Uncertainty Evaluation of Reservoir Simulation Models using Particle Swarms and Hierarchical Clustering

Muhammad Kathrada

Submitted for the

Degree of Doctor of Philosophy

Institute of Petroleum Engineering

Heriot-Watt University

June 2009

Abstract

History matching production data in finite difference reservoir simulation models has been and always will be a challenge for the industry. The principal hurdles that need to be overcome are finding a match in the first place and more importantly a set of matches that can capture the uncertainty range of the simulation model and to do this in as short a time as possible since the bottleneck in this process is the length of time taken to run the model. This study looks at the implementation of Particle Swarm Optimisation (PSO) in history matching finite difference simulation models.

Particle Swarms are a class of evolutionary algorithms that have shown much promise over the last decade. This method draws parallels from the social interaction of swarms of bees, flocks of birds and shoals of fish. Essentially a swarm of agents are allowed to search the solution hyperspace keeping in memory each individual's historical best position and iteratively improving the optimisation by the emergent interaction of the swarm. An intrinsic feature of PSO is its local search capability. A sequential niching variation of the PSO has been developed viz. Flexi-PSO that enhances the exploration and exploitation of the hyperspace and is capable of finding multiple minima. This new variation has been applied to history matching synthetic reservoir simulation models to find multiple distinct history

matches to try to capture the uncertainty range. Hierarchical clustering is then used to post-process the history match runs to reduce the size of the ensemble carried forward for prediction.

The success of the uncertainty modelling exercise is then assessed by checking whether the production profile forecasts generated by the ensemble covers the truth case.

Acknowledgements

I would like to thank the Herriot-Watt Uncertainty Joint Industry Program for funding of this work, the sponsors being BG, BP, Chevron, ConocoPhillips, DTI, JOGMEC, Hydro, ENI, Shell & Transform. At Shell, I'd like to thank Dick Eikmans, whom it was always great to bounce ideas off.

Contents

1 Introduction 7

1.1. Introduction to Numerical Reservoir Simulation 11

1.2. A Brief History of History Matching 18

1.3. General History Matching Approaches 24

1.4. Swarm Intelligence 35

2 Review of Particle Swarm Optimisation 39

2.1. Background to Particle Swarms 39

2.2. The Canonical PSO 42

2.3. The Inertia Weight PSO 43

2.4. The Constriction Factor PSO 47

2.5. Parameter Sensitivities 48

3 Development of a new Particle Swarm Variant 53

3.1. The Flexi-PSO 53

3.2. Qualitative Behaviour of the Swarm 64

3.3. Sequential Niching 72

3.4. Function Stretching 81

3.5. Handling Mixed Integer Problems 86

4 Mathematical testing of the Flexi-PSO 89

4.1. CEC 2005 benchmark test set 89

4.2. Neural network model of the IRIS dataset 98

4.3. Integer Problems 107

5 Hierarchical Clustering 109

5.1. Agglomerative Hierarchical Clustering 109

5.2. Clustering the IRIS dataset 114

6 History Matching & Forecasting : Case Study of the Imperial College Fault Model 116

6.1. Low Discrepancy Sequences 117

6.2. Model Definition 120

6.3. Results and Discussion 123

7 History Matching & Forecasting : Case Study of a North Sea Gas Field 139

7.1. Field Description 140

7.2. Results and Discussion 146

8 Conclusions 159

Appendix 166

Appendix A : CEC 2005 Mathematical Function Set 167

Appendix B : IRIS Dataset 200

Bibliography 204

Chapter 1

Introduction

Although much attention is focussed on new oil and gas developments, more than 70% of the worlds production comes from fields that are more than 30 years old. Maturing reservoirs come with a unique set of management challenges, from increased water cuts and gas-oil ratios through to aging technologies and health and safety implications. An added challenge to these reservoirs is that they often require more detailed forecasts of production behaviour, even though production volumes and hence revenues are lower. With the importance of understanding and forecasting the production increasing as well as the oil and gas becoming more difficult to extract, production costs also rise.

This leads to searching for an effective tool that can predict production behaviour. Reservoir simulation is one of the principal tools employed in the oil and gas industry to develop oil and gas bearing formations. This tool is used to evaluate different field development/management options against one another and thus maximise the economic value of the project. For the simulation model to be of any value, it needs to be representative of the subsurface structure, rock and fluid properties. For fields that have already been on production, the engineer can use the historical production data in an inverse manner to calibrate uncertain geological/fluid-flow parameters in the simulation model. This process of adjusting the reservoir model until it closely reproduces its past behaviour is typically referred to as "history matching", and is probably the number one topic of interest within the reservoir simulation community. History matching also plays a key role in developing an integrated approach to reservoir management because it allows the static geological model to be rationalised with production data.

Initially the objective of the history match study needs to be defined. The objective is mainly driven by the underlying business decision process in reservoir management e.g. reservoir planning, infill drilling campaigns, decisions on EOR incremental reserves, platform requirements, investigation of the impact of subsurface uncertainties on the reserves etc.

Multiple solutions exist to the history matching problem i.e. different history matched simulation models may not differ in the quality of their match criteria, but they may produce different results in the forecasting stage. This model diversity provides a basis for the quantification of uncertainties related to production forecasts and the estimation of the remaining reserves of a producing field.

Quite often the history matching process is undertaken deterministically where the engineer defines a set of reservoir / well parameters and some sensible ranges through which these parameters can be varied. He then goes through a tedious trial and error process varying these parameters, often one at a time to gain a sensitivity of the effect of that parameter on the system, analyse the results on completion of each run and then try some other combination of parameters that he intuitively feels would result in a lower error between the simulated and the historical data. This can often take many months, the outcome of which is not certain to yield a decent match at all particularly if the field is large and there are complex mechanisms at play within the reservoir.

In addition there is no guarantee that the match would be able to predict future reservoir performance either, which is why an ensemble of matches would give a better idea of what the prediction range may be. The shortcoming of the deterministic method is that the human brain can hardly visualise in more than four dimensions and most field history matches have many parameters that can be varied. With such a large number of unknown parameters to consider, traditional manual history matching remains very much a work in progress.

There are technological developments in both history matching and reservoir simulation that are helping to address today's reservoir management challenges. The rise of computer assisted history matching is an example of this. Computer assisted history matching allows the engineer to focus on developing an understanding of reservoir mechanisms and their relative impact on production behaviour. Through such tools, match modifiers are updated intelligently to try to increasingly improve the history match. It also makes it possible to consider more information when developing a history match or sensitising an appraisal. With manual history matching it can be impossible to evaluate all aspects of the reservoir description that could have an effect on the reservoir behaviour.

With computer assisted history matching however, large numbers of modifiers can be evaluated in a full physics simulator and in fewer runs to provide multiple matches of the reservoir to the production history. The results are then used with the simulator to predict how a field will perform and give measures of the uncertainty of these predictions. This in turn leads to valuable information on the economics of the reservoir.

This thesis addresses the area of assisted history matching where an algorithm is devised to search the hyperspace, and be quicker than a human at finding combinations of the uncertain parameters that would match the historical production data. We begin with a brief journey through the Society of Petroleum Engineers (SPE) literature to put into perspective the various approaches that have been used over the years and where the proposed methodology fits in. It is also to delineate the key advantages and disadvantages of the various methodologies. The Particle Swarm Optimisation method and its performance on benchmark mathematical functions, training a feed-forward neural network model and integer problems will be discussed. Then the Flexi-PSO will be tested on the Imperial College Fault Model that is widely regarded as a benchmark test case for history matching due to its difficult fitness landscape. The Flexi-PSO is then used to history match a synthetic version of a real North Sea gasfield model.

1.1. Introduction to Numerical Reservoir Simulation

Numerical reservoir simulation is the mathematical replication of the real physical processes of fluid flow that occur within oil and gas reservoirs (Ertekin et al, 2001). It is a model that represents the reservoir by a set of mathematical equations derived from first principles of flow through porous media. These equations can be solved analytically or numerically. As is so often found in engineering systems, the model can require assumptions to simplify the problem statement. If however, there are too many simplifying assumptions or the simplifying assumptions deviate too far from the true physics of the system, then the simulation can lead to unreliable results.

A reservoir simulation model is typically composed of a representation of the reservoir as well as a set of equations describing fluid flow through the reservoir. The reservoir representation begins with the geophysics discipline where the boundaries of the reservoir are demarcated. This is followed by the geology and petrophysics disciplines that determine the content of this demarcated volume. This volume is then populated by a geological model which could be a river channels, turbidite systems, etc. This geological model then uses information from wells which have been drilled as well as seismic data from the geologist to populate a set of rock parameters within this volume.

This geological model is discretised into a grid of blocks or cells as they are commonly known. An example of this is shown in Figure 1.1. This figiure shows a reservoir grid with wells penetrating the gridblocks at locations where they are in reality. Each gridblock has an associated set of reservoir rock properties that represents the volume that the gridblock is associated with. These properties can change with time as the reservoir undergoes production and injection, however the model is initialised with properties as found when initially drilled.

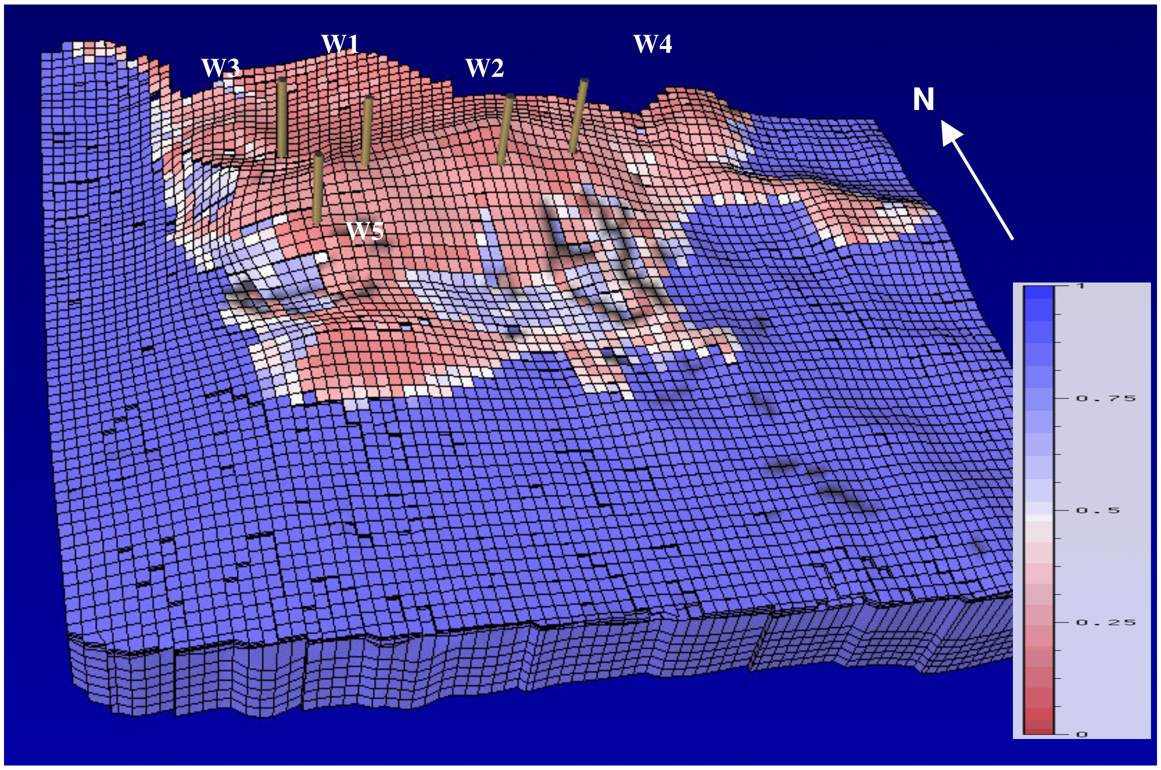

Figure 1.1. Example of a reservoir simulation grid

Typically the following data is required for any simulation model (Koederitz, 2005) :-

A. Gridblock location dependent parameters

- Location of each gridblock node in space viz. x, y, z co-ordinate
- Net to Gross (that amount of rock volume which can allow fluid flow)
- Effective Porosity (φ) – the ratio of connected void space to bulk volume of the rock
- Absolute permeability in each direction viz. k_x, k_y and k_z. This determines the speed of fluid flow through the reservoir rock.

- Pressure (P) expected over the gridblock volume
- Phase saturations typically oil, water and gas (S_o, S_w & S_g). However if enhanced oil processes are being undertaken, additional liquid and/or solid phases could be present)

B. Saturation dependent properties

- Capillary pressue (P_c) is the difference in pressure across the interface of two immiscible fluid phases. This is used to initialise the saturation profile of the various phases in the reservoir simulator
- Relative permeability (kr_o, kr_w & kr_g) is the measurement of the ability of two or more fluid phases to pass through a formation matrix. When more than phase is present in the reservoir rock, each phase tends to inhibit the flow of the other. Relative permeability (kr) is multiplied by absolute permeability (k) to give an effective permeability (ke) for each phase flow

C. Fluid and Rock parameters which are pressure dependent

- Formation volume factors of oil, water and gas (B_o, B_w and B_g) which is the ratio of a unit volume of reservoir fluid to the volume it would occupy at standard conditions (1 atm, 60 °F) at the surface

- Gas-Oil Ratio (Rs) which is the ratio of the volume of gas dissolved in the oil to the volume of oil itself at standard conditions
- Densities of each fluid phase viz. oil, water and gas (ρ_o, ρ_w & ρ_g)
- Viscosities of each fluid phase (μ_o, μ_w & μ_g)
- Fluid (oil, water and gas) and Rock Compressibilities (c_o, c_g, c_w & c_f). This is a measure of the change in volume of the fluid and rock with a change in pressure

D. Well and Surface Facilities data

- Location of perforations of each well in the grid co-ordinate system. This is important as these gridblocks act as pressure sinks for the movement of fluid from other parts of the reservoir
- Production and injection data comprising of phase rates and pressure when history matching
- Production and injection constraints due to facilities handling limits and pressure drawdown constraints on the wells when forecasting

The reservoir simulator uses all the above data in a set of mathematical equations to describe the simultaneous fluid flow of multiple phases as well as transfer of mass between the phases (usually between oil and gas) in the reservoir. The equations essentially describe the interaction between gravity, viscous and capillary forces within the porous media. Darcy's Law is the basis of these fluid flow equations which when applied to multiple phases over time is formulated as partial differential equations which are solved numerically in the simulator.

Darcy's Law is based on experimental work done by a civil engineer Henry Darcy in1856 on the water filtration systems in Dijon, France. In 1-dimension and for linear flow for a fluid with viscosity μ, his law expounds that in a horizontal plane the volumetric flow rate, q, through a porous medium of length L and cross-sectional area A (Figure 1.2) is given by the following equation (1.1.1) :-

$$q = -\frac{kA(P_{out} - P_{in})}{\mu L} \tag{1.1.1}$$

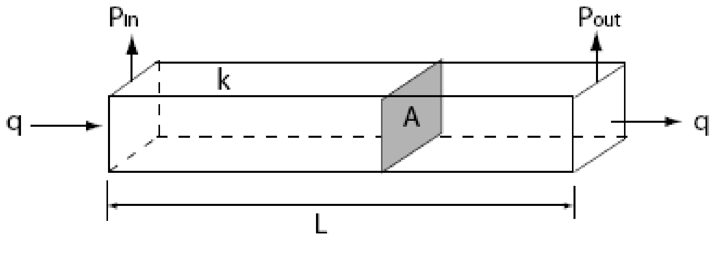

Figure 1.2. Diagram of Darcy's Experiement

k (permeability) in this equation is a derived property since all the other parameters are experimentally known. The equation can be formulated in the x, y and z directions by introducing pressure gradient and directional permeability tensor terms.

The equations used in the reservoir simulator are derived from Darcy's Law that honour the mass balance between flow for each phase through adjacent gridblocks and from gridblocks into wells and hence give the saturation and pressure changes at any spatial point in the reservoir with time. The equations are complex nonlinear partial differential equations which are difficult to solve analytical and typically numerical methods are used. Finite difference techniques are used to discretise the reservoir model in space and time. The equations then need to be linearised and can be solved explicitly or implicitly. Explicitly means that gridblock, fluid, rock and saturation dependent parameters are updated at the end of every timestep with the calculated pressure whereas Implicit schemes solve all the parameters including pressure simultaneously at the end of the timestep. Usually a direct or an iterative technique e.g. Newtons method is used to solve the system of linearised equations.

Simulation models with a large number of gridblocks can take quite long to simulate particularly if a detailed fluid model using an Equation of State is required. An Equation of State is a rigourous thermodynamic representation of the reservoir fluid at any pressure and temperature (Whitson et al, 2000).

The reservoir simulator now needs to solve an additional set of thermodynamic equations for each compositional component in all the active gridblocks. This increases the computing cost tremendously and for large reservoirs with many gridblocks can take an uncertainty modelling exercise into many months. However the reservoir simulator is the best tool in assessing the performance of a reservoir and is the preferred technique used in uncertainty modelling.

1.2. A Brief History of History Matching

This section covers methods attempted in assisted history matching viz. derivative and non-derivative techniques, stochastic methods, population based evolutionary techniques and the use of designed experiments/proxy modelling.

One of the first attempts at assisted history matching was by (Solorzanom et al., 1973) using a direct search method. Direct search is a method for solving optimization problems that does not require any information about the gradient of the objective function. As opposed to more traditional optimization methods that use information about the gradient or higher derivatives to search for an optimal point, a direct search algorithm searches a set of points around the current point, looking for one where the value of the objective function is lower than the value at the current point. You can use direct search to solve problems for which the objective function is not differentiable, or even continuous.

With direct searches, the algorithm computes a sequence of points that get closer and closer to the optimal point. At each step, the algorithm searches a set of points, called a mesh, around the current point, which is the best point computed at the previous step of the algorithm. The algorithm forms the mesh by adding the current point to a scalar multiple of a fixed set of vectors called a pattern. If the algorithm finds a point in the mesh that improves the objective function at the current point, the new point becomes the current point at the next step of the algorithm.

Other methods that have been proposed are those using sensitivity coefficients (e.g. Cui et al, 2005) where a sensitivity coefficient matrix of production data to reservoir parameters is built up by perturbing each reservoir parameter individually and then calculating the change in history match quantities (e.g. pressures and saturations) per change in reservoir parameter. This was found to be prohibitively expensive when dealing with a large number of dimensions as observed by (Yang et. al, 1988), particularly when using the classical finite difference method as it meant rerunning the simulation for each reservoir parameter perturbation.

(Chen et al., 1974) proposed using optimal control theory where the gradient of the performance index is computed. This in conjunction with first-derivative minimization methods like steepest descent and conjugate gradient were the focus of attention of many researchers (Chavent et al., 1975, Watson et. al, 1980, Wasserman et. al, 1975, Brun et. al., 2004, Bissell et al., 1994). (Yang et al., 1987) proposed quasi-Newton methods viz. Broyden-Fletcher-Goldfarb-Shanno (BFGS) and Self-Scaling Variable Metric (SSVM) as these methods could incorporate constraints unlike steepest descent and conjugate gradient techniques.

(Parish et al., 1993) created a knowledge-based system in conjunction with Sequential Bayes methods to assist the engineer with history matching. The knowledge-based element contained a rule base derived from interviews with engineers. The rules were typically IF … THEN … statements and though no quantitative results were reported, they concluded that the tool was effective in assisting the engineer with decision support rather than replacing him.

Whilst these techniques were of assistance to the simulation engineer, a caveat soon became apparent. These methods were great at finding a minimum of a function but who was to say whether that minimum was really the global optimum of the system particularly when one had no real clue as to what the fitness landscape looked like (Yamadi,2000, Mantica et al, 2001). Hence the realization of the non-uniqueness of a particular history match dawned and that the non-convex nature of the problem would be better tackled by global optimization methods as these techniques have a better chance of escaping local optima as opposed to local search techniques. To this end, attention was turned towards generating multiple matches. (Mantica et al, 2001) proposed a stochastic chaotic search method combined with a gradient based optimizer. Other attempts have also been made to use global and local optimization techniques. (Gomez et al, 2001) tried using a limited memory BFGS gradient optimization technique and once there was no improvement in the objective function, a tunnelling method was employed to escape the local minimum.

Other stochastic methods such as simulated annealing are worth mentioning. Simulated Annealing (Kirkpatrick et al, 1983) operates analogously to the physical process of annealing where the temperature of a metal is reduced to its minimum energy level by a slow cooling process. Rapid cooling would lead to the metal being left in a brittle state, however the usual tradeoff of time versus strength needs to be made. The method is able to escape local minima by accepting an uphill move dependent on a temperature function. The probability of an uphill move is reduced during the course of the run hence it is anticipated that many minima would have been visited during this trip and that the system would finally settle in the global optimum (Ouenes et al, 1983, Ouenes et al, 1994).

The principal drawback of the above mentioned techniques is that they are sequential, hence time consuming from a simulation time point of view. This is where evolutionary population based techniques become attractive. (Schulze-Reigert et al, 2001) proposed an evolutionary algorithm that made use of distributed computing. The nature of evolutionary algorithms is that they are slower to converge than gradient based search algorithms, but their parallel nature does not limit them to be solved on a single processor. They are also attractive in that they are much simpler to understand than gradient based techniques and do not require any derivative information. Other evolutionary based methods like genetic algorithms have been extensively studied (Sen et al, 1995, Romero et al, 2000). A genetic algorithm tries to drive towards a better objective function value by mating the fittest members of the population. It also has a mutation operator often seen as a necessary evil to prevent the algorithm from converging too rapidly. Population based algorithms however do require many iterations and hence are slower to converge.

Experimental design and response surface modelling methods have been attempted to address this problem. (Allessio et al, 2005, Li et al, 2006, Cullick et al, 2007) amongst others, used designed experiments in the initial stage of the history match to which a response surface was fitted. This response surface acts as a proxy to the simulator and guides future sampling. [Ramgulam et al, 2007] used a neural network to model the response surface and claimed that such a model reduced the number of simulations required to find a history match. Such experimental design-response surface techniques need to be approached with caution. Whatever their sophistication, they would be effective as interpolative tools and should never be used to extrapolate. Another issue associated with experimental design is that high dimensional problems require an exponentially increasing number of design points, something that may not be practical.

Scatter Search Metaheuristics have been used by (de Sousa et al, 2007) to history match two synthetic models. The term metaheuristic refers to methodologies that combine a high level controlling heuristic with a low level local search engine. In Scatter Search, in an initial random set of solutions (RefSet), two or more solutions are used to generate new trial solutions. This is done via a non-convex linear combination of solutions in the RefSet. The new trial solutions are ranked by their fitness, and the fittest members then undergo a local search. A collection of the best points is then extracted to be used as the RefSet for the next iteration. This method is advantageous as it is virtually parameterless and simple to understand, however the drawback is that there is not much that you can further do to the algorithm to increase its performance. (de Sousa et al, 2007) report good scalability of the algorithm but found it to be simulation intensive particularly with the addition of the local search.

Uncertainty analysis has also been used in assisted history matching. (Costa et al, 2006) statistically analyzed simulations and uncertainty variables to create a risk curve to avoid unnecessary simulation runs. (Erbas et al, 2007) used a Neighbourhood Algorithm (multiple start non-derivative local search which can be used in distributed computing) in a Bayesian framework to sample the parameter space and generate an ensemble of history match models, which are then assigned probabilities by posterior inferencing. An uncertainty range in a set of forecasts from these models can then be assessed.

1.3. General History Matching Approaches

History matching is essentially an inverse problem where plausible parameter values need to be determined given inexact (uncertain) data from an assumed theoretical model that relates the observed data to the model

(Oliver et al, 2008). Simply put, the parameter set x needs to be determined that fits data y in model f:-

$$y = f(x)$$

From a mathematical standpoint, the history matching process reduces to an optimisation problem for which a large number of numerical algorithms are available. Generally, optimisation algorithms are from two distinct classes :-

a) Techniques that use derivatives like Levenberg-Marquardt and Quasi-Newton. They have relatively fast convergence but are capable of only finding local minima.
b) Techniques that donot use derivative information like genetic algorithms and particle swarms. They are slower to converge since they search a wider area of the parameter space but are capable of finding multiple minima. They also lend themselves to distributed processing and treating the simulator as a black box.

This thesis deals with the latter category, however it is worth discussing the former category as well. Firstly it must be noted that for simple convex problems, there is no need to use vastly complicated algorithms. Often using something simple like Newton-Raphson is sufficient. With the Newton-Raphson technique for root finding, one starts with an initial guess somewhere on the function *f(x)*. A tangent is then drawn from the initial guess to the x-intercept and typically this point would be a better approximation to the functions minimum than the original starting point as depicted in Figure 1.3.

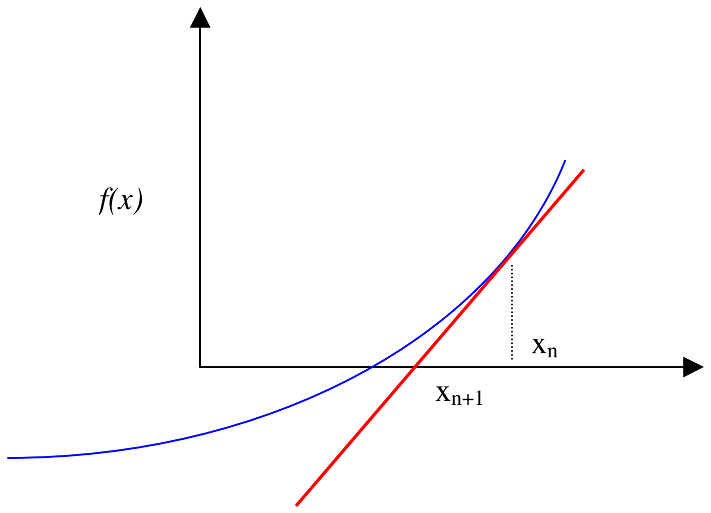

Figure 1.3. Diagram of Newton-Raphson Method

In optimisation, if a real number x^* is a minimum of *f(x)*, then x^* is a root of the derivative of *f(x)* and hence x^* can be solved by applying Newton-Raphson to *f(x)*. The Taylor expansion of a function *f(x)* (1.3.1) :-

$$f(x+\Delta x) = f(x) + f'(x)\Delta x + \frac{1}{2} f''(x)\Delta x^2 \tag{1.3.1}$$

has a minimum (or maximum) when (1.3.2) is met :-

$$f'(x) + f''(x)\Delta x = 0 \tag{1.3.2}$$

and if *f''(x)* is positive. This implies that it must be possible to calculate the second derivative of *f(x)*, something that is not achievable is discontinuous functions. Hence the solution will converge to *x** from an initial guess x_o, using the sequence as follows (1.3.3) :-

$$x_{n+1} = x_n - \frac{f'(x_n)}{f''(x_n)}, n \geq 0 \tag{1.3.3}$$

There are two main classes of methods to calculate the derivates viz. the forward method, also known as the simulator-gradient and the adjoint method. The adjoint method requires a backward in time simulation, but it is able to compute the gradient of the objective function with cost proportional to a single simulation no matter how many parameters there may be. This property makes the adjoint method much better to solve models with a large number of parameters. (Rodrigues et al, 2006) showed field models with more than 250 parameters which this technique was still able to solve efficiently. However (Oliver et al, 2008) noted that the sensitivity coefficients to partial derivatives could not be reliably calculated for those parameters to which the observed historical data was not very sensitive to.

Experimental design together with response surface modelling can also be effective emulator in history matching. (Busby et al, 2008) proposed a hierarchical nonlinear approximation scheme to obtain an accurate approximation of the response surface using few function evaluations. The response surface from their sequential experimental design results was generated by kriging. Response surface or proxy models as they are more commonly known are attractive since they are very quick to solve, and a full simulation run is not required. Further evaluation points for the simulator are obtained by optimising on this response surface, and these results are added to experimental design to update the response surface. The technique was tested on the Imperial College Fault Model. (This model is presented later in Chapter 6). Very low errors were achieved using relatively few function evaluations attesting to the efficacy of this method.

By and large, the challenge of statistical prediction is to assess the uncertainty in the predicted results. This reduces to the propagation of errors from the input parameters to the simulated results. The biggest hurdle in analysing the impact of uncertainties is the "curse of dimensionality" (Christie et al, 2005). High dimensional spaces can lead to complex fitness landscapes which can be impossible to resolve within a reasonable timeframe, particularly for systems that require simulation.

When solving inverse problems, scientists and engineers are faced with firstly trying to find at least one model that can be consistent with observations. Secondly, in problems where multiple models are consistent with observations, how can the non-uniqueness of these results be quantified? (Tarantola, 2006). The intention of the various history matching algorithms is to generate an ensemble of models that can be used in the quantification of the uncertainty of the model to the true reservoir behaviour.

Uncertainty arises from a lack of information, therefore uncertainty quantification means describing the state of information at hand which is typically done by probability distributions. Two different philosophies exist for quantifying uncertainty. The first avoids using any *a priori* information on the model parameters that could 'bias' the inferences drawn from the data. This means the parameter set is defined as a uniform distribution. The second philosophy is Bayesian which asks the question: how does the newly acquired data modify our previous information?

The Bayesian framework for statistical inference provides a methodical procedure for updating current knowledge of a system based on new information (Kaipio et al, 2005). Let simulation model n represent the system at hand, and be a formalisation of all information necessary to solve an objective. n would contain the fundamental equations describing the system (usually in the form of partial differential equations), the model parameters and their ranges, as well as initial and boundary conditions. In real world applications, much of the information in system n can contain uncertainty. This uncertainty can be represented by an ensemble of models N, with $n \in N$. A probability distribution on N can be defined, and is referred to as the prior distribution *p(n)*. Hence the uncertain parameters in the model and their prior distributions *p(n)* need to be determined; a process called parameterisation.

If some information exists as to the likely values of *n* then a prior distribution that reflects this can be selected. As an example, permeability (*k*) normally has a log-normal distribution due to the heterogeneity in the reservoir rock. If there is plenty of core data available, then the shape of the distribution can be delineated and if little data is available then a distribution that supports a wide range of *n* should be selected.

Additional information from observations of the system behaviour (*O*) can be used to update the estimate for the probability of *n*. This is referred to as the posterior distribution and denoted as *p(n / O)* by using Bayes' formula. Bayes theorem (Bayes, 1763) states that considering two events *A* & *B*,

$$p(A \mid B) = \frac{p(B \mid A)p(A)}{p(B)} \qquad (1.3.4)$$

This formula describes how a belief about an event changes as new information is obtained. Let event A have an initial prior probability *p(A)* of occurring. If event *B* then occurs then the description of how likely *A* is considering that *B* has occurred is the posterior probability *p(A| B)*. Bayes theorem updates the prior probability to the posterior by multiplying the $p(B|A)/p(B)$. The following example illustrates Bayes theorem.

Suppose there is a co-ed school having 60% boys and 40% girls as students. The girls wear trousers or skirts in equal numbers whilst all the boys wear trousers. An observer sees a (random) student from a distance and that this student is wearing trousers. What is the probability this student is a girl? The correct answer can be computed using Bayes' theorem.

The event A is that the student observed is a girl, and the event B is that the student observed is wearing trousers. To compute $P(A|B)$, we first need to know:

- $P(A)$, or the probability that the student is a girl regardless of any other information. Since the observers sees a random student, meaning that all students have the same probability of being observed, and the fraction of girls among the students is 40%, this probability equals 0.4.
- $P(A')$, or the probability that the student is a boy regardless of any other information (A' is the complementary event to A). This is 60%, or 0.6.

- P(B| A), or the probability of the student wearing trousers given that the student is a girl. As they are as likely to wear skirts as trousers, this is 0.5.
- P(B| A'), or the probability of the student wearing trousers given that the student is a boy. This is given as 1.
- P(B), or the probability of a (randomly selected) student wearing trousers regardless of any other information. Since P(B) = P(B| A)P(A) + P(B| A')P(A'), this is 0.5×0.4 + 1×0.6 = 0.8.

Given all this information, the probability of the observer having spotted a girl given that the observed student is wearing trousers can be computed by substituting these values in Bayes' formula :-

$$p(A \mid B) = \frac{p(B \mid A)p(A)}{p(B)} = \frac{0.5 \times 0.4}{0.8} = 0.25$$

(1.3.4) is the discrete form of Bayes' Theorem. For continuous distributions the posterior probability density function of n is expressed as (1.3.5) :-

$$p(n \mid O) = \frac{p(O \mid n)p(n)}{\int_N p(O \mid n)p(n)dn} \tag{1.3.5}$$

p(O| n), the probability of observations *O* given parameter/s *n* is referred to as the likelihood function. This together with the prior distribution *p(n)* must be specified in any Bayesian computation.

Relating this to reservoir simulation, the posterior distribution of reservoir parameters *n* (e.g. pore volume and permeability multipliers, aquifer sizes etc) are estimated from the observed field production data *O* (e.g. phase rates, bottomhole pressures etc). By comparing reservoir simulation production profiles to the observed field production data, one can create the likelihood function. Consider a certain phase rate measurement. If measurement errors are independent i.e. at time *t* is not dependent on a measurement at any other time t_n, are normally distributed around zero with variance σ^2 for all measurements, then the likelihood function for *M* measurements can be defined as (1.3.6) :-

$$p(O \mid n) = \left(\frac{1}{\sigma\sqrt{2\pi}} \right)^M \prod_{m=1}^{M} e^{-\frac{(q_{obs}-q_{sim})_m^2}{2\sigma^2}} \tag{1.3.6}$$

$\left(\frac{1}{\sigma\sqrt{2\pi}} \right)^M$ is constant and if the misfit is defined from the least squares formula as $misfit = \sum_{m=1}^{M} \frac{(q_{obs} - q_{sim})_m^2}{2\sigma^2}$ then the likelihood function becomes (1.3.7) :-

$$p(O \mid n) \propto e^{-misfit} \tag{1.3.7}$$

A general Bayesian framework as developed by the Uncertainty Quantification Group at Heriot-Watt University is shown in Figure 1.4.

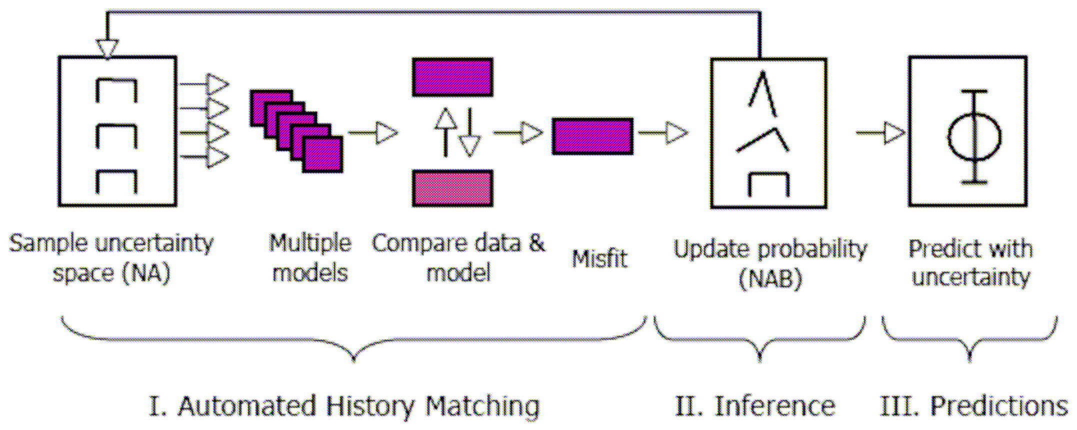

Figure 1.4. Bayesian Framework for Uncertainty Quantification

The cumulative distribution function of the posterior can now be calculated and credible intervals reported. As an example, a 10% maximum credible interval *(a,b)* is the widest interval whose posterior probability of containing the true *n* is 0.1. If *a* = 0, then *b* corresponds to the 0.1 quantile of the cumulative distribution. Subsurface quantities such as recovery and porosity/permeability are often reported as P10, P50 and P90. These terms correspond to the 10%, 50% and 90% probabilities that the actual value is below the reported value.

Against this backdrop of historical work, a simple attractive population based evolutionary technique is investigated.

1.4. Swarm Intelligence

Increasingly the trend in the scientific community is to use algorithms employing natural metaphors to model and solve complex optimisation problems. This is primarily due to the inefficiency of classical optimisation algorithms in solving large scale combinatorial and highly non-linear problems. The situation is exacerbated if integer/discrete variables are also present in the problem formulation.

It is well known that classical optimisation techniques impose limitations on solving mathematical programming and operations research models. This is due to the intrinsic solution mechanisms of these techniques. Solution strategies of classical optimisation algorithms are generally dependent on the type of objective and constraint functions (linear, non-linear etc) and the type of variables used in the problem modelling (discrete, real etc) and are hence weak in their general applicability to a wider set of problems which have a combination of different types of variables and or constraints. An example is

the Simplex method used in Linear Programming, where only real variables, linear objectives and linear constraint functions can be used.
However most of the time real-life problems require different types of variables, constraint and objective functions in their problem formulation and hence classical methods are often not adequate or easy to use. Their efficiency is also very much dependent on the size of the solution space, number of variables and constraints used in the problem definition, the structure of the solution space (convex, non-convex), and the starting point in the solution space for the optimisation procedure. If the starting point is in the wrong place you could easily land in a local optimum and not be able to escape from there.

Researchers in many areas have spent a great deal of effort in order to adapt their optimisation problems to classical procedures by sometimes rounding or transforming variables, relaxing constraints etc. This certainly affects solution quality and creates a challenge to find alternative optimisation methods that are more generic in their use.

Insects that live in colonies like ants and bees have fascinated naturalists for decades. “What is it that governs here? What is it that issues orders, foresees the future, elaborates plans, and preserves equilibrium?,” wrote (Maeterlinck, 1901). This is indeed very puzzling. Every insect in a social insect colony seems to have its own plans, yet an insect colony as a whole appears so well organised. The seamless integration of all the individuals does not seem to require any controlling supervisor.

Social insects like ants, bees, termites and wasps can be viewed as powerful problem solving systems with sophisticated collective intelligence. Composed of simple interacting agents, the intelligence lies in the networks of interactions among individuals, and between individuals and the environment. Social insects lend themselves to metaphors for artificial intelligence. The problems they solve viz. finding food, dividing labour among nestmates, building nests, responding to external threats – all have important counterparts in engineering.

A branch of nature inspired algorithms viz. Swarm Intelligence which derives inspiration from natural populations like bees, insects, birds and fish, have meta-heuristics which can mimic an individual's behaviour in a population as well as the population as a whole, thus taking advantage of their natural problem solving abilities. Particle Swarm Optimisation and Ant Colony Optimisation (Socha et al, 2008) belong to this domain of algorithms. The meta-heuristics mimic the communication mechanisms for food foraging/group motion behaviour and exploit this for solving engineering objectives.

Swarm Intelligence being derived from this kind of paradigm has as its intrinsic property a system whereby the collective behaviours of (unsophisticated) agents interacting locally with their environment cause coherent functional global patterns to emerge. Swarm Intelligence provides a basis from which it is possible to explore collective (or distributed) problem solving without centralized control or the provision of a global model.

Swarm Intelligence was popularised by (Crichton, 2002) in the book *Prey* which dramatised the use of nano-robots. Though fictional, the book did expound the mechanisms of swarm intelligence where a population of individuals are programmed with an objective (military reconnaissance imaging, medical nanotech-based imaging) and have mechanisms to communicate with each other to achieve this objective. The key concept here is "communication". Evidence of swarm intelligence in humans is also common. A recent BBC report revealed that oil market traders' principal mechanism of decision making is actually the use of Instant Messaging (Yahoo! in particular) with other traders to glean information from one another as to market movements (Reuben, 2008).

Chapter 2

Review of Particle Swarm Optimisation

2.1. Background to Particle Swarms

Particle Swarm Optimisation was first introduced by (Kennedy and Eberhart, 1995). Since then there has been a significant increase in publications on this optimisation methodology. Particle swarms are attractive to the user as they do not require gradient and derivative information, are intuitive to understand and can be parallelised (Schutte et al, 2003). They can be used to solve a wide variety of problems, including neural network training (Eberhart et al, 1995), static function optimisation (Shi et al, 1995), dynamic function optimisation (Blackwell et al, 2005), multimodal optimisation (Brits et al, 2002) and data clustering (Cohen et al, 2006).

The idea was originally derived from modelling social behaviour, in particular modelling the flight of a flock of birds, the social outlook of this methodology being discussed in (Kennedy and Eberhart, 2001). This population based approach is different from other population based evolutionary methods which use some form of evolutionary operators in order to move the population towards the global optimum. Here the “particles” which make up the population move in the search range with a velocity that is determined by a simple equation relating the experience of each individual particle and the population. In essence each individual particle memorises the best position it has encountered and uses this together with the memory of the best position of its neighbours/population found thus far. Hence changes in the particles trajectory from these influences are then made to its velocity in each iteration and this gives the particle direction in the search space. Position updates are then made from the new calculated velocity.

The resulting effect of these interactions is that particles move towards an optimal solution while still searching the surrounding territory. A large body of work is aimed at manipulating the particle's ability to move in the search space using different configurations and other operators to manipulate the particles velocity during the run of the optimiser. Ideally, an optimiser that has good exploration ability while still being able to do fine local searches would be highly desirable. Even more beneficial would be an optimiser that has the ability to escape from local minima, which is something that this thesis addresses later.

Each particle of a population of n members in d dimensions has the position

$$X_i = (x_{i1}, x_{i2}, \dots ,x_{id}) \qquad i \in [1,n], j \in [1,d]$$

All the particles are randomly initialised within a predefined search range for each variable ($X_{min,j}$, $X_{max,j}$). The velocity vector of each particle is represented as

$$V_i = (v_{i1}, v_{i2}, \dots, v_{id}) \qquad i \in [1,n], j \in [1,d]$$

An upper and lower bound, $V_{max,j}$, also cap the velocities. In this study $V_{max,j}$ is taken to be half the search range of each variable, as was suggested by (Eberhart and Shi, 2000) after doing numerical experiments on several benchmark functions.

$$V_{\max,j} = 0.5\left(X_{\max,j} - X_{\min,j}\right) \qquad (2.1.1)$$

In addition each particle has a memory of the best position it has attained thus far called the *pbest*

$$P_i = (P_{i1}, P_{i2}, \dots, P_{id}) \qquad i \in [1,n], j \in [1,d]$$

The particle with the best fitness found thus far is usually represented as P_g and known as the *gbest*. There is a variation of the neighbourhood topology where a localised neighbourhood is used and is known as *lbest*. This is usually represented as P_l. Here the swarm is divided into overlapping neighbourhoods of particles where each neighbourhood is usually about twenty percent of the size of the population and in each neighbourhood an *lbest* particle is defined as the particle with the best fitness. Dynamic neighbourhoods can also be defined and are discussed by (Suganthan et al, 1999, Zhang et al, 2003).

2.2. The Canonical PSO

The following formulation represents the canonical particle swarm optimiser introduced by (Kennedy & Eberhart, 1995) :-

$$v_{ij}(t+1) = v_{ij}(t) + c_1 r_1 \left(P_{ij} - x_{ij}(t)\right) + c_2 r_2 \left(P_{gj} - x_{ij}(t)\right) \tag{2.2.1}$$

$$\text{if } v_{ij} > V_{max,j} \text{ then } v_{ij} = V_{max,j} \tag{2.2.2}$$

$$\text{elseif } v_{ij} < -V_{max,j} \text{ then } v_{ij} = -V_{max,j}$$

$$x_{ij}(t+1) = x_{ij}(t) + v_{ij}(t+1) \tag{2.2.3}$$

(2.2.1) represents the velocity update for each dimension *j* of particle *i*. r_1 and r_2 are numbers in the range [0, 1] generated by a uniform random number generator. c_1 and c_2 are the acceleration constants for the personal and global bests respectively. Typically $c_1 = c_2 = 2$ is used. As can be seen from (2.2.1) the velocity update for each particle is a random weighted average of its personal best and the global best of the swarm, while the first (momentum) term in equation (2.2.1) allows the particle which may have just achieved the best fitness value to still move in the search space. (2.2.2) is a checking mechanism that limits the velocity in each dimension to the maximum allowable V_{max}. Finally the position of each particle in each dimension is updated according to (2.2.3).

2.3. The Inertia Weight PSO

The inertia weight method for particle swarm optimisation was first proposed by (Shi et al, 1998). It is a way of trying to balance the explorative and exploitative ability of the swarm particles. It also ensures that the particles do not accelerate out of the search range. The inertia weight parameter resembles simulated annealing in that initially the PSO can search a larger range as the particle velocities are allowed to be bigger, while at the end of the run exploitation is facilitated with a smaller value of the inertia weight. They show experimentally that varying the inertia weight results in better performance than using a fixed value of the inertia weight during the course of a run. The inertia weight method is defined by the following equations :-

$$v_{ij}(t+1) = wv_{ij}(t) + c_1r_1\left(P_{ij} - x_{ij}(t)\right) + c_2r_2\left(P_{gj} - x_{ij}(t)\right) \tag{2.3.1}$$

$$\text{if } v_{ij} > V_{max,j} \text{ then } v_{ij} = V_{max,j} \tag{2.3.2}$$

$$\text{elseif } v_{ij} < -V_{max,j} \text{ then } v_{ij} = -V_{max,j}$$

$$x_{ij}(t+1) = x_{ij}(t) + v_{ij}(t+1) \tag{2.3.3}$$

w is the inertia weight and is usually varied linearly decreasing from w_{max} to w_{min} during the course of an optimisation and is represented in (2.3.4),

$$w(t+1) = w_{\min} + (w_{\max} - w_{\min}) \times \frac{(t\_\max - t)}{t\_\max} \qquad (2.3.4)$$

where t_max is the user specified maximum number of iterations and t is the iteration number. w_{max} is usually 0.9 and w_{min} 0.4 as experimentally determined by (Shi et al, 1998). With time the decreasing inertia weight limits the movement of this particle and allows the swarm to converge. Figure 2.1 depicts the typical trajectory of a particle with respect to each term in (2.3.1).

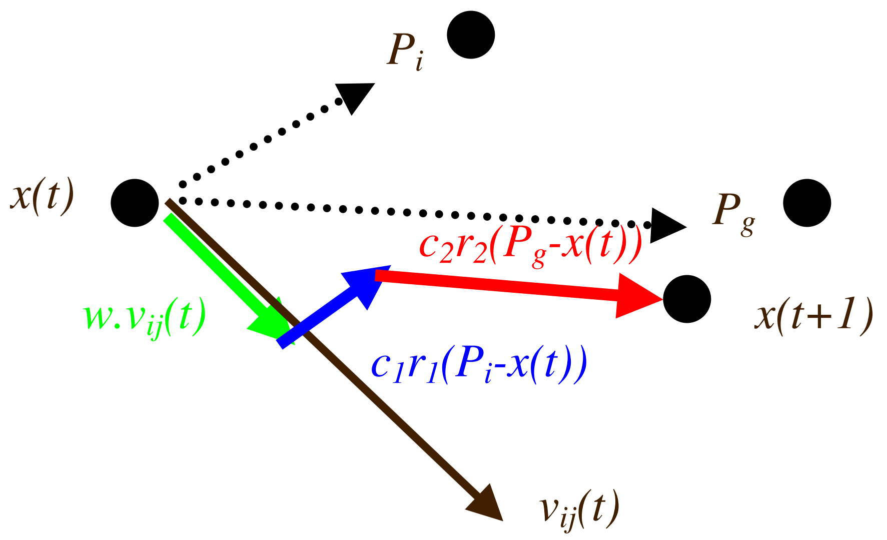

Figure 2.1. Inertia Weight Particle Trajectory

Figure 2.2 displays the typical velocity profile of a particle over each iteration. The energy dissipating effect of the inertia weight method can clearly be seen and it is this effect that leads to convergence of the particle at later times. Initially the particle can be seen exploring the search space while at later times it is exploitative by taking small velocity steps.

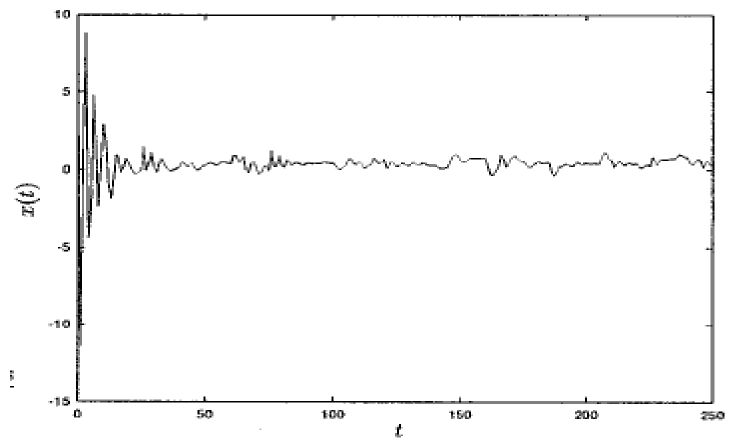

Figure 2.2. Inertia Weight Velocity Profile

Another PSO variant, known as the cognition only version was demonstrated by (Kennedy, 1997). Here $c_2 = 0$ and hence only the personal best position found thus far is used when calculating the new velocity. Hence there is no wider sharing of information between the particles and each particle is more likely to end up searching a local area where it was initialised. The algorithm keeps iterating until the maximum number of iterations is reached, the fitness function has reached a certain threshold or until velocity updates are close to zero. In this way, each particle in the swarm behaves as an individual hill-climber and this is beneficial if the objective function is multimodal. If $c_1 = 0$ then the swarm behaves as a stochastic hillclimber as no individual information is used and is beneficial when the objective function is unimodal.

The coefficients used in (2.2.1) determine the swarm behaviour, and many studies have been done in order to optimise these coefficients as well as maintain the explorative ability of the swarm. (Ratnaweera et al, 2004) proposed time varying acceleration coefficients and the mutation of particles to address this issue since it has been commonly observed particularly with benchmark functions, that the PSO finds a good local optima but can remain stuck in this optima sometimes for the entire duration of the run with little to no improvement.

A predator-prey type optimiser was introduced in (Silva et al, 2002, Silva et al, 2003) where a predator particle was used to chase the *gbest* particle and the predator randomly repelled particles in the swarm. The extent to which they were repelled also depended on how close the swarm particle was to the predator. This method however suffered from determining just how often swarm particles were to be repelled, and added another level of complexity to the tuning process. Other methods of gaining better performance include using mating, breeding and subpopulation mechanisms that were introduced by (Løvbjerg et al, 2001). Co-operative particle swarm optimisation is another promising area that has been introduced to allow the swarm to use information from the genes of different members of the population (van den Bergh et al, 2000).

2.4. The Constriction Factor PSO

The canonical PSO can still have fairly large velocities at the end of a run, hence the reason why inertia weights were introduced in an effort to control the velocities. The constriction factor PSO is another attempt to control the particle velocities and was proposed by (Clerc, 1999) as a way of ensuring convergence. This technique has the following formulation :-

$$v_{ij}(t+1) = K \times [v_{ij}(t) + c_1 r_1 (P_{ij} - x_{ij}(t)) + c_2 r_2 (P_{gj} - x_{ij}(t))] \qquad (2.4.1)$$

$$K = \frac{2}{\left|2 - \varphi - \sqrt{\varphi^2 - 4\varphi}\right|}, \text{ where } \varphi = c_1 + c_2, \text{ applicable for } \varphi > 4$$

In the above formulation, if $c_1 = c_2 = 2.05$, K will then be 0.729 and will result in the previous velocity (momentum term) being multiplied by 0.729 and the (P-x) being multiplied by 0.729*2.05 = 1.49445 (times a random number between 0 and 1). This is different from the inertia weight formulation where only the velocity of the previous iteration (momentum term) was lowered at every iteration, here the entire velocity step is reduced. Intuitively, it is expected that the velocities in the constriction factor method will decrease much more rapidly than the inertia weight method, hence leading to convergence. (Eberhart & Shi, 2000) analysed the constriction factor PSO and concluded empirically that setting $V_{max} = X_{max}$ significantly improved their results.

Furthermore (Zhang, Yu, Hu, 2005) analysed the effect of φ on the solution of unimodal and multimodal problems. φ was varied between 4.0 and 4.4. They concluded that the best choice for unimodal problems was to take φ = 4.1 and for multimodal problems φ = 4.05.

2.5. Parameter Sensitivities

It is important to have an understanding of the effect of the parameters of the PSO in order to design a version of the algorithm that would be suitable for history matching. In order to do this, a test is conducted here on the canonical, inertia weight and constriction factor versions to gain some insight to their behaviour. A test function (2.5.1) is used to get an idea of their velocity profiles.

$$f(x) = x_1^2 + 2x_2^2 - 0.3\cos(3\pi x_1) - 0.4\cos(4\pi x_2) + 0.7 \tag{2.5.1}$$

Firstly, the canonical version is tested by varying the acceleration coefficients. Typically $c_1 = c_2 = 2$. Figure 2.3 displays the effect of varying c_1 & c_2 from 1.0 to 3.0 on their velocity profiles. There are two aspects that should be noted from this Figure. Firstly, the velocity magnitudes are proportional to the acceleration coefficient. Secondly, it doesn't matter what the coefficient is, the velocities continue to increase with time since there is no damping mechanism in (2.2.1).

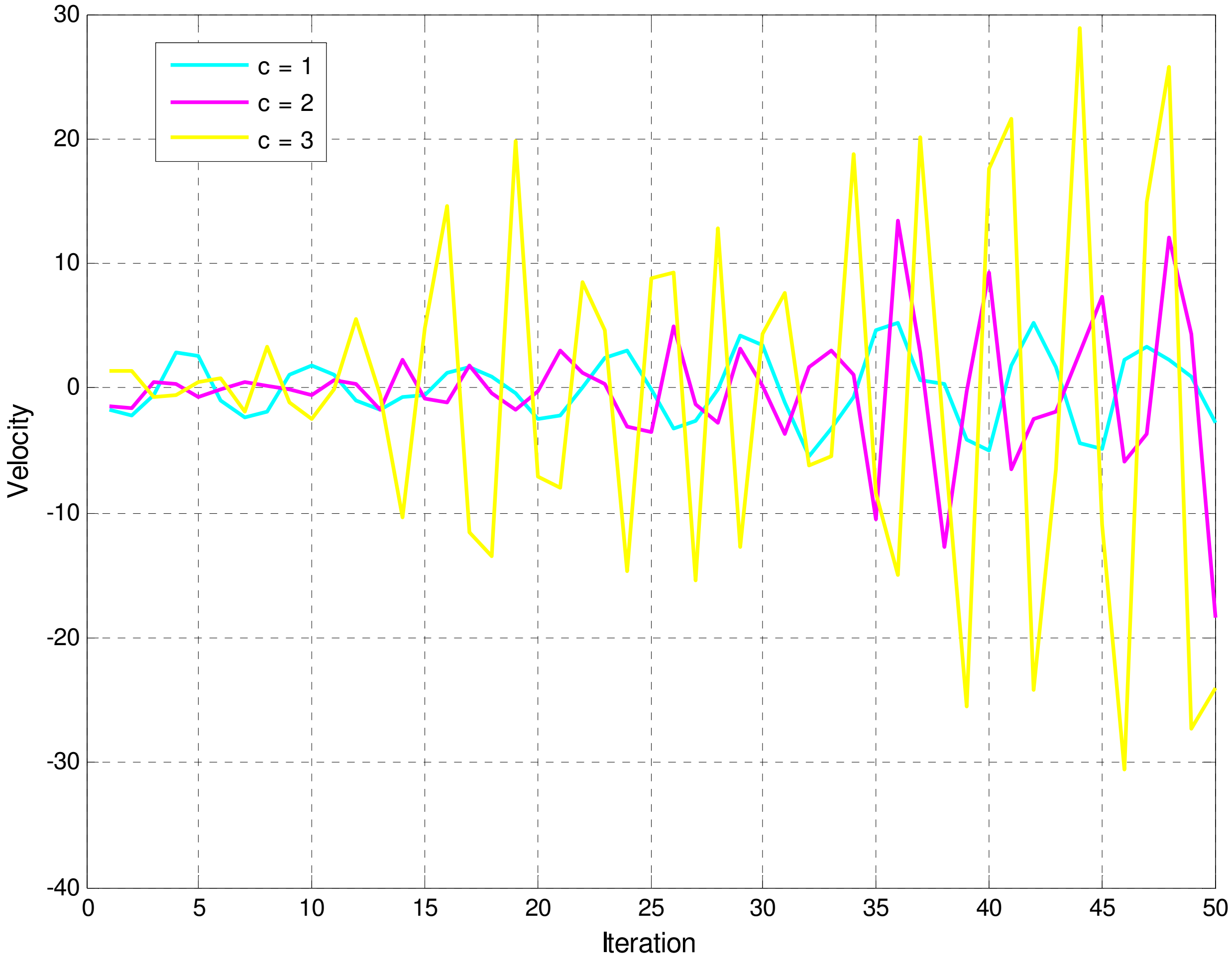

Figure 2.3. Acceleration Coefficient effect on the velocity profile of the Canonical PSO

The canonical PSO is clearly going to have convergence problems in history matching and can be rendered unusable. The next step is then to compare it with the inertia weight and constriction factor versions to see whether there is any benefit in using those techniques. Figure 2.4 displays the resulting profiles for 50 iterations of each PSO version. The canonical version suffers from high velocities all through the run and does not converge. The inertia weight version with w = 0.9 and linearly decreasing to w = 0.4 at the end of the run also shows fairly high velocities for most of the run, however does constrain itself towards the end. The constriction factor version quickly reduces its velocity and is able to make small steps for most of the run, hence fine tuning its solution.

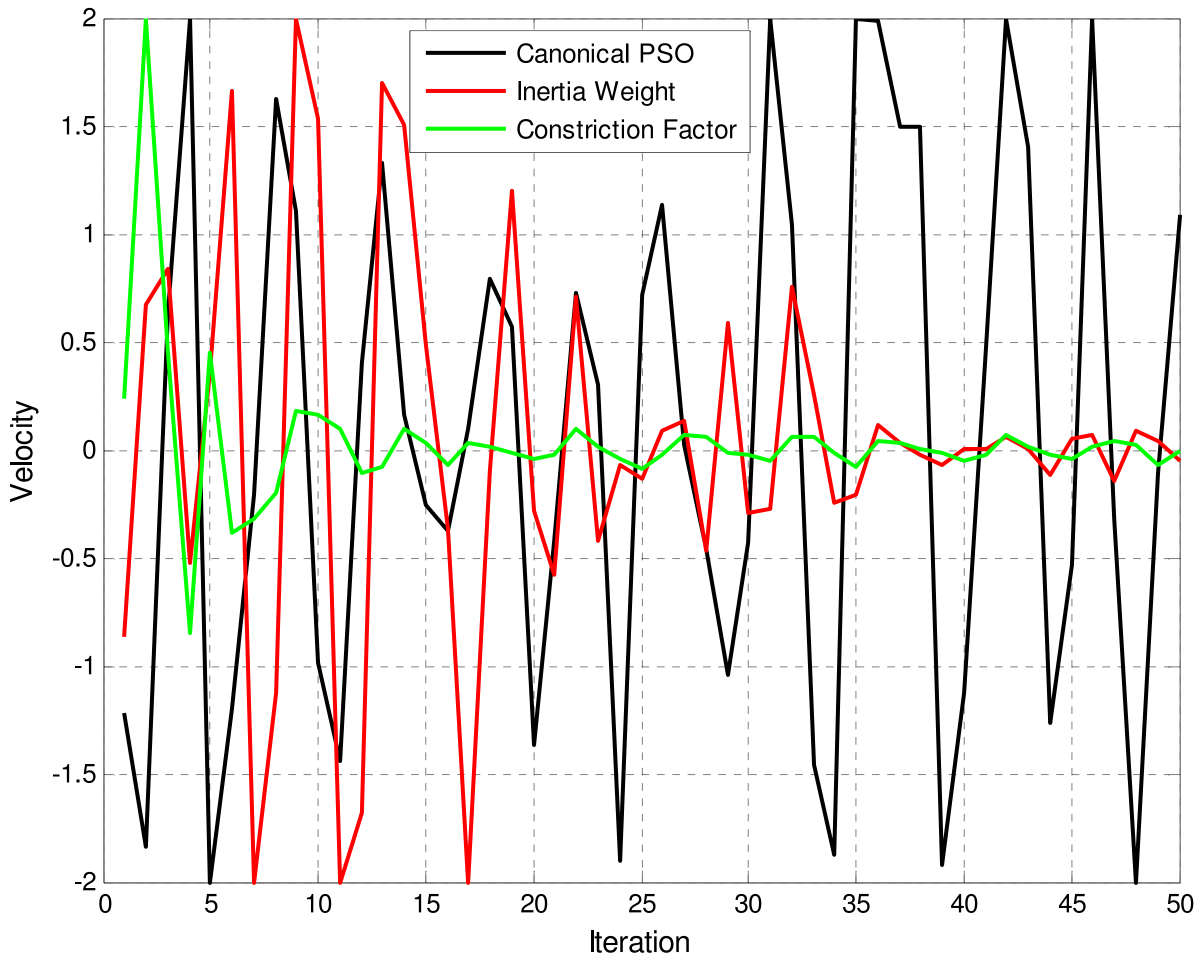

Figure 2.4. Velocity profile comparison of the Canonical, Inertia Weight and Constriction Factor PSO's

The next step is to investigate the effect of changing the inertia weight ranges to see if any improvement can be made to its convergence behaviour. A comparison is made with w = 0.9 $\rightarrow$ 0.4 (Shi et al, 1995), $w = 0.4 \rightarrow 0.9$ and $w = 0.5 \rightarrow 0$. Figure 2.5 displays the velocity profiles of this test. Clearly, varying $w = 0.5 \rightarrow 0$ shows convergent behaviour that is even better than the constriction factor in Figure 2.4.

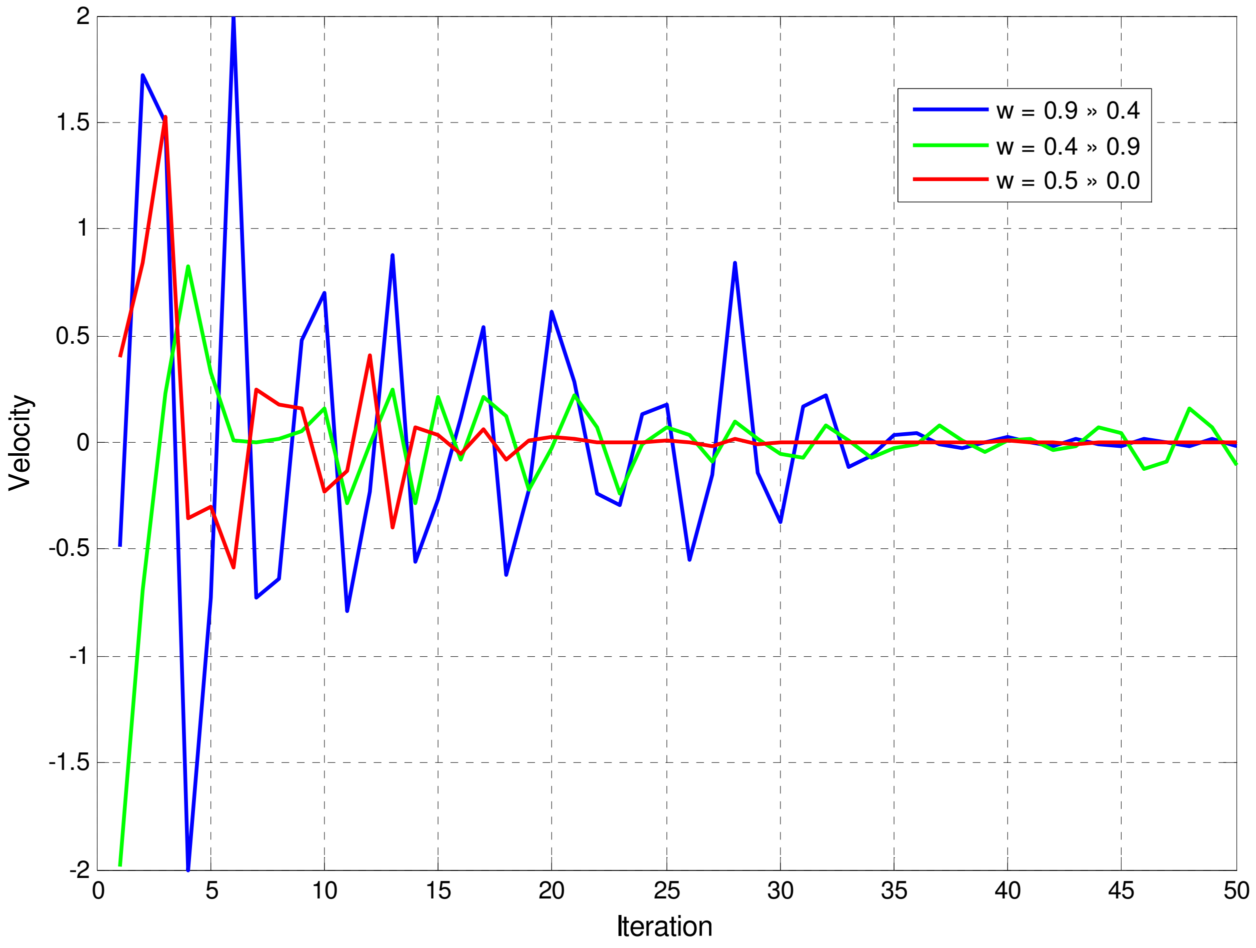

Figure 2.5. Velocity profile comparison of the Inertia Weight PSO with different w ranges

It does make sense to use this range for the inertia weight as taking it down to 0 will lead to very small velocities at later iterations and hence be able to fine tune a search. Although the constriction factor version does have velocities that are dampened with time, it does not have the flexibility of the inertia weight as the constriction factor K operates over the entire velocity update.

The objective is to design a Particle Swarm optimiser suitable for history matching purposes. The inertia weight version appears to be a better candidate for further development and it will be used as the basis for the rest of this thesis.

Chapter 3

Development of a new Particle Swarm Variant

3.1. The Flexi-PSO

Particle Swarms are similar to fractals. Fractals produced intricate patterns based on simple recursive equations. Similarly the swarm also produces an exciting emergence of interaction between its particles that leads to good solutions in global optimisation also using simple recursive equations. The analogy of particles interacting at the social level makes intuitive sense and heuristics can be developed to make the canonical algorithm much more powerful.

This thesis looks at intuitive mechanisms and heuristics to increase the effectiveness of the swarm. This will be judged by comparing a particle swarm variant developed in this thesis viz. the Flexi-PSO (Kathrada, 2009) to the original Inertia Weight method on a non-convex function. Further tests will be conducted on benchmark mathematical test sets and the training a neural network to assess the performance of the Flexi-PSO in relation to other state of the art techniques.

The first mechanism that is introduced here is to use an extended particle swarm optimiser that updates the velocities using *pbest*, *gbest* as well as *lbest*. *lbest* here is implemented for a neighbourhood with a ring topology where each particle has a neighbour on either side of it, with the end member particles also being connected and hence forming a ring as in Figure 3.1. Particles are numbered according to the sequence in which they are initialised.

If the neighbourhood size is taken to be two, then any particle *(i)* compares itself to particle *(i-1)* and particle *(i+1)*, e.g. particle 1 would compare itself to particle 2 and particle 8 since the topology is a ring. The neighbourhood size used in this study is 25% of the population size. This idea was also introduced by (Jun-jie & Zhan-hong, 2005), however it was applied to the constriction factor method of PSO (Eberhart and Shi, 2000). Here, advantage is taken of the neighbourhood best position, and this additional information helps the swarm to search more of the solution space.

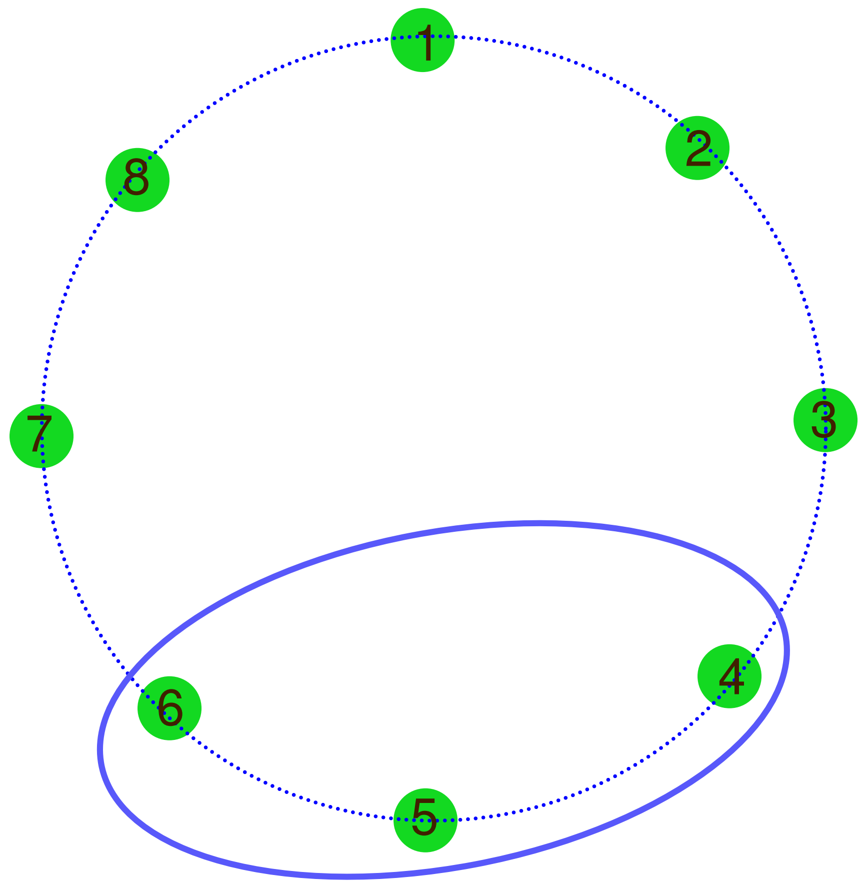

Figure 3.1. Ring Topology for a population of particles

(3.1.1) is the extended PSO equation :-

$$v_{ij}(t+1) = wv_{ij}(t) + c_1 r_1 \left(P_{ij} - x_{ij}(t)\right) + c_2 r_2 \left(P_{gj} - x_{ij}(t)\right) + c_3 r_3 \left(P_{lj} - x_{ij}(t)\right) \qquad (3.1.1)$$

r_1, r_2 and r_3 are numbers in the range [0, 1] generated from a uniform random number generator and are updated for each dimension in each iteration. w is the inertia weight parameter and is varied linearly down from $w_{max} = 0.5$ at the beginning of the run to $w_{min} = 0.0$ at the end of the run. The shorter range of w used here is to aid exploitation of the particles towards the end of the run.

The issue then arises as to how to assign the acceleration coefficients. (Jun-jie & Zhan-hong, 2005) chose various configurations in order to keep the sum of the acceleration coefficients equal to 4. This is in keeping with the original PSO where $c_1 = 2$ and $c_2 = 2$. In this study a dynamic approach has been used to select the acceleration coefficients for each particle and on every iteration. The simple heuristic that is followed is that a flexible PSO is desired to be able to deal with both multimodal and unimodal problems. The acceleration coefficient heuristic for d variables is represented as follows :-

```
for $i = 1:d$                                                    (3.1.2)
  if rand() < 0.333
        then  $c_{1i} = 2.0$, $c_{2i} = 0.0$, $c_{3i} = 0.0$
  elseif rand() > 0.666
        then  $c_{1i} = 0.0$, $c_{2i} = 2.0$, $c_{3i} = 0.0$
  else
        $c_{1i} = 1.333$, $c_{2i} = 1.333$, $c_{3i} = 1.333$
end
```

where rand() is a uniformly drawn random number in the range [0,1]. Hence each particle on each iteration has an equal probability of either acting as an individual hillclimber, a stochastic hillclimber or to use both cognitive and social information from the swarm. This makes the swarm as a whole much more flexible in being able to deal with an objective function, particularly if one does not have much idea of what the fitness landscape may look like.

The underlying motto behind this enhancement is "Big moves coupled with small moves". In the traditional inertia weight formulation, particles in the swarm are more likely to make big moves in the search space which progressively decreases with each iteration. Conceptually this leads to a big problem, in that a particle may be in a valley which contains the global minimum of the function, but because the particles are taking large steps, they can easily fly out of this region to a poorer region. However, if the swarm can be designed such that from outset, it does have the possibility of making small moves as well as big moves, this can greatly enhance its convergence and explorative ability.

There have been other techniques that have explored the same idea but with a different implementation. (Li et al, 2007) proposed a random velocity boundary condition on the swarm such that at each iteration, V_{max} was set randomly so that particles now had a higher probability of taking small moves early on in the run.

The next issue that arises in the implementation is how to deal with particles that go out of the boundary range. Figure 3.2 depicts different mechanisms that can be employed.

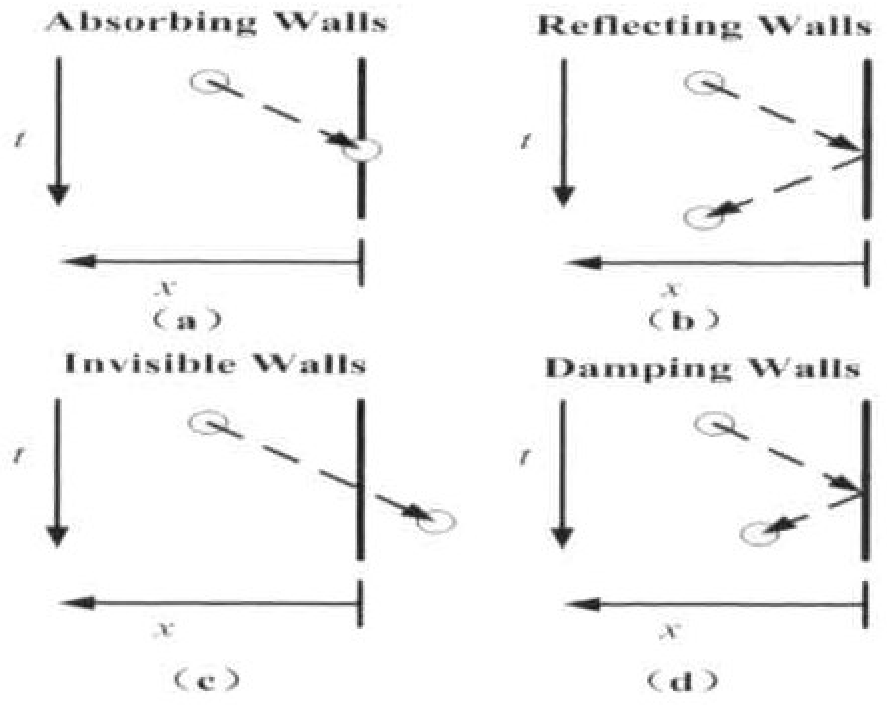

Figure 3.2. Boundary handling mechanisms

In Figure 3.2a, the boundary acts as an absorbing wall, effectively stopping the particle from going any further. This can be especially useful for those functions whose optimum is located at the boundary. In Figure 3.2b, the particle is reflected back into the search space by reversing its velocity after impact with the boundary wall. In Figure 3.2c the particle is allowed to escape the boundary but this particle is typically ignored when it comes to being function evaluated. Finally in Figure 3.2d the velocity is reversed and dampened when it impacts the boundary wall.

The damping wall boundary handling mechanism is chosen to be used in the Flexi-PSO. The absorbing walls mechanism does appear attractive at first glance particularly since functions can have their optimums on the boundary, however in practise it was found to lead to many redundant function evaluations. The problem arises that once the particle is stopped at the boundary, for it to get back into the search space can take many iterations since the sign of the velocity needs to be reversed. Reflecting walls were deemed to be inappropriate since the particle is reflected right back and this can equally lead to many redundant function evaluations if the optimum is near the boundaries. Invisible walls were not considered since a history match function evaluation is desired for every iteration and it would be a waste of the distributed computing resources to subtract a function evaluation on an iteration. Damping walls is the most attractive option since function evaluations are not wasted, and at the same time the particle can move progressively closer to the boundary if indeed the optimum is located close to it.

3-Dimensional animations over a benchmark function presented later in this paper are used to give a qualitative understanding of the behaviour of the swarm. It was found that while the acceleration coefficient heuristic did allow particles some degree of freedom, at the end of the run they still tended to congregate very closely around the *gbest* and lacked the desired explorative ability. This was wasteful as often the particles congregated around the *gbest* early on in the run with the result that the particles had very small velocities and from that point onward were only performing local exploitation with little improvement in the *gbest*. This is an intrinsic drawback of the particle swarm method as the entire swarm surrounds an attractor and cannot break free from it to search a wider area. If w were varied from $w_{max} = 0.9$ to $w_{min} = 0.4$ then the particles tend to flicker around the *gbest* with little ability to fine tune the search as also noted by (Vesterstroem et al, 2002).

This premature convergence problem was addressed using the following heuristics. One half of the population should be allowed to perform local exploitation (denoted as "exploitation" particles) while the other half (denoted as "exploration" particles) should be repelled from *gbest* if they came too close to it. As a measure of "closeness" to the *gbest*, the repulsion is induced in two ways. If an exploration particle comes to within a fitness tolerance or a distance tolerance of the *gbest*, then a perturbation to a randomly selected dimension of the velocity vector is added. The fitness repulsion is invoked when the difference between fitness of the exploratory and gbest particles is less than a fitness tolerance ε viz.

$$\left| f_i - f_{gbest} \right| \le \varepsilon \qquad (3.1.3)$$

The distance repulsion is invoked when the normalised absolute difference between the exploratory and *gbest* particles in all dimensions is less than a threshold of the search range viz.

$$\frac{\left| X_j - P_{g,j} \right|}{X_{j,\max} - X_{j,\min}} \le \alpha, \quad j \in [1,d] \qquad (3.1.4)$$

Once a repulsion is invoked for an exploration particle, the velocity is perturbed in a randomly selected dimension and is represented in equation (3.1.5):

$$v_{ij}(t+1) = r_4 \frac{V_{\max}}{2} \qquad (3.1.5)$$

where r_4 is a random number drawn uniformly in the range [-1,1]. Qualitative animations using this concept of exploration and exploitation particles showed “atomic-like” behaviour, similar to what was observed by (Blackwell and Branke, 2004). This “atomic-like” behaviour is explained by the observation that whenever an exploration particle came too close to the *gbest* it was repelled outwards only for it to be attracted back to the *gbest* where it was once again repelled outwards. However this repulsion often enables particles to find better solutions. The repulsion step size is set proportional to half of V_{max}. If there is some idea as to how far apart the optima are expected to be on the fitness landscape then this step size can be set accordingly. The exploitation particles on the other hand close in on the *gbest* and try to improve it by doing a fine local search. If an exploration particle finds a better *gbest*, then the rest of the swarm moves towards this new position and the process continues until the termination criterion is met. Figure 3.3 displays the pseudo-code for the entire procedure.

```
Begin
  initialize the population
  initialize the velocities
  evaluate fitness of all particles
  set current position as pbest, set particle with best fitness as gbest and find
  the neighbourhood lbests
    While  iter < total_iterations
              update inertia weight factor (2.3.4)
              set acceleration constants with (2.4.2)
                For i = 1 to population
                  update fitness distance (fd) and variable difference (vd) using
                  (2.4.3) and (2.4.4) respectively
                    If  fd > $\varepsilon$ |  fd = 0 | vd > $\alpha$ | $i \leq \frac{population}{2}$
                      For j = 1 to dimensions
                           update velocities (2.4.1)
                           check velocity magnitudes with (2.3.2)
                      EndFor j
                    Else
                      reset acceleration constants
                      pick = $\lceil$rand().dimensions$\rceil$   // $\lceil\rceil$ is the ceiling operator
                      For j = 1:dimensions
                        If j $\neq$ pick
                           update velocities with (2.4.1)
                    Else
                        update velocities with (2.4.5)
                        check velocity magnitudes with (2.3.2)
                     EndIf
                EndFor j
            EndIf
        EndFor i
        update positions with (2.3.3)
        evaluate fitness of all particles
        update pbest, gbest and lbest if necessary
    EndWhile
End
```

Figure 3.3. Pseudo-code for the Flexi-PSO

3.2. Qualitative Behaviour of the PSO

In order to gain a greater understanding of the behaviour of the swarm, some qualitative analysis from experiments is necessary. To this end 3-dimensional animations have been set up for the following function (3.2.1) {same as (2.5.1) presented earlier & will red thread its way through this thesis} :-

$$f(x) = x_1^2 + 2x_2^2 - 0.3\cos(3\pi x_1) - 0.4\cos(4\pi x_2) + 0.7 \tag{3.2.1}$$

This is a highly multimodal function with many local minima and is depicted in Figure 3.4.

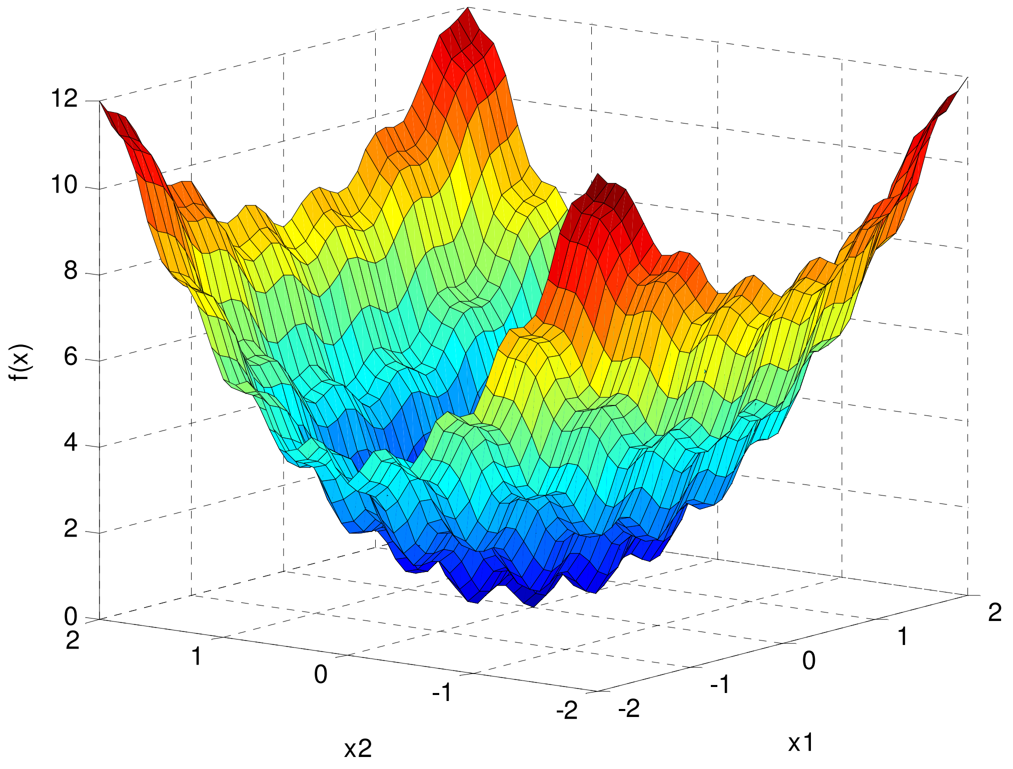

Figure 3.4. 3-D plot of multimodal Equation (3.2.1)

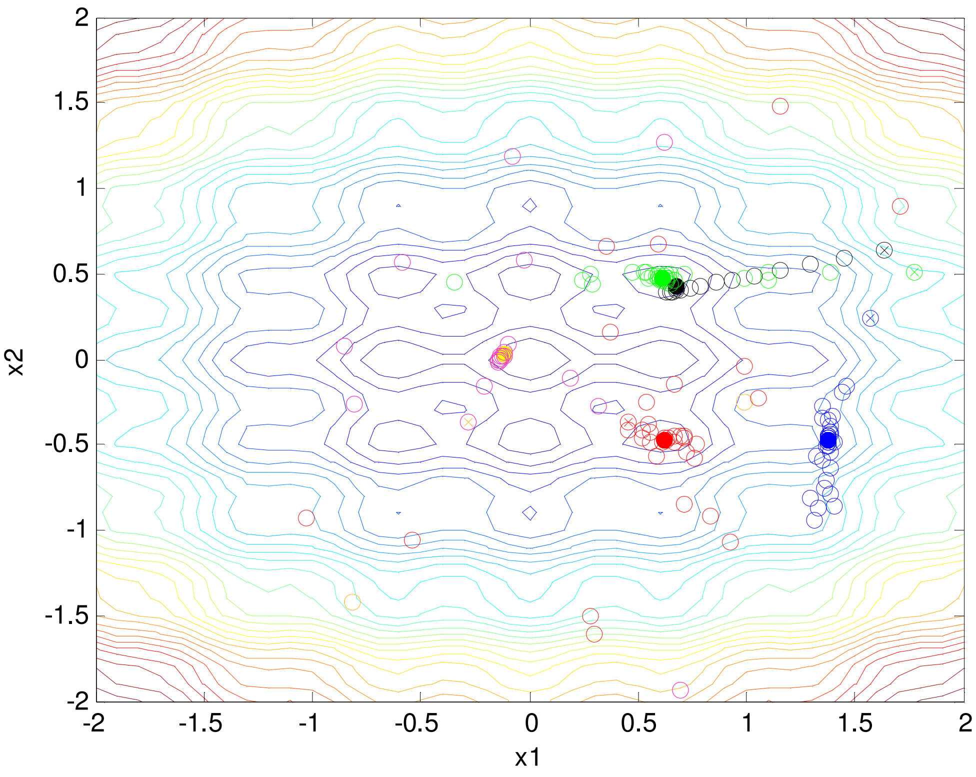

Figure 3.5. Cognition only inertia weight PSO

Figure 3.5 shows the behaviour of the cognition only particle swarm. This is the variation proposed by (Kennedy, 1997) and is essentially a local search. The particles in red are the initial population positions. It can clearly be seen that the global optimum has not been found but that each particle converges to its best found position. If a particles initial velocity is large, it can climb over the nearest hills to another area of the search space, but if it cannot improve upon its best position then it is attracted back to its best position. This makes the cognition only variation of the particle swarm an individual hill climber. This is however very useful and was used in the development of the Flexi-PSO, represented as heuristic (3.1.2). Convergence is achieved much quicker by allowing each particle to randomly use the cognition only variation.

Figure 3.6 and Figure 3.7 are contour plots of this function upon which the history of a swarm run using the Inertia Weight PSO and Flexi-PSO are superimposed respectively. Each run comprised of 10 particles and 100 iterations. The red circles in both figures are the initial population positions. In Figure 3.6 the population is deliberately initialised away from the global optimum and in a small volume of the search space yet the swarm is still able to migrate its way to the global optimum. The efficiency of the Flexi-PSO algorithm (Figure 3.7) is clear as there is a dense cluster of particles searching the niche with the global optimum and a sparse search away from this niche. Other nearby niches have also been searched. This is especially important in history matching due to the expensive computational time for each function evaluation and it is along these lines that further development of the algorithm has been carried out. In contrast the traditional inertia weight PSO (Figure 3.6) converges much slower to the global optimum.

In Figure 3.7 the Flexi-PSO exhibits repulsion along the principal axis as equation (3.1.5) is invoked for a single dimension only. For rotated functions, the repulsion can be invoked in multiple dimensions.

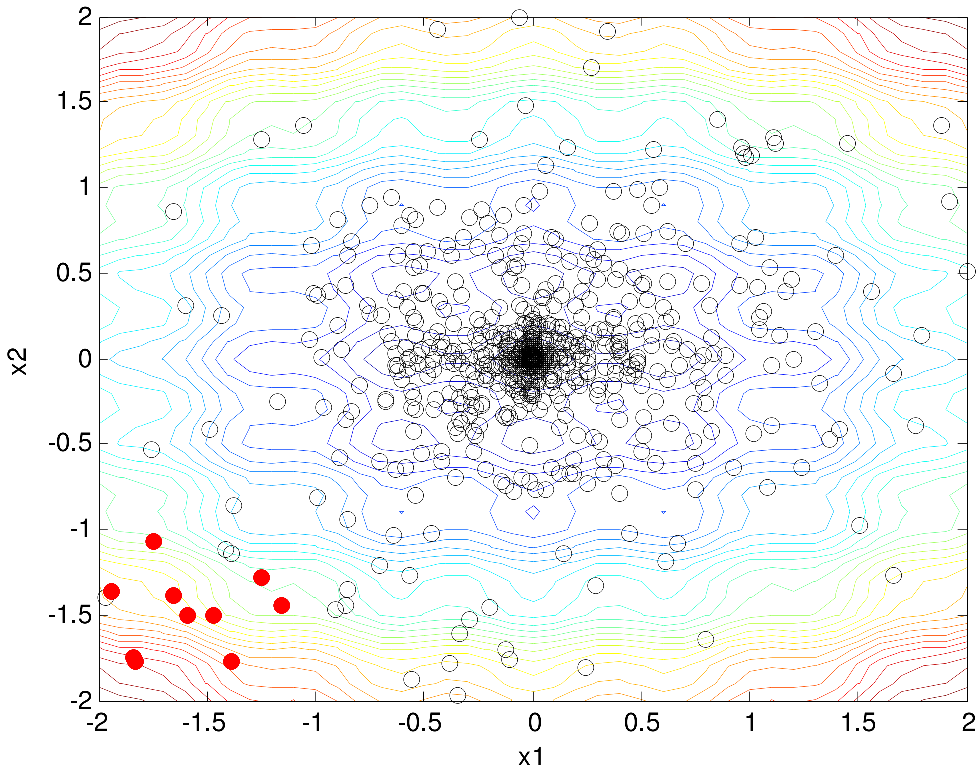

Figure 3.6. Inertia Weight PSO search of Equation (3.2.1)

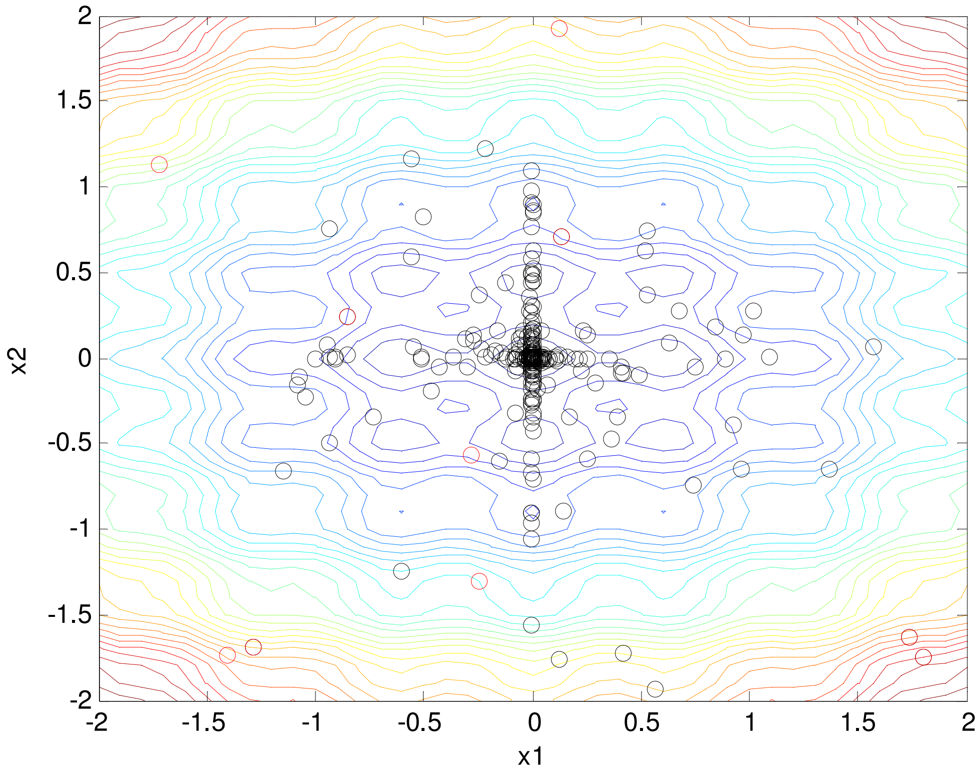

Figure 3.7. Flexi-PSO search of Equation (3.2.1)

(Vesterstroem et al, 2002) proposed a diversity metric in order to measure the convergence behaviour of the swarm. This metric is simply a summed average distance measure of each particle from the mean position of the swarm given in (3.2.2) where *n* is the number of particles and *d* the number of dimensions :-

$$diversity = \frac{1}{n}\sum_{i=1}^{n}\sqrt{\sum_{j=1}^{d}\left(x_{ij} - \bar{x}_j\right)^2} \qquad (3.2.2)$$

This metric is independent of the shape of the objective function, and is a qualitative indicator of the behaviour of the swarm. Figure 3.8 is an illustration of the diversity of the traditional inertia weight PSO versus the Flexi-PSO.

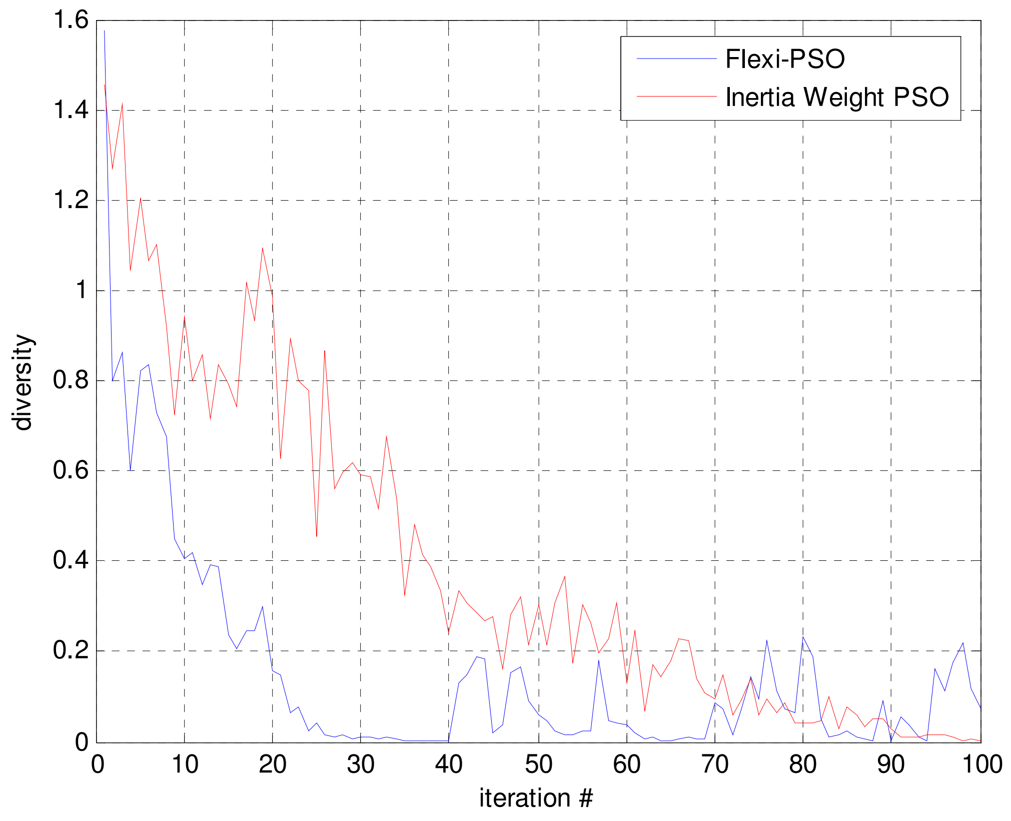

Figure 3.8. Diversity metric of the swarm history

It can be immediately seen that the Flexi-PSO converges quicker than the traditional inertia weight formulation but that it also maintains a level of diversity at later iterations by repulsion of the exploration particles thus enabling the Flexi-PSO to escape local minima more easily. These are key elements for history matching as we do want to get to a match as quick as possible but be flexible enough to move on searching for other suitable matches as well. This is further illustrated in the velocity profiles of both methods in Figure 3.9 of variable x_1.

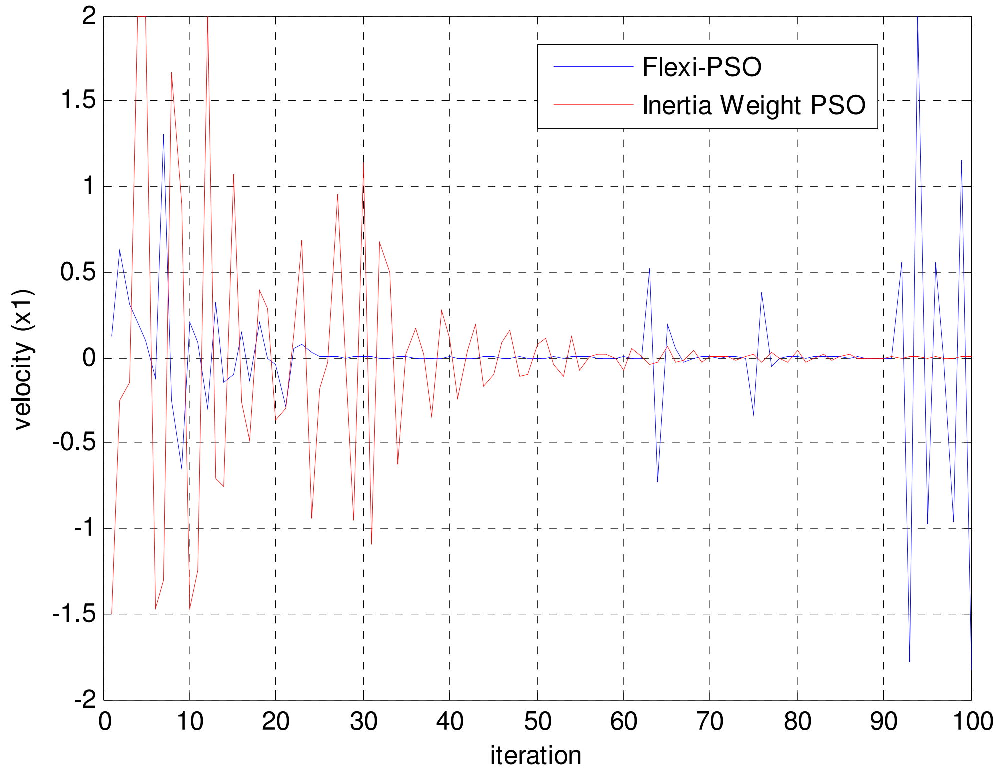

Figure 3.9. Velocity profile of variable x_1

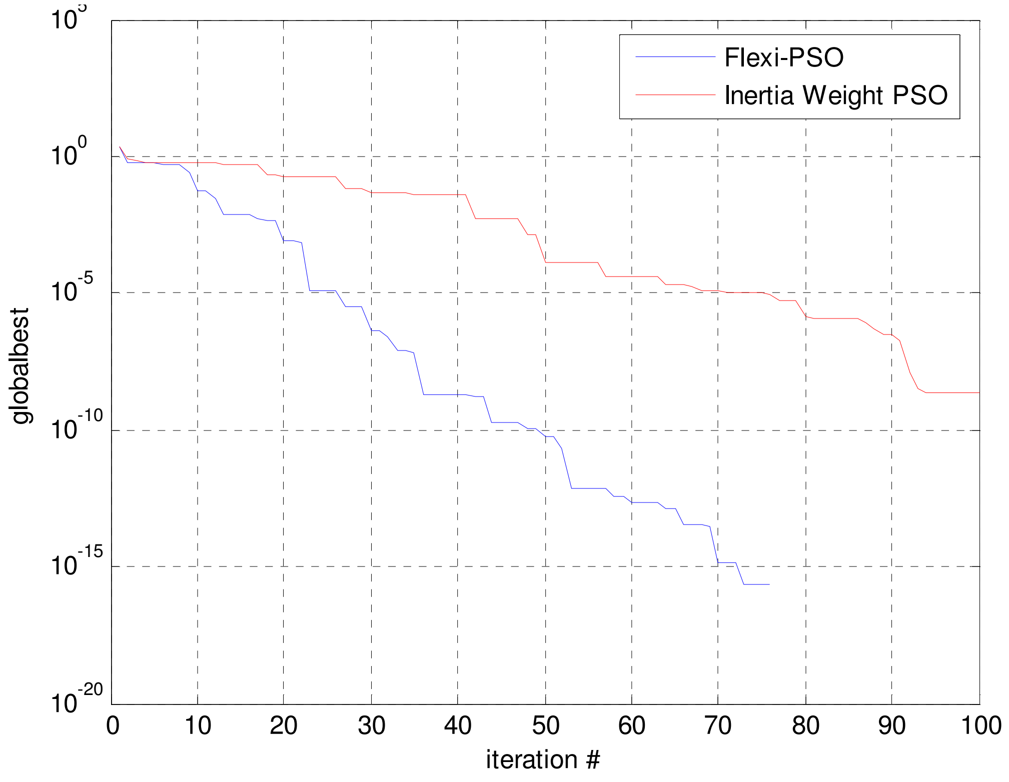

Figure 3.10. Global best value history

Figure 3.10 also shows that Flexi-PSO reaches the true global optimum faster than the inertia weight method, once again due to the modifications made to it. The Flexi-PSO appears to halt at around iteration 75 however this is just due to the precision of MATLAB® being reached.

3.3. Sequential Niching

The Flexi-PSO does have the ability to escape local minima more easily than traditional PSO formulations, however the goal of this thesis is to develop an algorithm for history matching that would be able to find multiple niches to be used in uncertainty modelling. To this end niching variations of the PSO have been investigated.

Two variations of niching algorithms exist viz. parallel and sequential niching. Parallel niching seeks to locate and maintain several niches in a population simultaneously and the fitness landscape is not modified in doing so. The challenge is in finding a good measure to locate possible solutions and to organise individuals in the population around solutions. Sequential niching methods on the other hand successively locate and isolate niches such that future searches do not duplicate sampling in niches that have already been identified, usually by modifying the fitness landscape around the niche.

There have been many studies on niching using genetic algorithms but very little using particle swarms. Fitness sharing and deterministic crowding are popular techniques employed in genetic algorithms for locating multiple optima. A seminal paper on sequential niching using fitness sharing GA's is by (Beasley et al, 1993). In this paper, fitness sharing was used to locate niches, and derating functions applied to modify the fitness function within the niche radius. Fitness sharing was introduced by (Goldberg, 1987) and is a technique that modifies the fitness landscape by lowering an individual's fitness by an amount nearly equal to the number of individuals within the same niche.

The primary drawback to this approach is that the niche radius calculation requires prior knowledge of the number of optima in the fitness function. This is something that clearly cannot be used in history matching or when working with "black boxes" as the number of optima are unknown. Nevertheless this paper did highlight key elements in sequential niching viz. selection of an appropriate derating function such that false optima are not created (mexican hat effect) and estimation of the niche radius. Deterministic crowding is another method introduced by (Mahfoud, 1995) that uses competition between parents and children in the same niche. Essentially after crossover and mutation, each child replaces its nearest parent if it has a better fitness.

There have been a few attempts at using particle swarms to find multiple niches. (Engelbrecht, 2005) argued that the *gbest* PSO was incapable of niching while the *lbest* PSO was inefficient. Nevertheless there have been studies on modifying the basic algorithm that have achieved some success. (Kennedy, 2000) used a clustering technique that assigns each particle to a cluster and substitutes the cluster centre for the particle's personal best. Although a niche radius is not employed in this approach, it is necessary to set the number of clusters before hand, which can be difficult to estimate for different functions particularly "black boxes". (Brits et al, 2002) proposed a cognition only model that iterates and when there is little improvement, a sub-swarm is created around the particle in a small area to further refine the search. The algorithm is however dependent on proper initial distribution of the particles, something which cannot be guaranteed for complex functions.

(Zhang et al, 2005) attempted using the concepts in fitness sharing GA's to train multiple sub-swarms by employing a power law derating function and calculating the niche radius from a prior knowledge of the fitness landscape. They do however introduce an interesting concept of convergence similar to the diversity metric used by (Vesterstroem et al, 2002) to stop the training of each sub-swarm.

(Vaz & Fernandes, 2005) used the inertia weight PSO in conjunction with an approximate descent direction to enable the computation of multiple niches. This is an interesting approach though somewhat computationally expensive since gradients need to be calculated for each particle at each iteration, and would not be appropriate for functions with discrete variables.

(Zhang et al, 2006) proposed one of the most rigorous methods of sequential niching in particle swarms with the only drawback being the computational expense of additional function evaluations to estimate the niche radius. They successively train sub-swarms to find new niches by isolating old niches using the hill valley function approach which continuously moves in each dimension taking interior sample points until the monotonic change in the fitness stops. This is very well suited to mathematical functions but not expensive function evaluations.

Since run times in reservoir simulation models can be quite long, and the simulator is a "black box" many of these approaches would not be suitable. In niching the primary elements are choice of a suitable derating function to steer the algorithm away from previously identifies niches and estimation of the niche radius. The approach taken in this thesis is not to use a derating function due to the computational expense. Instead any particle falling within a previously identified niche is not evaluated but accelerated out of that niche instead. It is difficult to address the second problem of choosing a niche radius as each simulation model is going to have a completely different fitness landscape and hence we are left with either trying to rigorously evaluate the niche radius by making many more function evaluations or empirically set the niche radius beforehand and live with a certain amount of inefficiency.

In this study, neural networks were used to train the sampled points once there was less than a 2% improvement in the globalbest over the last 5 iterations. Once the neural network was trained, it was then interrogated in both directions of each dimension to estimate the niche radius, however this was found to be ineffective due to the scarcity of sample points. This becomes a contradictory problem since niches need to be identified with the fewest of function evaluations whereas neural networks being proxy models require large amounts of data to be trained with to be effective and this line of work was abandoned.

The niche radius is now taken as a user defined limit and in this study is set to 10% of the dimensional range of each variable. This radius is purely up to the user to define as the niche radius will vary within each function, vary with different objective functions and for different problem setups, hence there is no further sensitivity study on this parameter in this thesis. Figure 3.11 shows the effect of adding this to the Flexi-PSO.

The lowest valleys are extensively sampled by the swarm using the same number of function evaluations as in the previous cases. Once there is no user specified threshold improvement within a user specified number of iterations, the global best position is cordoned off by the niche radius and the swarm is reinitialised randomly ensuring that no particle is reinitialised in the cordoned off area. To preserve useful information that the swarm already has, the global best on re-initialisation is set to the best position visited by the swarm that is not in the niche cordoned area. Figure 3.12 shows the pseudo-code for this procedure.

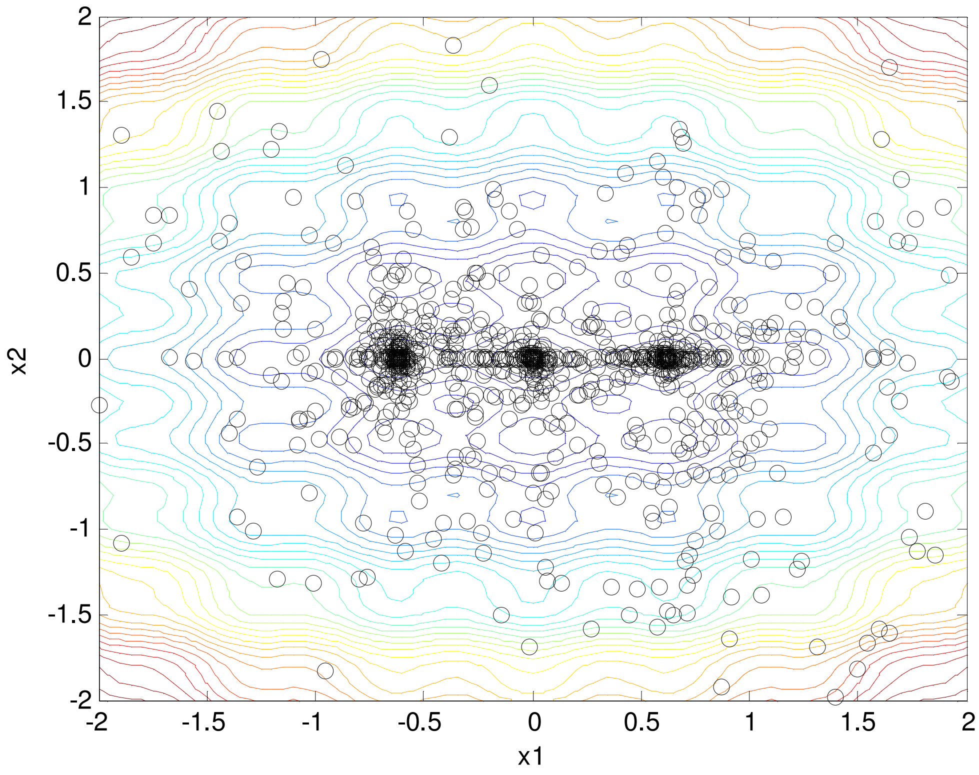

Figure 3.11. Sequential Niching Flexi-PSO search of Equation (3.2.1)

Figure 3.12 displays the pseudo-code for the Sequential Niching Flexi-PSO.

```
Begin
  initialize the population
  initialize the velocities
  evaluate fitness of all particles
  set current position as pbest, set particle with best fitness as gbest and find
  the neighbourhood lbests
    While  iter < total_iterations
            update inertia weight factor (2.3.4)
            set acceleration constants with (2.4.2)
              For i = 1 to population
                update fitness distance (fd) and variable difference (vd) using
                (2.4.3) and (2.4.4) respectively
                  If  fd > $\varepsilon$ |  fd = 0 | vd > $\alpha$ | $i \leq \frac{population}{2}$
                    For j = 1 to dimensions
                        update velocities (2.4.1)
                        check velocity magnitudes with (2.3.2)
                    EndFor j
                  Else
                    reset acceleration constants
                    pick = $\lceil$rand().dimensions$\rceil$   //  $\lceil\rceil$  is the ceiling operator
                    For j = 1:dimensions
                      If j $\neq$ pick
                        update velocities with (2.4.1)
                    Else
                       update velocities with (2.4.5)
                       check velocity magnitudes with (2.3.2)
                     EndIf
                 EndFor j
             EndIf
        EndFor i
        update positions with (2.3.3)
        For I = 1 to population
             While (niches > 0 & particle lies within any niche)
                  Reinitialise particle randomly
             EndWhile
        EndFor
        evaluate fitness of all particles
        update pbest, gbest and lbest if necessary
        if |gbest(iter) – gbest(iter-user_iter)| < tolerance
             set niche boundary = gbest ± niche_radius
             reinitialise population
             reinitialise velocities
             set gbest = best position found outside niche boundary
    EndWhile
End
```

Figure 3.12. Pseudo-code for the Sequential Niching Flexi-PSO

3.4. Function Stretching

Function Stretching is a technique that can be used to find multiple minima. (Parsopoulos et al, 2004) proposed a two-phase transformation of the objective function once a detected minimum has been found. The first phase stretches the objective function upwards eliminating all minima with values higher than the detected minimum. In the next stage, the detected minimum is turned into a maximum whilst still leaving all minima with objective function values lower than the detected minimum unaltered.

Let x^* be a minimiser of an objective function *f.* The stretching is defined as :-

$$G(x) = f(x) + \gamma_1 \|x - x^*\| (sign(f(x) - f(x^*)) + 1) \tag{3.4.1}$$

$$H(x) = G(x) + \gamma_2 \frac{sign(f(x) - f(x^*)) + 1}{\tanh(\mu(G(x) - G(x^*)))} \tag{3.4.2}$$

where γ_1 = 5000, γ_2 = 0.5 and μ = 10e^{-10} are arbitrary parameters. The following function is used to evaluate whether this transformation process can be useful in the history matching process.

$$y = \sin(x) + x.\cos(x) + 10 \tag{3.4.3}$$

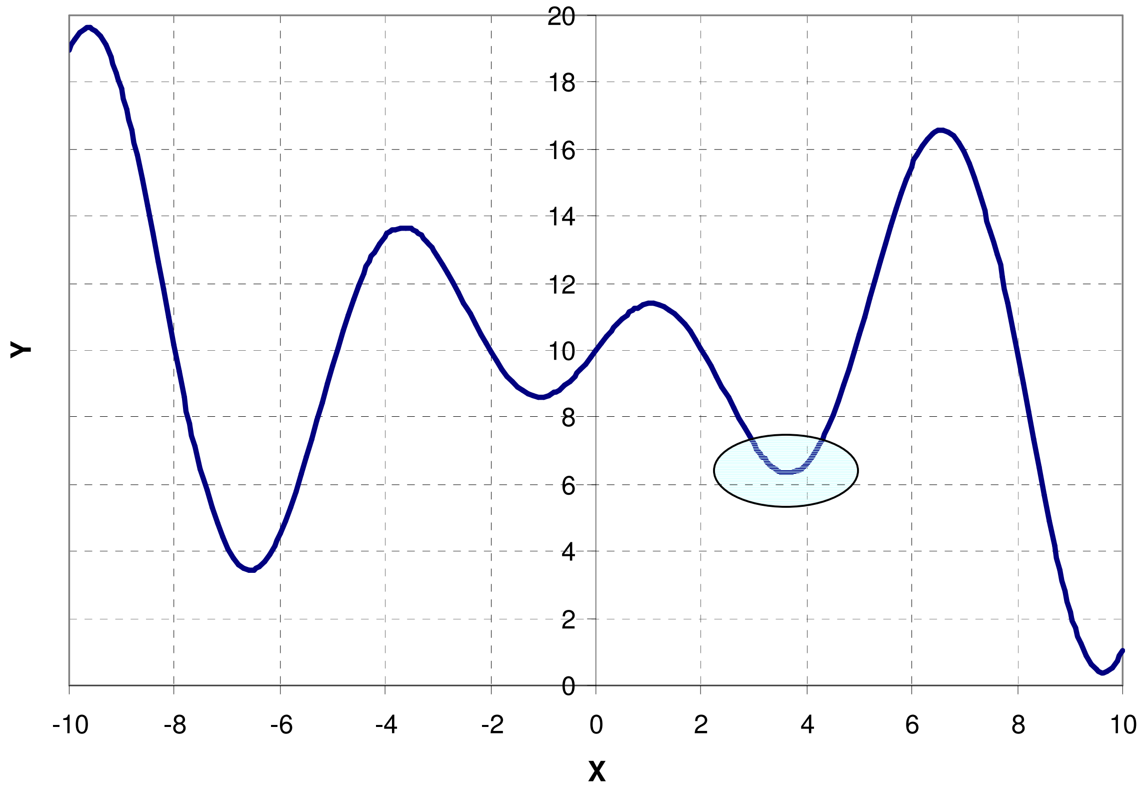

Figure 3.13. Plot of (3.4.3)

Figure 3.13 illustrates (3.4.3). This function is then taken through the two-stage transformation process and is depicted in Figure 3.14. The local minimum used is $x^* = 3.68$ (highlighted in Figure 3.12). G stretches the function upwards and H has turned this local minimum into a maximum whilst leaving everything lower than $f(x^*) = 6.328$ intact. This appears to be a promising technique that can be used in conjunction with the PSO however, if the first detected minimum is indeed the global minimum, then no other minima will be detectable thereafter and the algorithm will have to be rerun, albeit you are better off since the global minimum is now known.

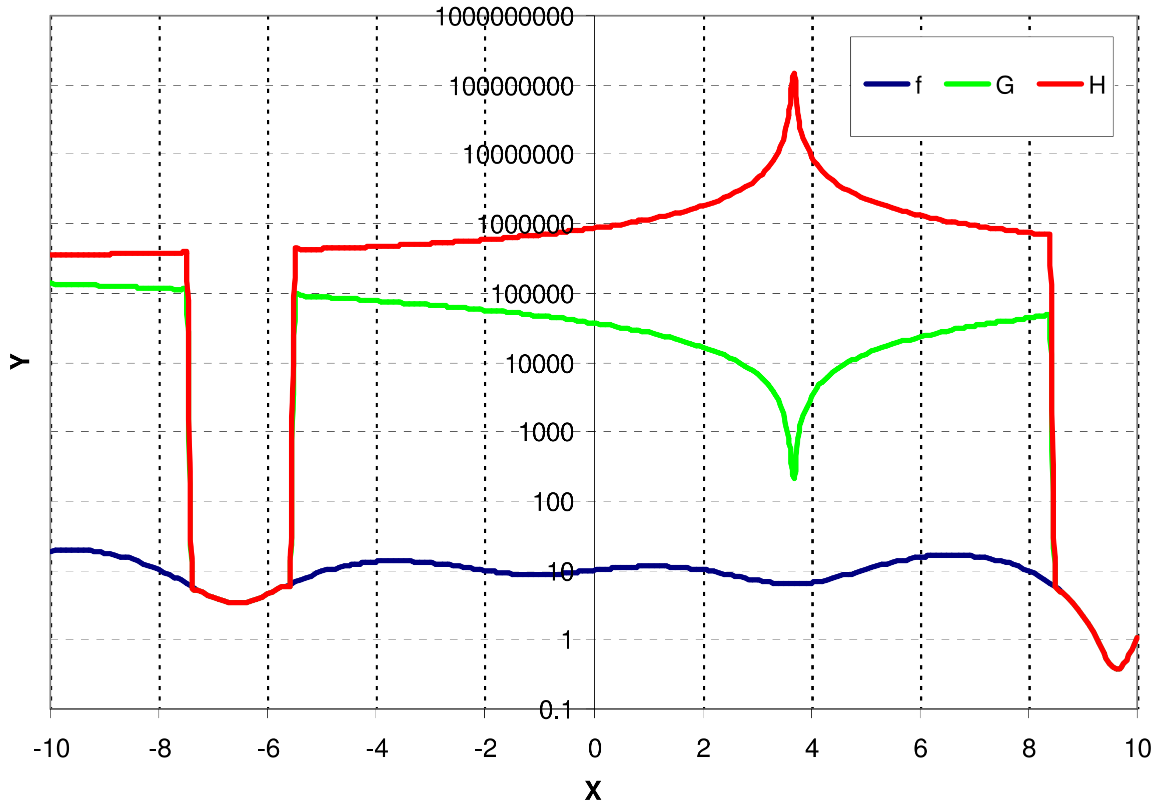

Figure 3.14. Function Stretched depiction of minimum @ x^* = 3.68

Figure 3.15 shows the effect of the stretching transformation on the global minimum at $x^* = 9.61$. In a way, one would actually hope that the first minimum that is found is not the global minimum with this technique, but it does lend itself to the Flexi-PSO since the Flexi-PSO has the ability to take small steps and hence find a local minimum quicker than its counterparts. Testing this technique on a local minimum ($x^* = [-0.6\ -0.5]$, $f(x)^* = 0.9127$) gives the transformed fitness landscape in Figure 3.16. Figure 3.17 then shows the globalbest progression when the Flexi-PSO is run on this transformed function.

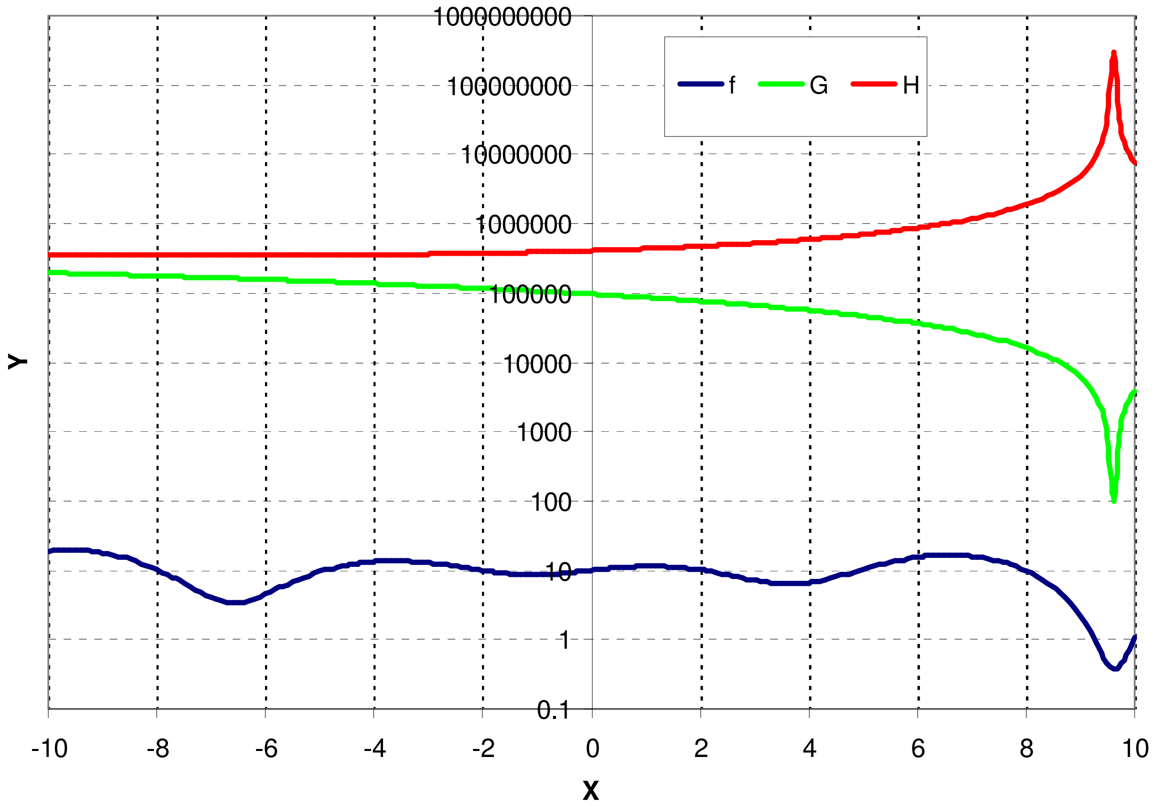

Figure 3.15. Function Stretched depiction of global minimum @ $x^* = 9.61$

The Flexi-PSO is not initialised anywhere in the area of the hollows of Figure 3.15, since the initial globalbest value is in the region of 10^5, and the Flexi-PSO is still able to make its way into the hollows of the transformation and find the global optimum. This technique looks promising and will be attempted when history matching the case studies presented later in this thesis.

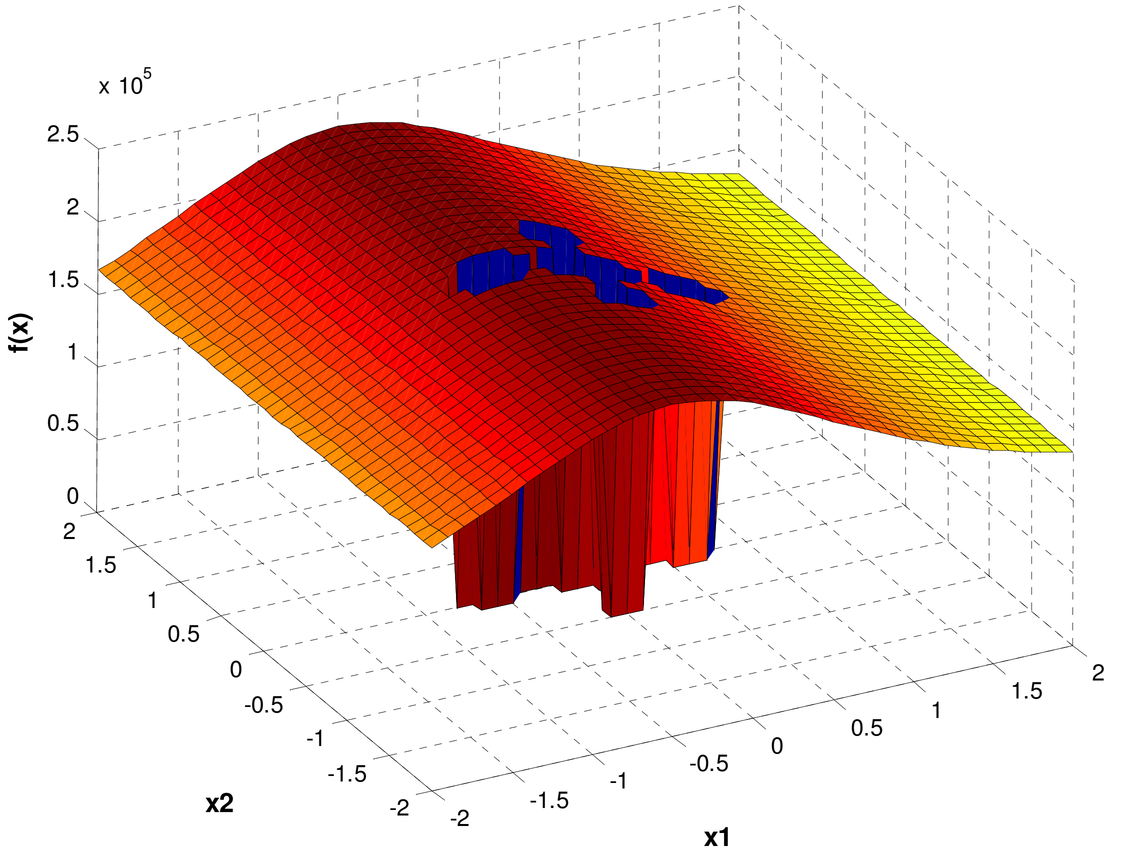

Figure 3.16. Function Stretched depiction of local minimum @ x^* = [-0.6 –0.5] on (3.2.1)

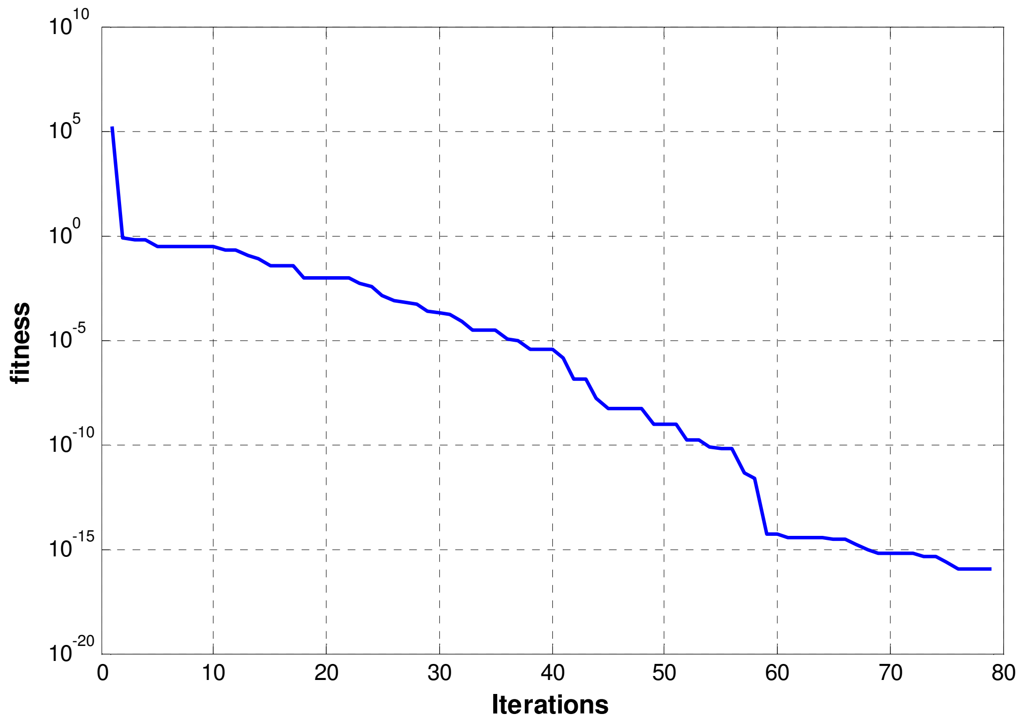

Figure 3.17. Flexi-PSO performance on the function stretched transformation of (3.2.1)

3.5. Handling Mixed Integer Problems

Another area of particular importance in history matching is mixed integers. Mixed integer problems are where you have both discrete variables and continuous variables simultaneously in the problem formalisation. This is relevant to history matching as the most common approach has been to use a single static model and deterministically find a suitable history match, but this approach was largely due to a lack of computing power. With widely available distributed computing resources and reservoir simulators that can decompose the grid and run the sub-grids in parallel over multiple processors, past limitations are no longer that critical. This opens the way for wider uncertainty handling by using multiple static models either based on different grids, geological models or property realisations. Hence when the assisted history match is launched, the Flexi-PSO will sample from the available static models (discrete variable/s) and fluid/rock parameters (continuous variables) simultaneously and gravitate towards the static model/s that give the best performance on the objective function.

This turns the history match problem from being solely in the continuous domain to the mixed integer domain. In our case it is unlikely that binary integer problems arise, but it is more of a case where an integer variable can take on a number of discrete values e.g. realisation 1, realisation 2 etc. There have been quite a few attempts at mixed integer problems using particle swarms of which a few will be mentioned. (Gaing, 2005) used a simple rounding off method in the velocity updates for the discrete variables. Hence (3.1.1) would be rounded off to give a discrete value that would then be used in the position update. (Rongshan & Xia, 2007) proposed using the sigmoid function (commonly used as transfer functions in neural networks) to deal with binary integer problems. The updated velocity is used as the sigmoid function argument and the position is updated as zero if the sigmoid function result is less than a uniform random value within [0,1] and 1 otherwise. (Kitayama & Masuda, 2006) developed a penalty function approach to handling discrete variables. In the velocity updates all variables are treated as continuous but the fitness function is augmented with a penalty if the continuous equivalent of the discrete variables departs from discrete values.

In this study a simple round-down approach to each discrete variable is taken, where the discrete variable represented in the swarm is just the index to the actual underlying variable value. This is by far the simplest approach to mixed integer problems and is used in a mathematical benchmark function test in the next chapter to test its effectiveness. (3.5.1) formalises this representation for tubing sizes :-

Actual size (ID) ： [1.867”, 2.259”, 2.323”, 2.441”, 3.068”]

PSO index ： $X = [1, 2, 3, 4, 5]$

PSO update (2.3.3) ： $x = 1.45 \rightarrow X = \mathrm{floor}(x) = 1$ (3.5.1)

Function evaluation ： $f(X) = f(1.867”)$

Chapter 4

Mathematical Testing of the Flexi-PSO

4.1. CEC 2005 benchmark test set

There have been many optimisation methods proposed over the years for history matching but there has been no qualitative way of judging their effectiveness in relation to other each other, except for those that have used a common benchmark test model like the Imperial College Fault model. In this study 25 non-linear functions have been used as an experiment to gauge how well the Flexi-PSO can deal with unimodal and highly multimodal functions. The test set is developed by (Suganthan et al., 2005) for the 2005 Congress on Evolutionary Computation Special Session on Real Parameter Optimisation. This test set in particular is good to assess bias in algorithms as many functions are shifted and rotated. Details of these functions can be found in Appendix A.

Some functions are asymmetrically initialised to assess the robustness of the algorithm. When the PSO was first introduced, symmetric initialisation was common where the initial population was uniformly distributed in the entire search space. (Angeline, 1998) suggested initialising the population asymmetrically, where the population is initialised in only a portion of the search space and away from the global optimum.

Each function was run twenty five times so as to obtain a mean fitness value and standard deviation, and each run used a different seed for the random number generator hence each population initialisation was different. All the runs were conducted in 10 dimensions, using a population size of 20 particles for 500 iterations resulting in 10 000 function evaluations per trial. A comparison is made with another PSO paper presented by (Liang & Suganthan, 2005) in which a dynamic multi-swarm inertia weight method is combined with a quasi-Newton search method to improve local optimisation. In order to maintain parity, the Flexi-PSO is combined with the quasi-Newton (Fletcher, 1970) option FMINUNC within MATLAB®. The Flexi-PSO uses the first 9500 function evaluations whilst the last 500 function evaluations use the FMINUNC function. Figure 4.1 and Table 4.1 displays the comparison of the mean values achieved between these two methods in addition to a differential evolution (Tasgetiren et al, 2005) and memetic algorithm (Molina et al, 2005) presented at the conference. (Tasgetiren et al, 2005) present results for only the first 14 functions.

The first five functions are unimodal functions; function 1 is the Shifted Sphere Function, function 2 the Shifted Schwefel's problem 1.2, and function

3 the Shifted Rotated High Conditioned Elliptic function. These three functions have different condition numbers leaving them in increasing order of difficulty respectively. The condition number associated with a problem is a measure of that problem's amenability to digital computation, that is, how numerically well-conditioned the problem is. A better result is achieved for function 1 than function 2 which in turn is better than function 3. Function 4 is shifted Schwefel's problem 1.2 with noise in fitness which makes the search process much more difficult. The Flexi-PSO does show good performance on this function relative to the other techniques but is still far from the optimum.

Function 5 is Schwefel's problem 2.6 with the global optimum on the bounds. For 10-*D,* 3 dimensions are on the low bounds, 3 dimensions on the high bounds and other 4 dimensions randomly distributed in the search range. The Flexi-PSO does not perform very well on this problem mainly due to the fact when a particle goes out of the search space it is damped back in the search space rather than limiting the position to the boundary. In practice this can be problematic with particle swarms as it can take many iterations for the particle to move back into the search space if it is stopped at the boundary and many function evaluations are wasted during this time.

Functions 6-25 are multimodal problems. Function 6 is the Shifted Rosenbrock's Function, a problem between unimodal and multimodal and an algorithm with good local search ability can achieve good results on Rosenbrock's Function. The Flexi-PSO achieves a good comparable performance. Function 7 is the Shifted Rotated Griewank function without bounds, only the initialization range is given and the search range is $[-\infty,+\infty]$. Griewank's function is more difficult with decreasing dimension and it is difficult to achieve the global optimum. The Flexi-PSO performs relatively well on this function. Function 8 is the Shifted Rotated Ackley function with global optimum on bounds, which has a very narrow global basin and half the dimensions of this basin are on the bounds. This is akin to finding a needle in a haystack and the Flexi-PSO is not able to find the minimum on any run.

Functions 9 and 10 are shifted Rastrigin's function and shifted rotated Rastrigin's function respectively, both of which have a huge number of local optima. The Flexi-PSO performs well on all 25 runs for function 9, but the results are poorer for function 10 owing to the rotation. Function 11 is the Shifted Rotated Weierstrass function and the poor results that the Flexi-PSO achieves is due to the complexity of this function. Function 12 is Schwefel's problem and for the 100 000 feval case, the optimum is found more than half the time but when it fails to locate the optimum region, it results in a solution with a poor fitness. Functions 13 and 14 are expanded functions on which the Flexi-PSO performs relatively well, while functions 15-25 are eleven novel composition functions. They are composed of basic functions and are extremely challenging to any search algorithm. The Flexi-PSO performs poorly on all these functions but as can be seen from Figure 4.1 and Table 4.1, to be relatively the same as the other algorithms.

The Flexi-PSO compares well with other methodologies and gives confidence for further use. Figure 4.2 and Table 4.2 compare the performance on the same function set but this time in 30 dimensions and for 100 000 function evaluations. The population size is increased to 40 particles for this test and the results are once again averaged over twenty five runs. The Flexi-PSO is compared to a Flexible Evolutionary Algorithm (Alonso et al, 2005), Real Coded Memetic Algorithm (Molina et al, 2005) and a steady state Real Parameter Genetic Algorithm (Ballester et al, 2005).

It is evident from Table 4.2 that the Flexi-PSO outperforms the other techniques on most of the functions underlining its scalability to higher dimensions. One reason for this is that the Flexi-PSO maintains explorative capability through the exploration particles even when the exploitative particles begin to converge, hence the swarm as a whole can continually search the dynamic range.

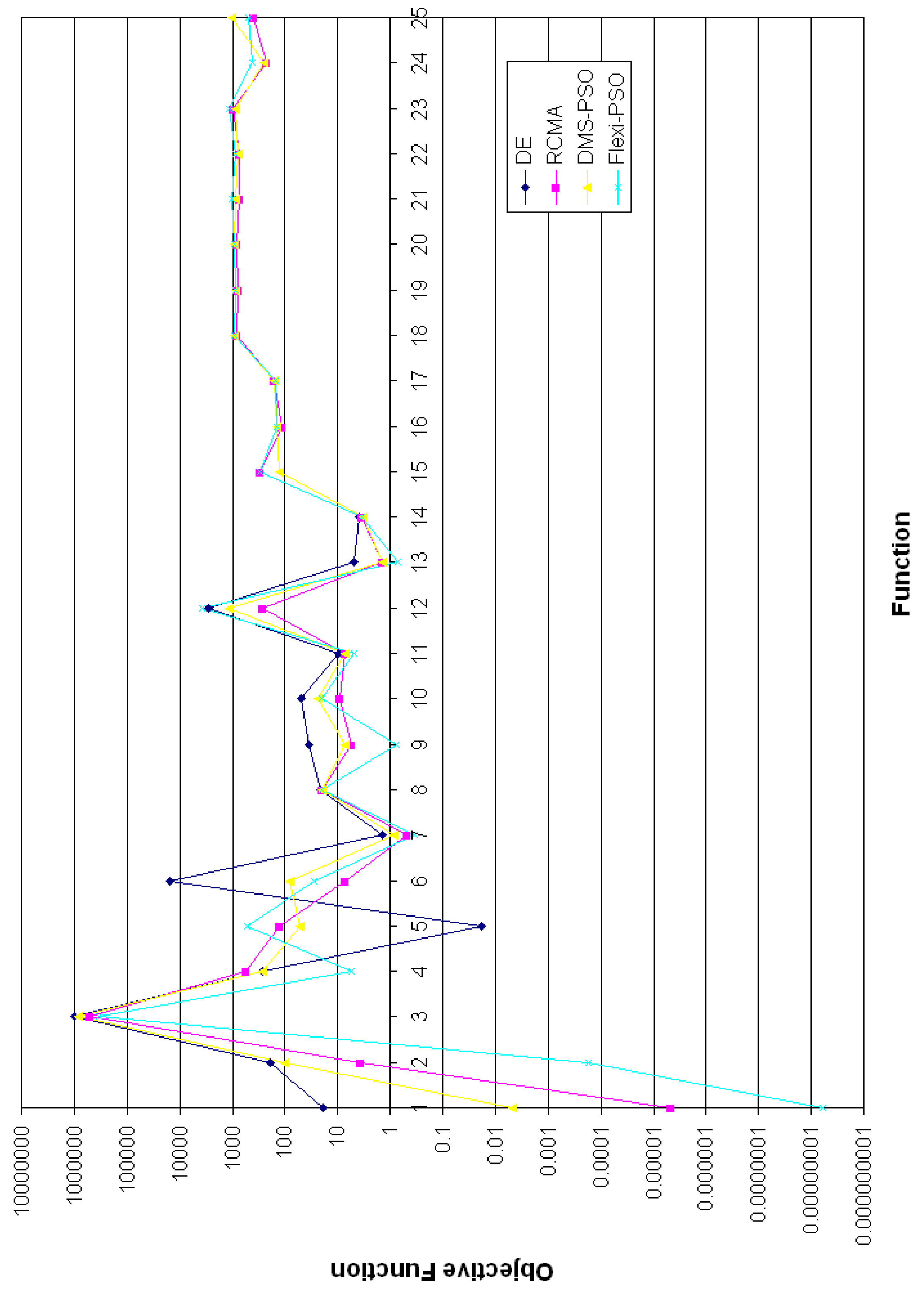

Figure 4.1. CEC-2005 Comparison (10-D, 100 000 fevals)

Function	Random Search	DE	RCMA	DMS-PSO	Flexi-PSO
1	3972.6	18.816	0.00000459	0.0048732	**6.0999E-09**
2	9856	194.33	3.659	100.7	**0.0001715**
3	6.32E+07	1001049	515354.8	843760	**343160**
4	7777.8	267.16	553.511	270.52	**5.5735**
5	11920	**0.0188126**	125.378	52.905	516.32
6	3.83E+08	15560	**7.10789**	82.235	27.273
7	2271.6	1.3767	0.484082	0.84928	**0.33796**
8	20.509	20.547	**20.247**	20.365	20.415
9	74.54	35.894	5.309446	7.4393	**0.75681**
10	90.36	50.082	**8.832397**	23.521	19.82
11	10.798	9.78996	7.334553	7.3131	**4.9684**
12	54498	2912.3144	**264.37**	1180.7	3813.8
13	6.6614	4.99484	1.425342	1.3832	**0.70825**
14	4.1269	3.99999936	3.513988	**3.3758**	3.4664
15	727.08		305.706	131.28	296.6
16	340.69		**112.8299**	141.05	142.41
17	414.52		156.661	161.23	**155.1**
18	1178.6		**806.7819**	897.28	922.45
19	1118.3		**772.03**	879.85	863.56
20	1079.9		**800.116**	901.32	935.48
21	1352.4		**741.413**	851.41	1023.9
22	1045.2		**721.052**	756.64	854.66
23	1377.8		981.28	**860.76**	1127.8
24	1312.2		**224.017**	248.75	421.75
25	1338.4		**399.9965**	1005.7	499.89

Table 4.1. Comparison between Random Search, Differential Evolution, Real-Coded Memetic, Dynamic Multi-Swarm and Flexi-Particle Swarm Optimisation Algorithms on the CEC 2005 Mathematical Benchmark Test Set (best solution in bold) for 10-D, 10 000 fevals

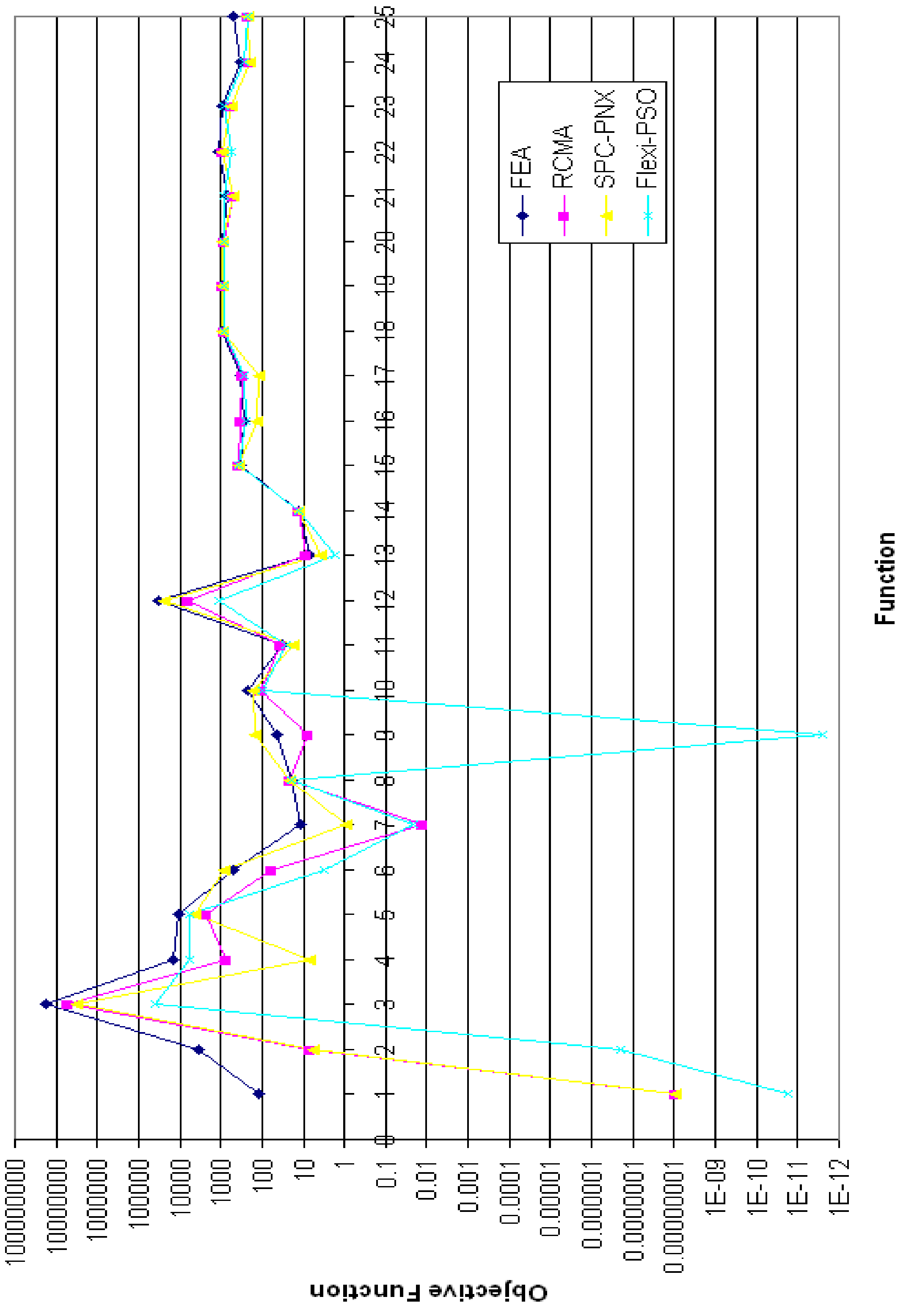

Figure 4.2. CEC-2005 Comparison (30-D, 100 000 fevals)

Function	Random Search	FEA	RCMA	SPC-PNX	Flexi-PSO
1	61517	117.33	9.53E-09	9.3524E-09	**1.6389E-11**
2	74634	3573.8	7.289625	5.8753	**1.9705E-07**
3	5.47E+08	17094000	5508628	3317500	**40481**
4	77629	14525	779.1663	**6.8783**	5614.6
5	31898	10174	**2213.529**	4336.6	6035.8
6	1.96E+10	514.15	61.4232	868.07	**3.2214**
7	9833.6	11.137	**0.01329727**	0.95537	0.020672
8	20.975	20.464	20.79068	21	**20**
9	415.46	42.879	7.550987	143.38	**2.6034E-12**
10	638.52	217.37	110.197	170.61	**103.63**
11	40.951	31.486	34.65414	**18.119**	26.395
12	1.13E+06	31652	6432.686	23408	**1193.8**
13	181.72	7.3701	8.659078	3.7176	**1.6729**
14	13.784	13.057	12.747	13.452	**12.521**
15	926.61	**331**	356.1009	368.29	354.35
16	701.59	269.95	335.0033	**133.34**	250.61
17	776.21	338.36	296.6728	**124.14**	270.19
18	1236.1	967.17	877.9795	907.64	**832.97**
19	1236.5	943.55	882.1409	907.15	**831.1**
20	1233	973.6	879.902	907.23	**832.67**
21	1385.6	695.48	**500**	500.06	821.83
22	1404.8	1082.5	913.7631	908.67	**579.96**
23	1407.3	965.89	559.1006	**534.17**	797.6
24	1418.8	328.16	**200**	**200**	260.51
25	1433	517.86	**212.8011**	226.76	231.07

Table 4.2. Comparison between Random Search, FEA, Real-Coded Memetic, Real Parameter GA (SPC-PNX) and Flexi-Particle Swarm Optimisation Algorithms on the CEC 2005 Mathematical Benchmark Test Set (best solution in bold) for 30-D, 100 000 fevals

4.2. Neural Network model of the IRIS Dataset

A further test of the effectiveness of an optimisation algorithm is the training of a neural network. In this study the Iris dataset (Appendix B) is used to test the effectiveness of the Flexi-PSO and a comparison made with the standard backpropagation method of updating the weights of a feed-forward single hidden layer neural network. This subsection first introduces the basics of a feedforward neural network before moving on to comparing the performance of the Flexi-PSO and typical backpropagation error minimisation techniques long used in the training of neural networks. The commonly used IRIS dataset used for classification of three different flower types is used in this comparative study.

An Artificial Neural Network (ANN) is an information processing paradigm that is inspired by the way biological nervous systems, such as the brain, handle information (Masters, 1993). The key element of this paradigm is the novel structure of the information processing system. It is composed of a large number of highly interconnected processing elements (neurons) working in unison to solve specific problems. Typically they are used on problems involving pattern recognition or data classification, proxy or response surface modelling, time-series modelling and have seen implementation in most industries.

ANNs, like people, learn by example. An ANN is usually configured for a specific application through a learning process. Learning in biological systems involves adjustments to the synaptic connections that exist between the neurons. This is true of ANNs as well. From a computational point of view we also know that the fundamental processing unit of the brain is a neuron. A neuron consists of a cell body, or soma, that contains a nucleus (Figure 4.3). Each neuron has a number of dendrites that receive connections from other neurons. Neurons also have an axon that goes out from the neuron and eventually splits into a number of strands to make a connection to other neurons. The point at which neurons join other neurons is called a synapse.

Signals move from neuron to neuron via electrochemical reactions. The synapses release a chemical transmitter that enters the dendrite. This raises or lowers the electrical potential of the cell body. The cell body sums the inputs it receives and once a threshold level is reached an electrical impulse is sent down the axon (often known as firing). These impulses eventually reach synapses and the cycle continues. Synapses that raise the potential within a cell body are called excitatory. Synapses that lower the potential are called inhibitory. It has been found that synapses exhibit plasticity. This means that long-term changes in the strengths of the connections can be formed depending on the firing patterns of other neurons. This is thought to be the basis for learning in the brain.

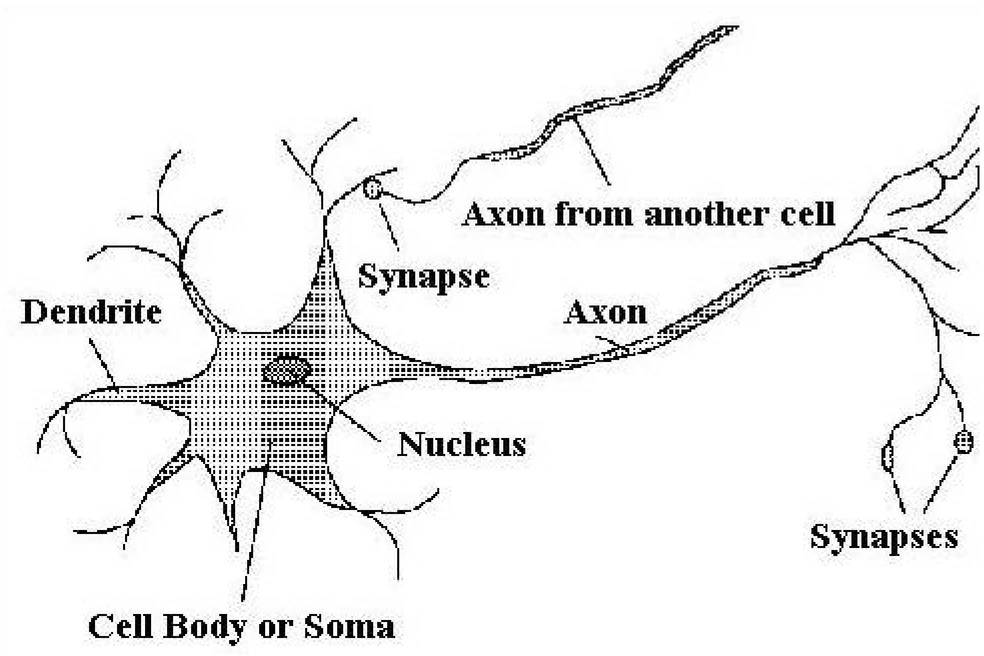

Figure 4.3. Schematic of a biological neuron

Artificial neural networks “artificially” replicate the behaviour of a system of biological neurons. Figure 4.4. displays a feed-forward neural network with 2 inputs, 2 hidden neurons, and a single output neuron. I_1 and I_2 contain the input data that is used to train the network which is usually scaled before use in the network. This is done to remove biasness towards variables that are large in magnitude or vary over log scales as opposed to other variables that are linear. Weights (W_{ij}) are usually real numbers and can take on any value.

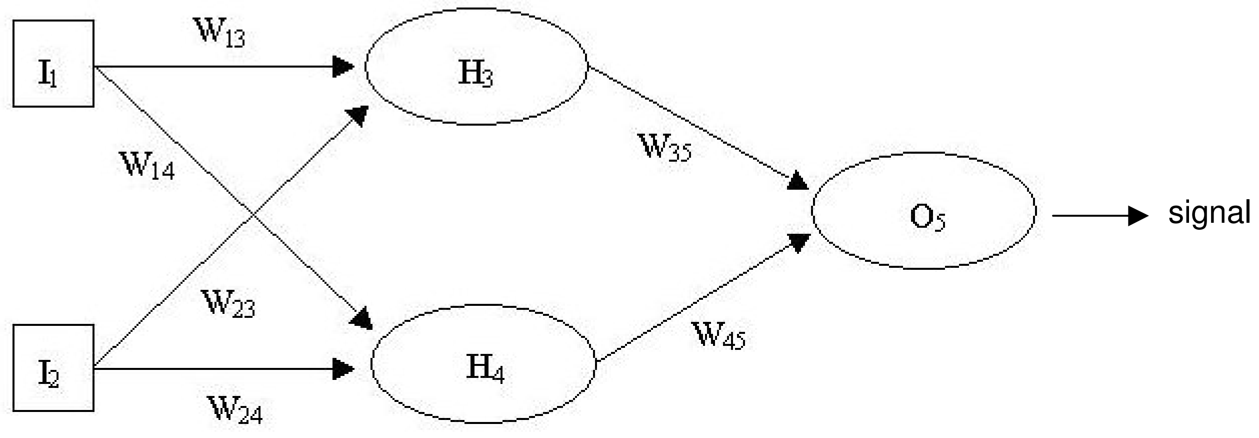

Figure 4.4. Schematic of an artificial neural network

The neurons in the hidden and output layers of Figure 4.3. are represented by transfer functions that could in theory take on any shape. Typically sigmoid transfer functions in the hidden layer are used together in conjunction with linear transfer functions in the output layer. This design is reported to be capable of approximating any continuous function arbitrarily well (Mathworks, 2005). Figure 4.5 depicts the processing in an artificial neuron with a sigmoid function. The signal into the neuron is the product of each input and its weight to the neuron in addition to a bias (threshold). This is then mapped onto the transfer function and the evaluation thereof is sent as an output signal.

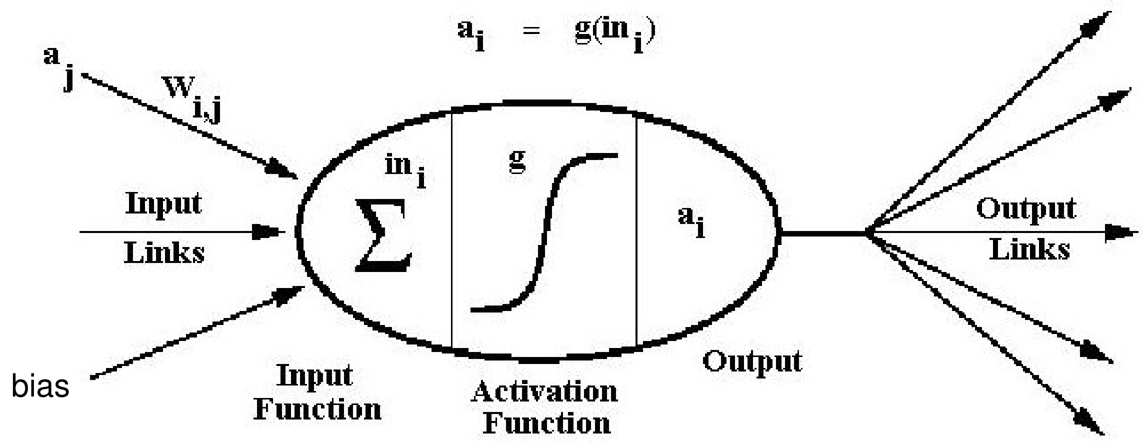

Figure 4.5. Processing in an artificial neuron

This inner workings can be represented as the following for neuron *i* (in this study a tan-sigmoid function is used) :-

$$in_i = \sum_{j=1}^{inputs} a_j W_{ij} + bias \tag{4.2.1}$$

$$a_i = g(in_i) = \tanh(k.in_i) \tag{4.2.2}$$

The tan-sigmoid function has *k* = 1, however in this study, *k* (the slope of the sigmoid functions) is allowed to vary to increase the flexibility of the network. Networks used for data classification usually use step functions as transfer functions that give a hard threshold for a neuron to fire, thus making clear distinctions in data. Step functions can be approximated with a sigmoid function that has a relatively large value of *k*. Figure 4.6 illustrates the effect of *k* on the shape of the transfer function. Naturally if k = 0 there is a flat response from the neuron for any input and hence this neuron can be removed.

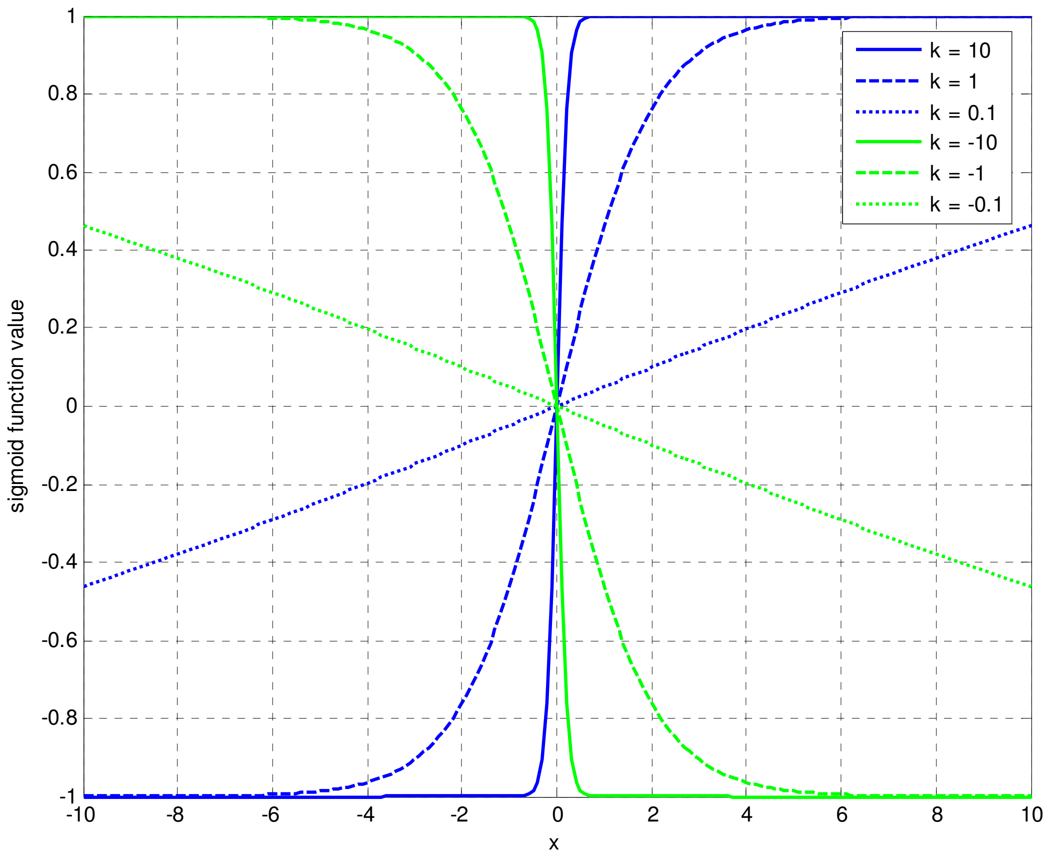

Figure 4.6. Effect of *k* on the transfer function (4.2.)

There has been work done before in this area using particle swarms and is worth testing as neural networks pose highly non-convex fitness landscapes due to the number of weights (variables) involved and the non-linearity of the transfer functions within each neuron.

(Ribeiro & Schlansker, 2004) used the canonical particle swarm to train a neural network for reactive power systems successfully. (Al-kazemi & Mohan, 2002) used a multi-phase PSO to train a feed-forward neural network on the commonly used Iris, New Thyroid and Glass classification datasets (Blake et al, 1998). This variation of the algorithm only uses the global best and current position of the particle in the velocity updates. (Eberhart and Shi, 1998) went as far as to state that scaling was unnecessary in pre-processing input data to a neural network when using the inertia weight PSO and a high slope threshold on the sigmoid transfer function.

A test was put forward to the Flexi-PSO to train a feed-forward neural network with a single hidden layer on the IRIS dataset (Appendix B). The hidden and output layer neurons contained the tan-sigmoid transfer function and the Flexi-PSO is used to update the weights and evolve the structure of the network. This is then compared to a standard back-propagation (Masters, 1993) technique of updating the weights.

The IRIS dataset is commonly used as a test case for data classification algorithms. There are fifty samples each of flowers of three species viz. Setosa, Veriscolor and Virginica. There are four attributes used to distinguish each species, viz. Sepal Length, Sepal Width, Petal Length and Petal Width.

This set is commonly used as the Veriscolor and Virginica flower types are not linearly separable from each other. The network is trained to 10 000 epochs using the Flexi-PSO and standard backpropagation. Results of the classification are presented in Figure 4.7.

The Flexi-PSO achieves a very good match to the actual classification whereas the standard backpropagation fails on many samples. The backpropagation algorithm has two parameters to be set viz. learning rate (η) and momentum (α). In this comparison $\eta = 0.5$ and $\alpha = 0.8$. Testing on other combinations of the learning rate and momentum did not yield any better results. This is another test in robustness that the Flexi-PSO passes.

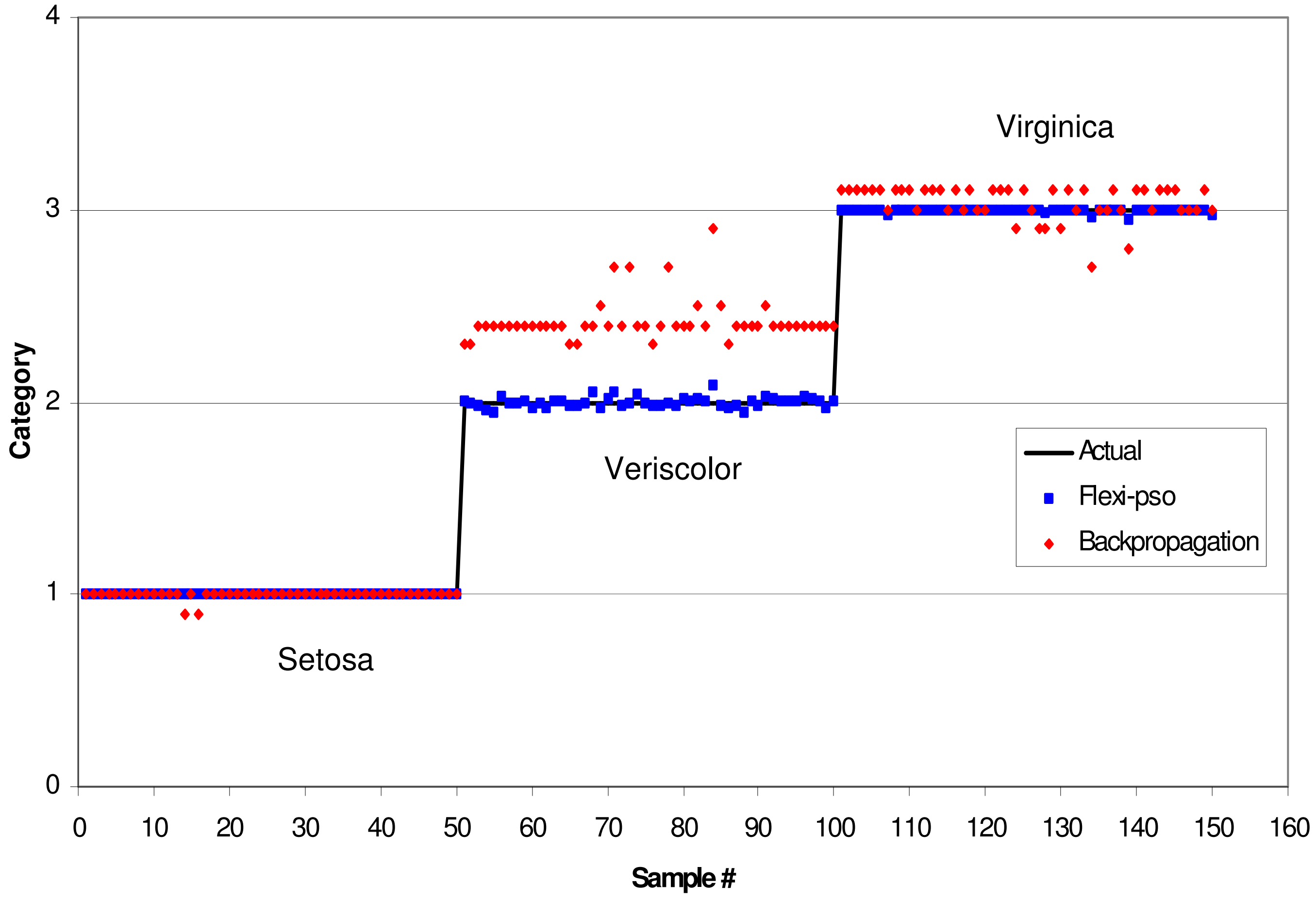

Figure 4.7. Measured and Predicted Comparison of the Flexi-PSO and Standard Backpropagation techniques on the IRIS Dataset

4.3. Integer Problems

In testing integer problems, the method used is as discussed in Section 3.4. Three commonly used test problems found in the literature (Laskari et al, 2002) are used to test the Flexi-PSO. These problems are defined as follows :-

$$F_1(x) = (9x_1^2 + 2x_2^2 - 11)^2 + (3x_1 + 4x_2^2 - 7)^2 \tag{4.3.1}$$

with solution $x^* = (1, 1)$ and $F_1(x^*) = 0$

$$F_2(x) = (x_1 + 10x_2)^2 + 5(x_3 - x_4)^2 + (x_2 - 2x_3)^4 + 10(x_1 - x_4)^4 \tag{4.3.2}$$

with solution $x^* = (0, 0, 0, 0)$ and $F_2(x^*) = 0$

$$F_3(x) = -3803.84 - 138.08x_1 - 232.92x_2 + 123.08x_1^2 + 203.64x_2^2 + 182.25x_1x_2 \tag{4.3.3}$$

with solution $x^* = (0, 1)$ and $F_3(x^*) = -3833.12$

A comparison is made with results obtained by (Laskari et al, 2002) who used an inertia weight (PSO-In), constriction factor (PSO-Co) and both inertia weight and constriction factor (PSO-Bo) particle swarm to solve the above problems. Table 4.3 reports the comparison in both function value and mean number of function evaluations required to find the optimum over an average of 30 runs. All methods do find the global optimum but the Flexi-PSO is able to do so much quicker.

Function	Method	Mean F(x')	Mean fevals
F_1	PSO-In	0	304.0
	PSO-Co	0	297.3
	PSO-Bo	0	302.0
	Flexi-PSO	**0**	**76.0**
F_2	PSO-In	0	1728.6
	PSO-Co	0	1100.6
	PSO-Bo	0	1082.0
	Flexi-PSO	**0**	**438.0**
F_3	PSO-In	-3833.12	334.6
	PSO-Co	-3833.12	324.0
	PSO-Bo	-3833.12	306.6
	Flexi-PSO	**-3833.12**	**65.3**

Table 4.3. Comparison performance on benchmark integer problems

Chapter 5

Hierarchical Clustering

An assisted history match run could lead into hundreds of simulations and in order to select matches that fall into distinctly different niches, some post-processing of the results is required. This is even more essential for the Sequential Niching Flexi-PSO, as it has already been shown that it has the capability of moving into different niches. However, many other niches could also have been searched by some particles during the course of the run and these need to be isolated as well. It may be difficult to analyse a table of results directly particularly if there a large number of variables, hence clustering would be useful in this regard.

5.1. Agglomerative Hierarchical Clustering Methods

Many clustering techniques exist viz. self-organising maps, k-means, fuzzy-c means and hierarchical clustering to name a few. The goal of this thesis is not to design a new clustering method but to use it in conjunction with other graphical tools. Hence for simplicity hierarchical clustering has been chosen. Hierarchical clustering is a method of cluster analysis that builds a hierarchy of clusters. There are different methods that can be used to generate the hierarchical cluster tree information based on ways of measuring the distance between two clusters of objects. If n_r is the number of objects in cluster r and n_s is the number of objects in cluster s, and x_{ri} is the ith object in cluster r, the definitions of the various measurements are as follows :-

Nearest neighbour, uses the smallest distance between objects in the two clusters :-

$$d(r,s) = \min(\, dist(\, x_{ri}, x_{sj})\,),\ \ i \in (1, \ldots, n_r),\ \ j \in (1, \ldots, n_s) \tag{5.1.1}$$

Furthest neighbour, uses the largest distance between objects in the two clusters :-

$$d(r,s) = \max(\, dist(\, x_{ri}, x_{sj})\,),\ \ i \in (1, \ldots, n_r),\ \ j \in (1, \ldots, n_s) \tag{5.1.2}$$

Average linkage uses the average distance between all pairs of objects in cluster r and cluster s :-

$$d(r,s) = \frac{1}{n_r n_s} \sum_{i=1}^{n_r} \sum_{j=1}^{n_s} dist(x_{ri}, x_{sj}) \tag{5.1.3}$$

where *dist* is the normalised Euclidean distance function.

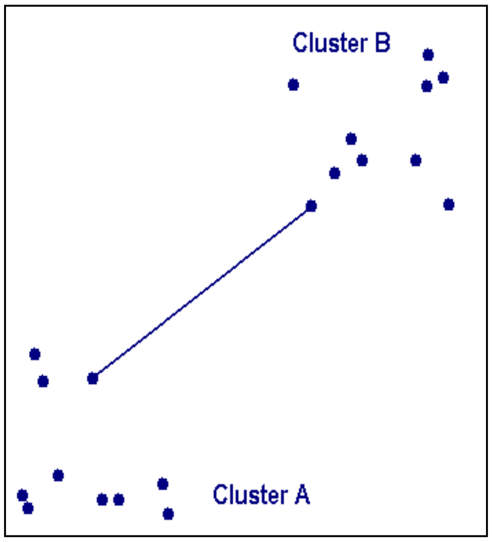

Fig. 5.1. Nearest Neighbour

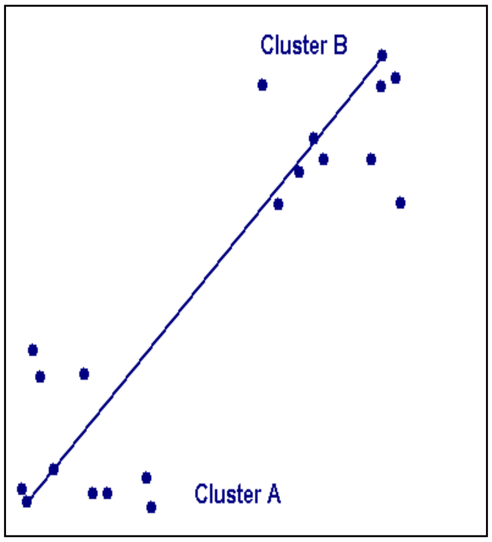

Fig. 5.2. Furthest Neighbour

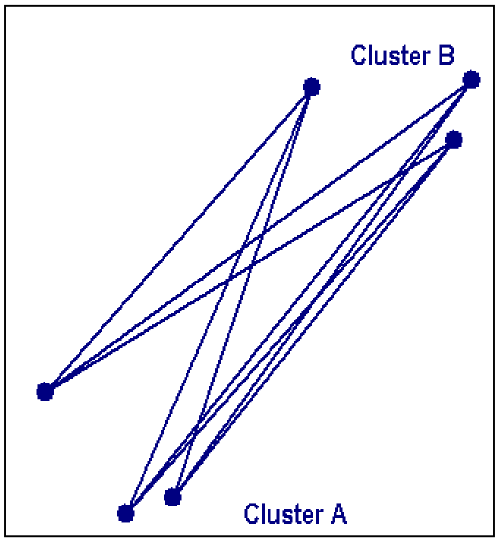

Fig. 5.3. Average Linkage

The following is the procedure for the nearest neighbour measure implementation :-

Consider a set *S* of m-dimensional data points within a tree structure *Y*.

a) Place each data point instance of *S* in its own cluster (singleton), creating a list of clusters *L* (initially, the leaves of *Y*): *L* = S_1, S_2, S_3, ..., S_{n-1}, S_n

b) Compute the shortest normalised Euclidean distance between every pair of elements in *L* to find the two closest clusters {S_i, S_j}

c) Remove S_i and S_j from *L*

d) Merge S_i and S_j to create a new internal node S_{ij} in *Y* which will be the parent of S_i and S_j in the result tree

e) Go to (b) until there is only one set remaining

An example illustration of the resulting dendrogram is shown in Fig. 5.4.

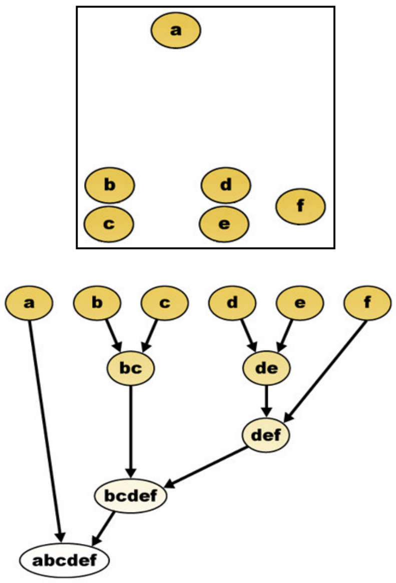

Fig. 5.4. Simple Dendrogram

5.2. Clustering the IRIS Dataset

This section examines a few hierarchical distance measures in clustering the IRIS dataset. Figure 5.5 is the cross plot of the dataset and illustrates the non-separability of the Veriscolor and Virginica flower types. Table 5.1 displays the numbers of samples misclassified by each distance measure. Average linkage has the least number of classification errors and will be used later in this study. It is to be expected that the nearest neighbour measure would result in more errors, as it would be less susceptible to picking up linearly non-separable clusters.

Distance Measure	Misclassifications
Nearest neighbour	51
Furthest neighbour	18
Average	17

Table 5.1. Classification errors on the IRIS dataset

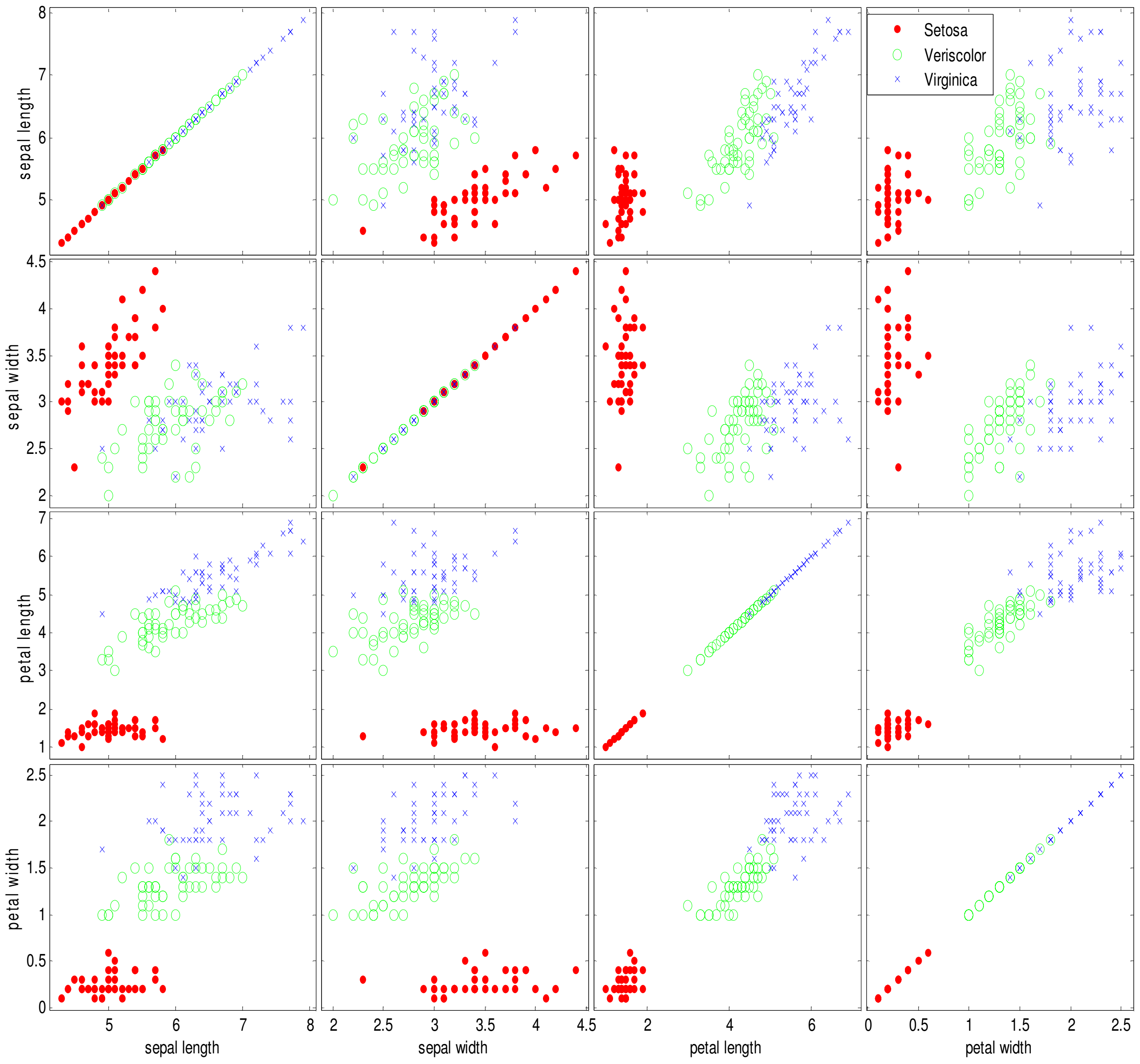

Fig. 5.5. Cross plots of the IRIS dataset

Chapter 6

History Matching & Forecasting : Case Study of The Imperial College Fault Model

This section deals with the Imperial College fault model as a case study. A description of the model is given followed by the results of the history matching exercise using the Flexi-PSO and an overall uncertainty evaluation that includes forecasting with the ensemble that is generated in the history matching phase. But firstly, lets look at some qualitative ways in which to enhance the performance of the algorithm. As was discussed in Chapter 3.2, the swarm is more than capable of finding optima even it is asymmetrically initialised. However the goal of this thesis is to find ways to quicken the process of history matching due to the expensive nature of running simulation models, and to minimise the number of simulations to be run. It is intuitively better to initialise the swarm as uniformly as possible over the hypercube and this chapter begins with a technique to address this issue.

6.1. Low Discrepancy Sequences

Faure sequences are low discrepancy sequences where successive numbers are added in a position as far as possible from one another in order to avoid clustering (Faure, 1992). The numbers generated sequentially fill in the gaps between the previous numbers in the sequence. These sequences produce low error bounds for multidimensional integration and global optimisation (Fox, 1986) and have seen extensive application in finance (Joy et al, 1996).

(Van der Corput, 1935) was the first to introduce low discrepancy sequences and many sequences developed thereafter are based on this work. In general for base *b*, if the n'th term of the sequence is indexed as decimal-base :-

$$n = \sum_{j=0}^{m} a_j(n) b^j \tag{6.1.1}$$

The reflection of (6.1.1) is then used to generate the n'th term as :-

$$b(n) = \sum_{j=0}^{m} a_j(n) b^{-j-1} \tag{6.1.2}$$

The n'th term of the van der Corput sequence, for base *b*, is generated as follows:-

the decimal–base number *n* is expanded in the base *b*, example *n* = 4 in base 2 is 100 ($4 = 1 \times 2^2 + 0 \times 2^1 + 0 \times 2^0$) from equation (6.1.1). The number in base *b* is reflected. In the example, 100 becomes 001. Mapping into interval

[0,1). 001 becomes 0.001 (binary decimal) and this corresponds to the decimal number 1/8, that is 1/8 (= 0x(1/2) + 0x(1/4) + 1x(1/8)) from equation (6.1.2). The algorithm for the Faure sequence uses (6.1.1) and (6.1.2), however before (6.1.2) is used, there is a combinatorial rearrangement of the a_j. This is performed using a *recursive* equation, from dimension (*d*-*1*) to the new dimension *d*:-

$$a_i^d(n) = \sum_{j \geq i}^{m} \frac{j!}{i!(j-i)!} a_j^{d-1}(n) \bmod b \tag{6.1.3}$$

The first dimension uses the van der Corput sequence with the specific Faure's base *b*, then the numbers are reordered for dimension *d* > 1 with (6.1.3). Figure 6.1 compares the difference between the internal random number generator within MATLAB® and a Faure sequence for 200 points in 2 dimensions. Clearly the Faure Sequence tends to fill in the space much more evenly than the random number generator and it is this greater uniformity of spacing that intuitively is sensible to use in the initialisation of any population based optimiser.

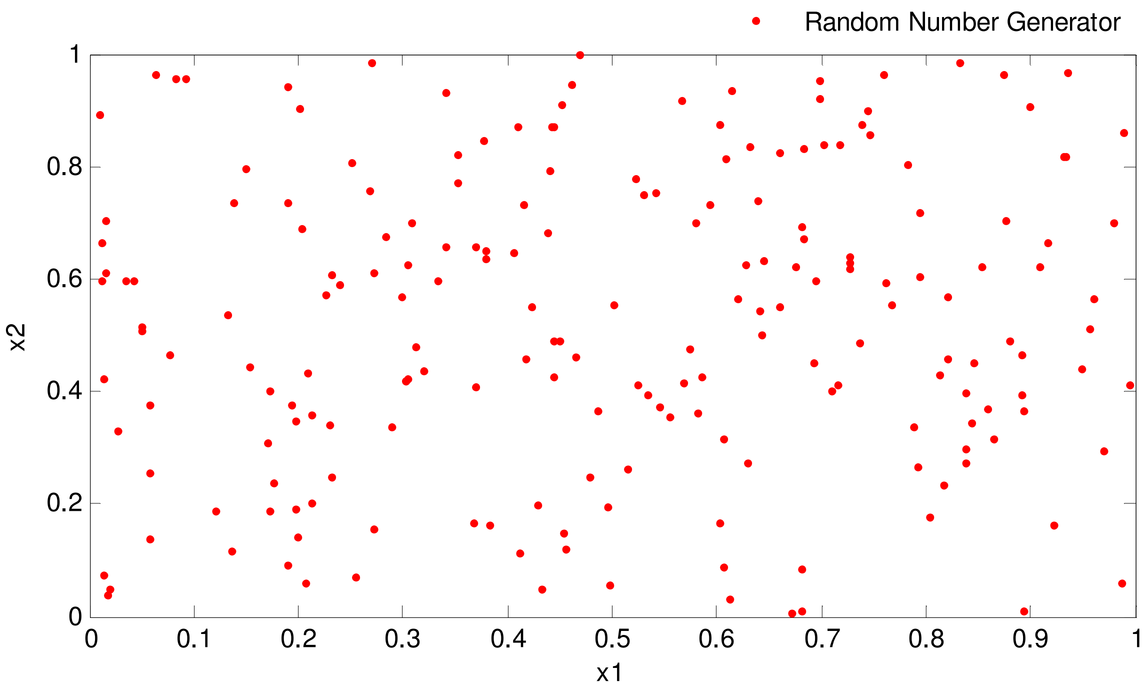

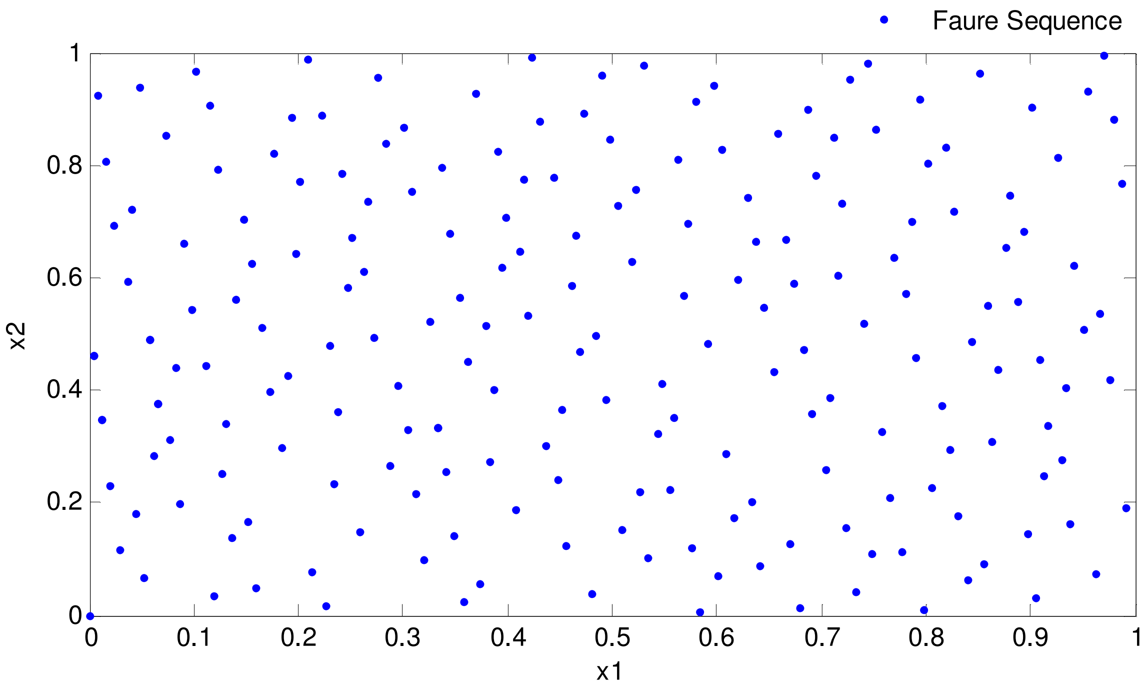

Figure 6.1. 2-D comparison of a random number generator and a Faure Sequence

6.2. IC Fault Model Description

The Imperial College Fault Model has become a well known benchmark history matching model. It is a simple model that is quite difficult to history match (Carter et al, 2006). The geological model with no-flow boundary conditions consists of six layers of alternating good and poor quality sands (Figure 6.2). The good and poor quality layers have identical properties respectively. Starting from the top layer, the thicknesses are 12.5ft, 11.5ft, 10.5ft, 9.5ft, 8.5ft and 7.5ft for each layer resulting in a total thickness of 60 feet. The simulation model is 100 x 12 grid blocks, with each geological layer divided into two simulation layers with equal thickness, each grid block is 10 feet by 10 feet aerially. The width of the model is 1000 feet, with a simple fault at the mid-point, which offsets the layers. Water is injected at the left-hand edge, and a producer well on the right-hand edge. Both wells are completed on all layers, and are operated on bottom hole pressures. The model is constructed such that the vertical positions of the wells are kept constant and equal, even when different fault throws are considered. The well depths are from 8325 feet to 8385 feet. This model has been simulated in the Shell proprietary simulator MoReS.

There are three parameters in this model viz. fault throw (h), high permeability (k_g) and low permeability (k_p). A truth case is run for 5 years to generate synthetic monthly production data with the set of parameter values being fault throw = 10.4 ft, high permeability = 131.6 md and low permeability = 1.31 md. The first three years of production data is used in the history match and the last 2 years used as prediction data to measure the predictive quality of the history matches. The swarm is initialized from a random uniform distribution in the ranges viz. $h \in [0,60]$ ft, $k_g \in [100,200]$ md and $k_p \in [0,50]$ md.

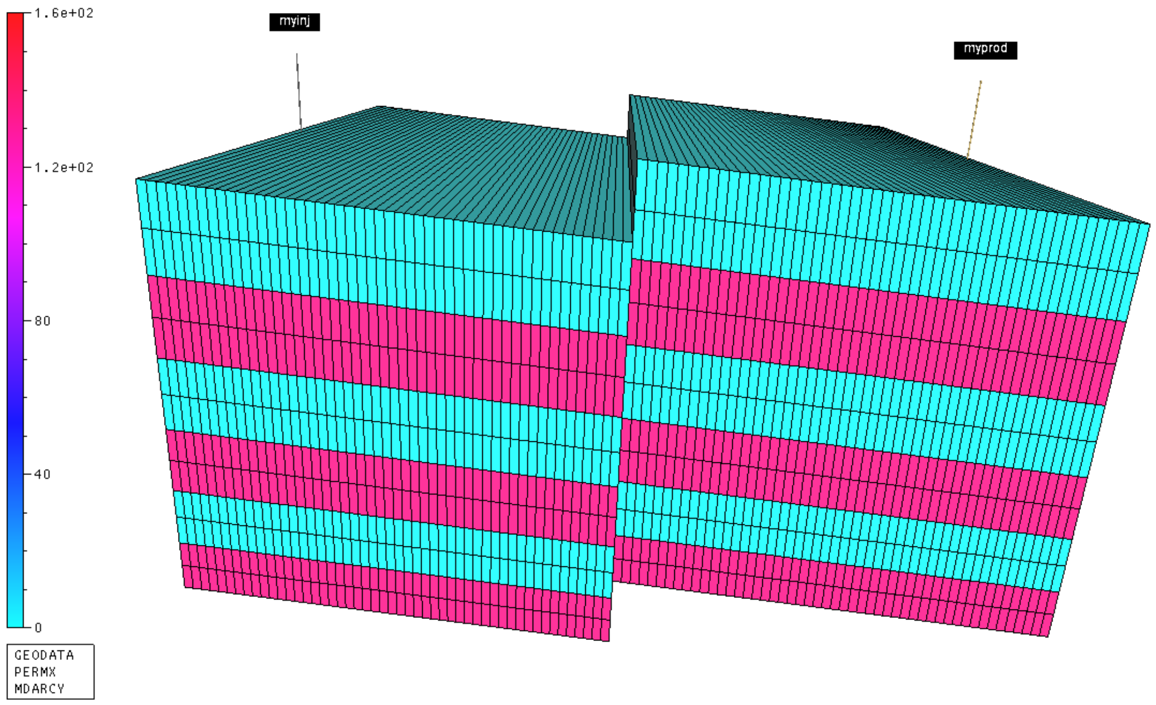

Figure 6.2. Imperial College Fault Model

The fitness is defined as the root mean square error between the simulated data of each realisation and the production data from the truth case :-

$$fitness = \frac{1}{n}\sqrt{\sum_{i=1}^{n}\left[\frac{Q_o^{obs,i} - Q_o^{sim,i}}{\sigma_o^i}\right]^2 + \sum_{i=1}^{n}\left[\frac{Q_w^{obs,i} - Q_w^{sim,i}}{\sigma_w^i}\right]^2} \qquad (6.2.1)$$

Here *n* denotes the number of measurements in the history matching period which is thirty six. The superscript *obs* refers to the truth case production data and the superscript *sim* refers to the realization case production data for oil and water respectively. σ_o and σ_w are the standard deviations for oil and water production rates respectively in the truth case and behave as weighting factors for normalization purposes. In this instance they are taken to be 3% of the truth case production data viz.

$$\sigma_o = 0.03\,Q_o^{obs} \qquad (6.2.2)$$

$$\sigma_w = 0.03\,Q_w^{obs} \qquad (6.2.3)$$

The Flexi-PSO is set up with 20 particles running for 50 iterations leading to a maximum of 1000 function evaluations.

6.3. Results and Discussion

The aim of this history matching exercise is to use the sequential niching capability of the Flexi-PSO to capture as much of the uncertainty range as possible, in other words to identify as many distinctly different minima as possible in the search space thus creating an ensemble of history matches. Creating an ensemble of matches that are similar to one another is just taking a set of points from around single minima and that is not the objective of this study. Such an approach would in all likelihood lead to similar prediction profiles and this study is aimed at searching for good history matches that in fact have divergent prediction characteristics and hence lead to more confidence in the predictive uncertainty range. Another reason is that in practical terms one can only take forward a reasonable number of history matches into the prediction phase. Taking forward too many history matches and multiplying them by the number of prediction scenarios, will likely give an unmanageable and undecipherable set of profiles that would be very time consuming.

The nature of the Flexi-PSO is that it explores and tries to exploit different valleys in the search space, hence it is anticipated that this behaviour would be reflected in the results. Models were ranked in increasing order of fitness and their history match profiles analysed. Models with a RMSE less than 3 were deemed acceptable. The RMSE value of 3 does not correspond to any statistical framework, but is chosen pragmatically by visual inspection of the matches. Fig. 6.3 is a normalized plot of each variable and it is immediately visible that the swarm has explored and exploited different areas of the search space. The throw axis shows distinctly different accepted fault throws indicating exploration and around these distinct areas are clusters of points indicating exploitation. The challenge now is to select a set of history matches from this set.

The normalized profile chart of Figure 6.3 is used in conjunction with hierarchical clustering. Firstly from Figure 6.3, there appears to be about ten cluster areas. The next step is to use agglomerative hierarchical clustering with the average linkage normalized Euclidean distance as a criterion for separation. To verify the appropriateness of the visually derived number of clusters, the dendrogram just needs to be cut at the level that leaves ten clusters. The clusters formed from this procedure are then visually checked against Figure 6.3 to ensure they are sensible. Such profile charts are valuable to visualise systems with many variables. Figure 6.4 displays the clusters in 3-D.

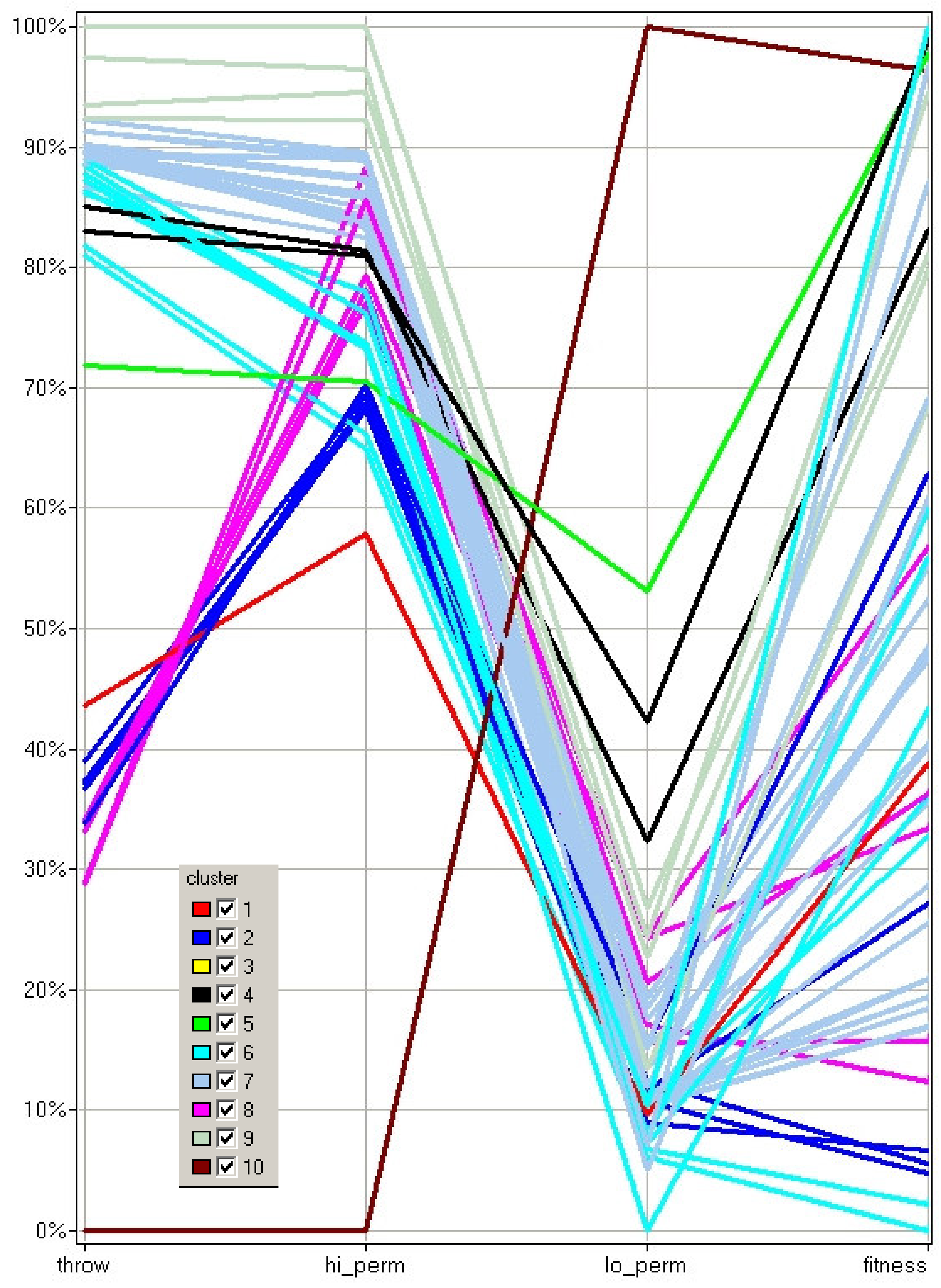

Figure 6.3. Normalised profile chart of acceptable matches

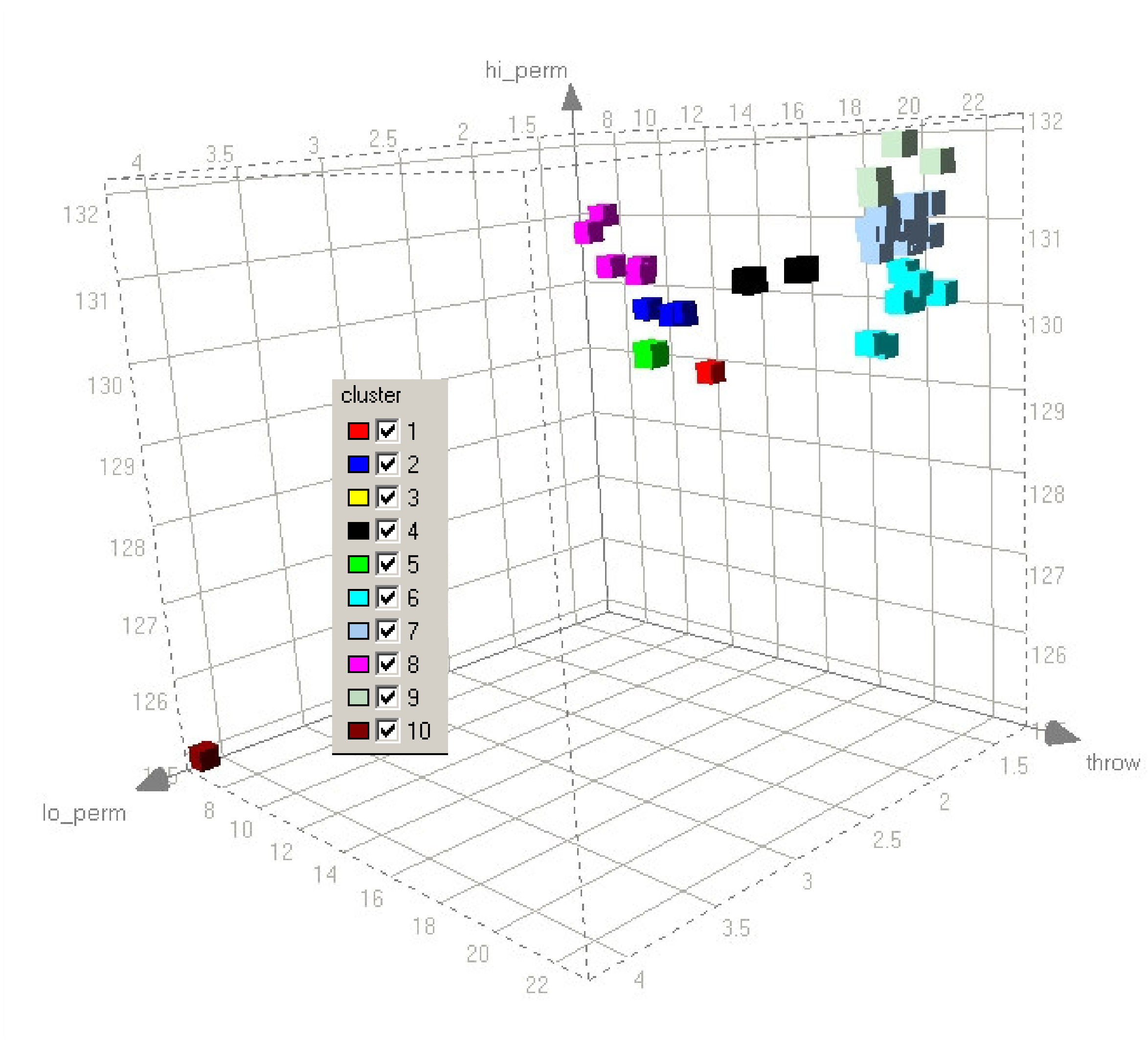

Figure 6.4. 3-D plot of acceptable matches that are clustered

The next step is to determine which members of each cluster to take into forecasting. In this thesis a practical approach is taken, considering CPU availability, disk space and most importantly time available to the engineer for an uncertainty study task. In this regard, the minimum of each cluster is only taken into a table for a final qualitative analysis as in Table 3.

It can be seen that there are still some similarities between the various matches, though they appear distinctly different on Figure 6.3. This is because Figure 6.3 is a normalised plot hence is very useful qualitatively, not quantitatively. Similar matches are grouped in Table 6.1, and the minimums of each group taken as the final set to carry forward into the prediction viz. Match 2, 7, 9 and 10. It can be seen that Match 9 is very close to the truth case, in fact the Flexi-PSO would be able to refine the match closer to the truth case if the improvement tolerance is slackened before reinitialisation.

	Throw	Hi-perm	Lo-perm	Fitness
Truth	10.60	131.60	1.31	0.00
Match 1	**20.41**	**130.44**	**1.50**	**1.67**
Match 2	**19.58**	**129.53**	**1.48**	**0.99**
Match 3	*20.25*	*130.69*	*2.21*	*2.62*
Match 4	*19.92*	*130.66*	*2.49*	*2.93*
Match 5	*17.91*	*129.86*	*2.17*	*2.86*
Match 6	*18.10*	*129.92*	*2.80*	*2.91*
Match 7	*22.66*	*131.99*	*2.05*	*2.58*
Match 8	***13.53***	***129.03***	***1.57***	***2.09***
Match 9	***11.13***	***130.98***	***1.99***	***1.73***
Match 10	6.47	124.96	4.14	2.88

Table 6.1. List of final history matches

Figures 6.5-6.8 show the production plots for five years. The first three years are the history match period and the last two years is the prediction phase. Matches 1-10 were all carried through to check whether eliminating them loses any valuable information. For the history match period the ensemble is able to track the truth case well, and the final reduced set (in bold lines) is adequate to capture the range of the ensemble. It must be noted from Figures 6.5 & 6.7 (oval demarcated area) that late in the prediction the ensemble is not able to track the truth case. This is important as it makes one realize that generating an ensemble is quite valuable to give an idea of the uncertainty range but is by no means definitive.

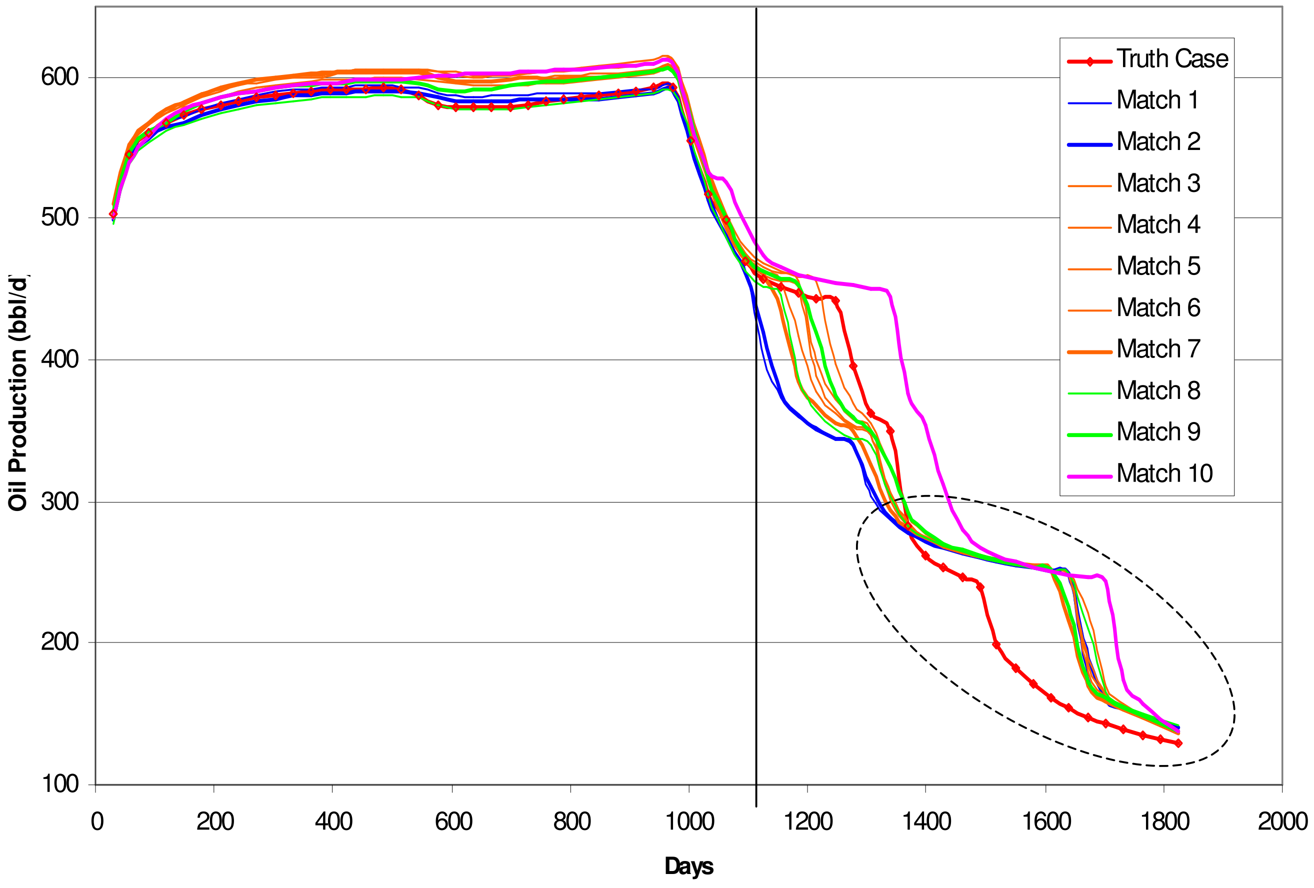

Figure 6.5. Oil Production Rate

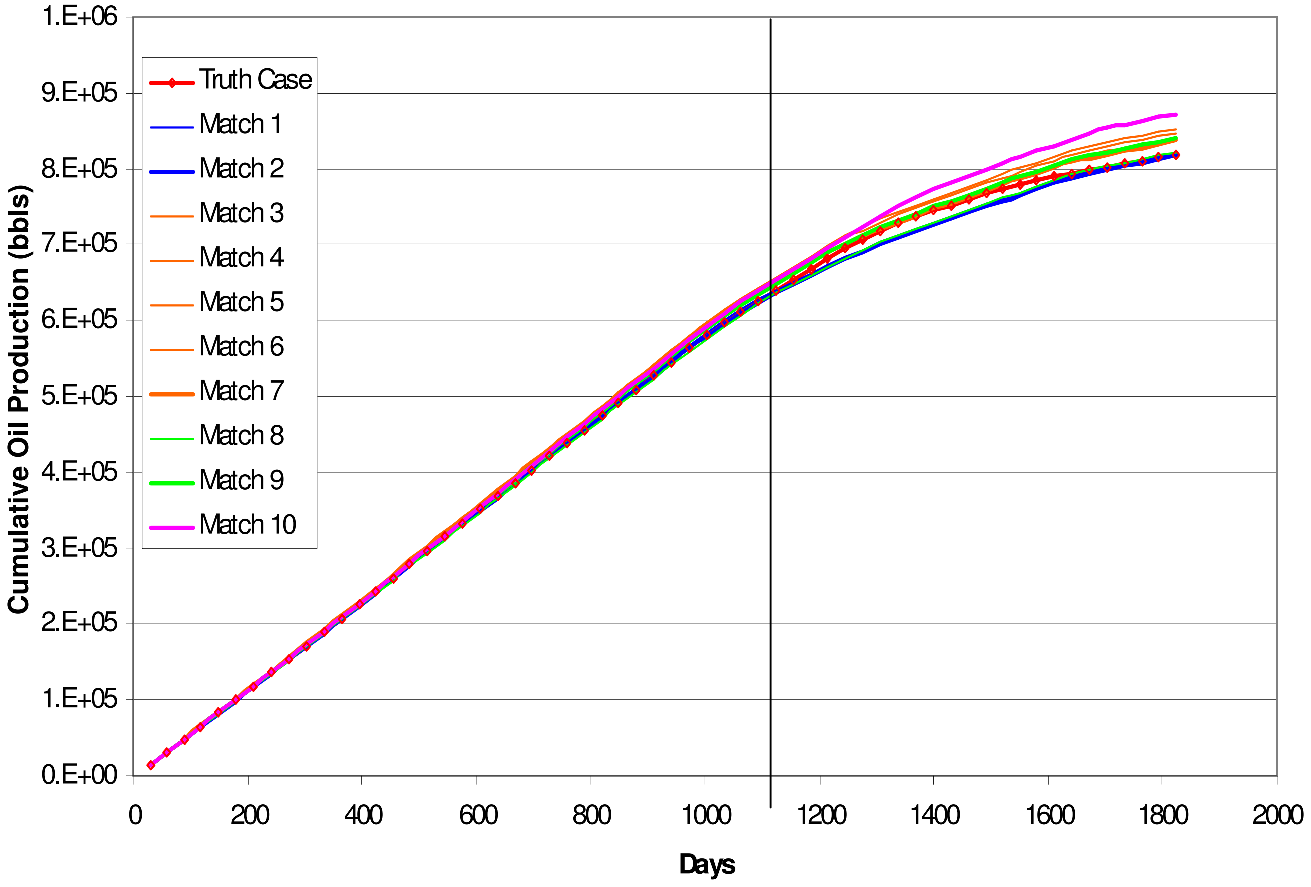

Figure 6.6. Cumulative Oil Production

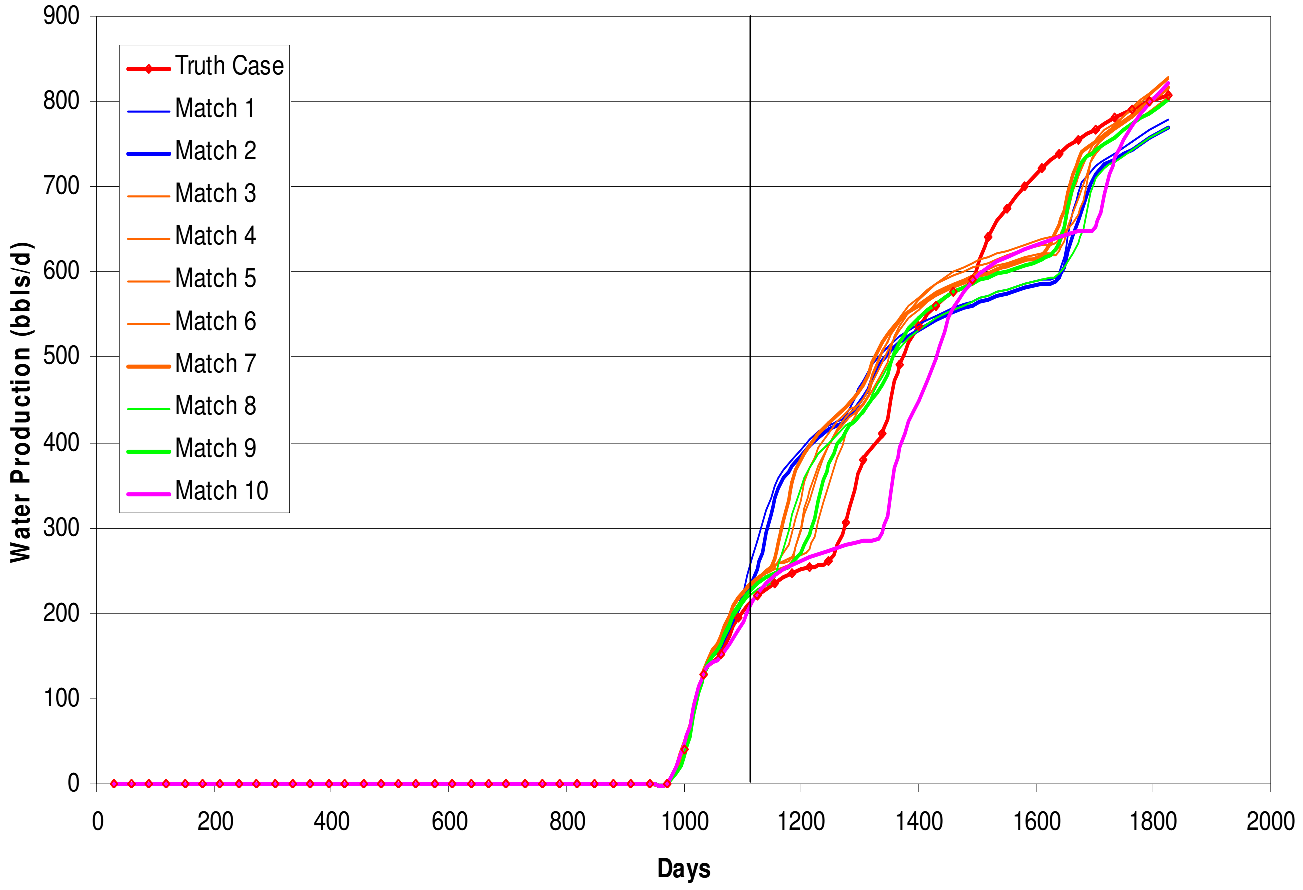

Figure 6.7. Water Production Rate

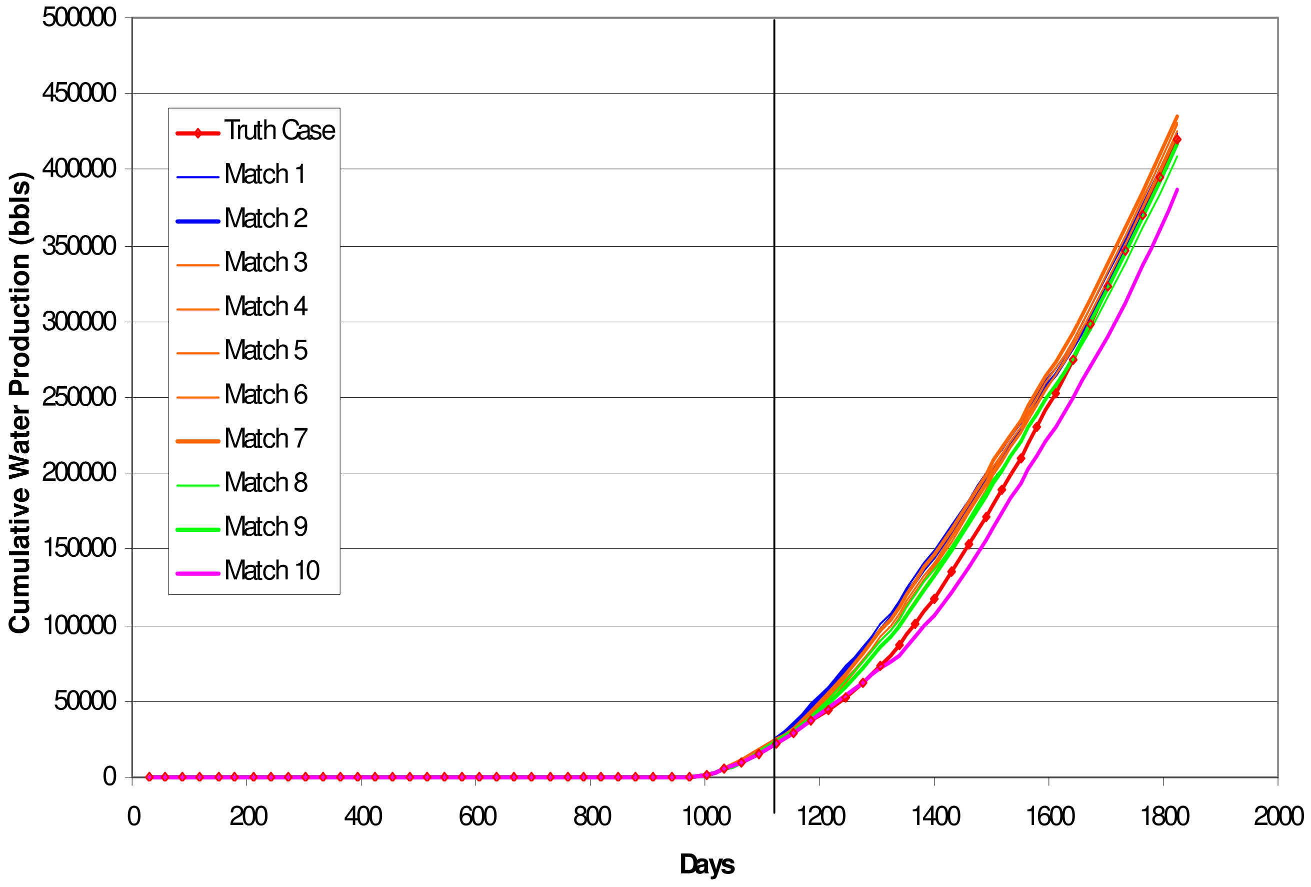

Figure 6.8. Cumulative Water Production

Figure 6.9 illustrates the fitness history of the Flexi-PSO. It can be seen that up to the 30th iteration the swarm converges very quickly but from here on (oval demarcated area) there doesn't appear to be any improvement in the global best solution and in fact the swarm appears to be finding progressively poorer solutions. This is due to the sequential niching nature of the Flexi-PSO, where minima that have already been found have been isolated and as the swarm is now exploring other areas of the search space it cannot find any other reasonable minima.

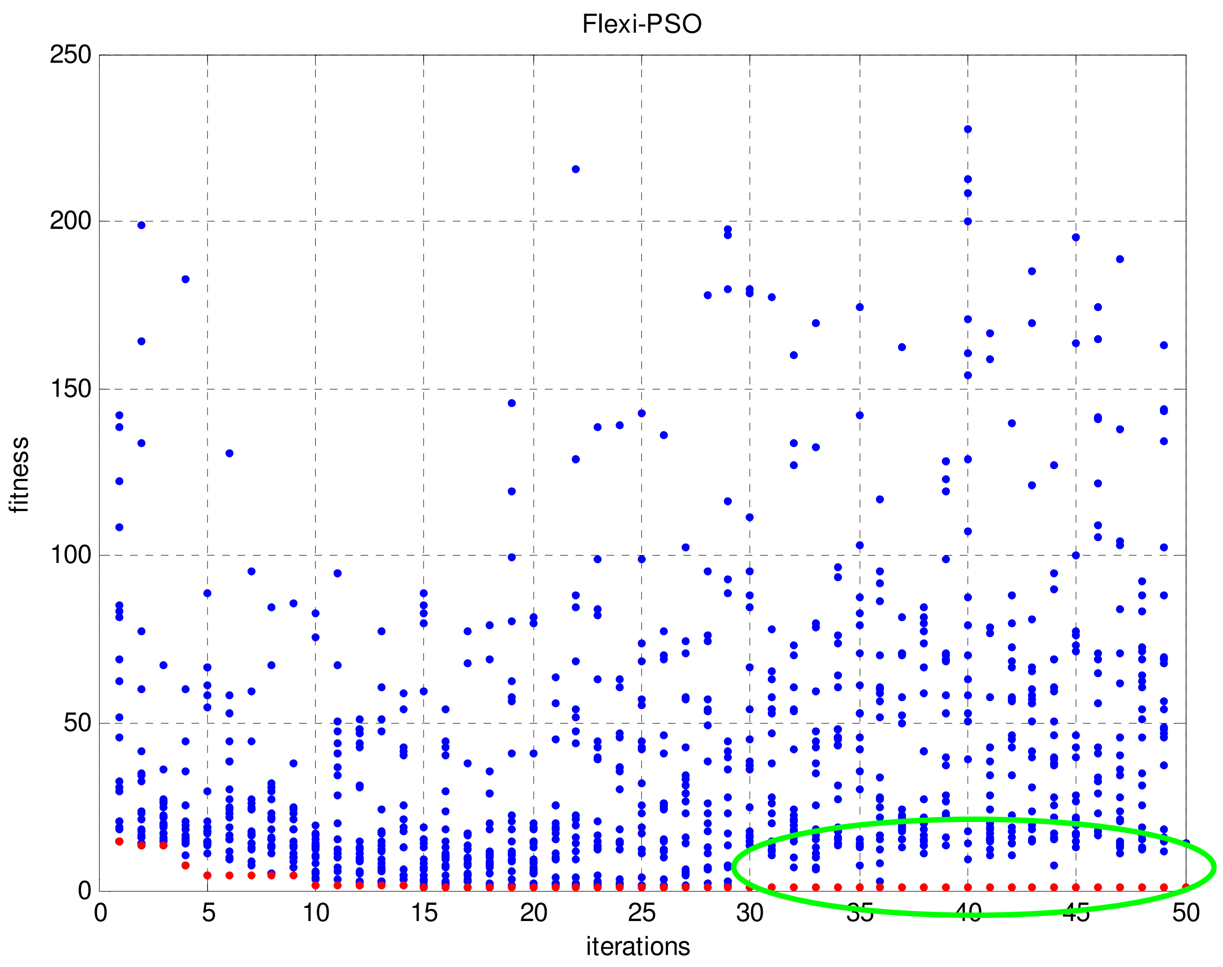

Figure 6.9. Fitness history

The minimum fitness is obtained on the 24th iteration and is represented by Match 2 (Table 6.1). Unlike any other method previously reported this divergence is in fact an encouraging indicator because one now has the option of stopping the global search procedure and complete the analysis of the assisted history match. Finally one always has the option of taking this a step further, time and resources permitting, to execute the cognition only version of the PSO or a local search algorithm to fine tune the final set of matches to see if any slightly better solution can be found.

A further attempt at history matching the ICF model using the Flexi-PSO and **function stretching** was investigated. This also serves to investigate the effect on a different starting population on another run. The final list of history matches is presented in Table 6.2. Distinct matches have been isolated using this technique, but this time the niche containing the truth case has not been found. Since function stretching elevates the fitness landscape, niches with a narrow valley can be even more difficult to identify as the stretching can lead to narrow needle like valleys in the transformed fitness landscape. This also leads onto the conclusion that any uncertainty modelling task should preferably be done with different starting populations on different runs to ensure that the fitness landscape has been searched more thoroughly.

	Throw	Hi-perm	Lo-perm	Fitness
Truth	10.60	131.60	1.31	0.00
Match 1	**5.5064**	**119.82**	**9.9581**	**2.4606**
Match 2	**5.9013**	**120.47**	**9.5479**	**2.6728**
Match 3	*17.566*	*129.32*	*1.9041*	*1.6375*
Match 4	*17.586*	*129.39*	*2.1557*	*1.2772*
Match 5	*17.589*	*129.38*	*2.3202*	*2.0165*
Match 6	*17.59*	*129.37*	*4.3485*	*2.7946*
Match 7	*17.601*	*129.35*	*2.1453*	*1.325*
Match 8	*17.64*	*129.26*	*2.1185*	*1.5769*
Match 9	*17.765*	*128.96*	*2.0321*	*2.4119*
Match 10	2.2419	121.61	2.9937	1.2027

Table 6.2. List of final history matches for function stretching transformation

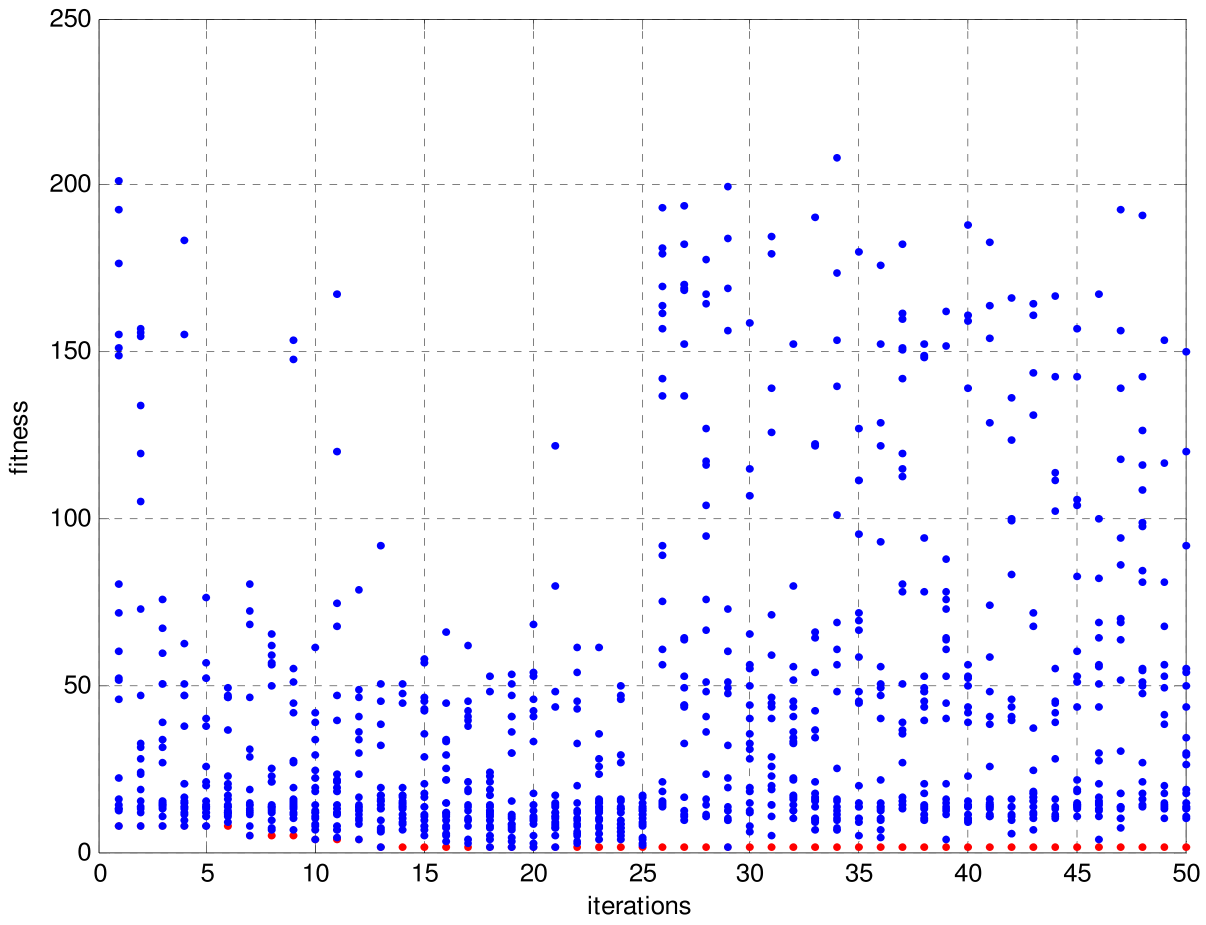

Figure 6.10. Fitness history for function stretched transformation

Figure 6.10 illustrates the fitness history of the function stretched transformation. For scale purposes the true fitness values are plotted and not the transformed fitness. Once the first niche is isolated at the 25th iteration, successive niches are then visited as the model objective is transformed. This is valuable as it directs the swarm fairly quickly to the non-transformed areas. The drawback is that it is much more difficult to get into the niche that contains the truth case since the transformation results in a very “spiky” fitness landscape. In a multimodal landscape this will result in niches residing in the spiked areas and hence being separated in a somewhat discontinuous fashion. This would require many more iterations to find the truth case as once the swarm finds the first niche, the objective function is transformed and the swarm will then search for the next niche and once a particle finds the next niche and the globalbest is updated, the rest of the particles will rush into that niche without much exploration of the rest of the search space since the contrast in fitness is so large.

This enhances the sequential niching nature of the Flexi-PSO but it does mean that the more spikes there are in the objective transformation, the longer it will take to find the region of the truth case as evidenced in this study.

Using the Nelder-Mead Simplex direct search method (Lasgarias et al, 1998) to history match the ICF Model makes a further test as to the efficiency of the Flexi-PSO. A brief description of direct search was given in Chapter 1.2. The FMINSEARCH option within MATLAB was employed for this task. Since the original formulation of the Nelder-Mead technique was not designed to handle bounds, direct usage of this option always led to solutions outside the desired range of the uncertainty parameters.

A modified version FMINSEARCHBND (D'Errico, 2006) that is able to handle boundary constraints by an internal transformation of the variables (quadratic for single bounds, sin(x) for dual bounds) was then used to history match the ICF Model. 10 attempts were made using random starting points and each attempt was allowed 1000 function evaluations to be commensurate with the Flexi-PSO. The results are shown in Table 6.3. Each attempt terminated once the improvement in the objective function was less than the specified tolerance that was set very low at 0.001 to allow FMINSEARCHBND to make as many function evaluations as possible.

The resulting best fitness on all attempts was very poor and it is clear that the Flexi-PSO outperforms it.

	Throw	Hi-perm	Lo-perm	Fitness	fevals
Truth	**10.60**	**131.60**	**1.31**	**0.00**	
Match 1	52.03	170.07	9.70	4.67	243
Match 2	49.56	162.02	9.70	4.98	303
Match 3	28.05	138.41	1.01	12.98	224
Match 4	54.16	174.61	11.78	4.64	252
Match 5	57.56	101.05	41.19	13.03	204
Match 6	12.33	136.00	1.22	18.16	175
Match 7	55.98	102.25	35.37	12.99	119
Match 8	55.98	180.29	13.33	4.53	184
Match 9	16.69	128.99	1.68	3.32	197
Match 10	47.10	152.41	2.82	11.16	216

Table 6.3. List of history matches from modified Nelder-Mead Simplex method

Chapter 7

History Matching & Forecasting : Case Study of a North Sea Gasfield

A North Sea Gasfield is now studied to check the effectiveness of the Flexi-PSO and to further investigate the uncertainty evaluation conclusions of the ICF model case study. It could be that since the ICF model has a very difficult fitness landscape and quite a simple cross-sectional grid that the uncertainty results are anomalous to it, hence further research into a real field model is warranted.

A Gasfield that Shell operates in the North Sea is selected for this case study. To be able to meaningfully assess the performance of the Flexi-PSO on history matching this real field model, a set of modifiers and a respective set of values are defined as the truth case for the model. The model is then run for ~ 4 years and this production regarded as the truth case history. The Flexi-PSO is then unleashed on the model modifiers with predefined ranges and the fitness history is then analysed and clustered to isolate a final set of matches to be taken into forecasting. A synthetic model like this is much more useful than matching to true production data since there is no way of evaluating whether the forecasts from the matches obtained will in fact encapsulate the true future production.

7.1. Field Description

This is a clastic reservoir with combined structural and stratigraphic traps. There is some internal faulting but the faults do not compartmentalise the reservoir. The sands were deposited in a sand-rich turbidite system. The reservoir section is subdivided into 4 lithostratigraphic units (E – laterally variable thin heterogeneous, D – laterally extensive massive sand, C – laterally extensive mudstone rich heterogeneous & A – laterally restricted sand rich) as in Figure 7.1. The bulk of the gas occurs in Unit D, which, with high overall net/gross, porosity and permeability, has excellent reservoir quality. The mud-rich Unit C is expected to mitigate against bottom-water influx, so that most of the water drive is expected to come from edge aquifers. The reservoir production mechanism is gas expansion drive supplemented by aquifer influx.

The fluid is a fairly dry gas with very little liquid dropout at the facilities. There are five vertical, partially penetrated wells, all completed in the E and D units. In this study, a set of modifiers are taken as the truth case (Table

7.1) which in fact reflect the real uncertainty in the field. The production rates used in the history match are derived from the real production as well.

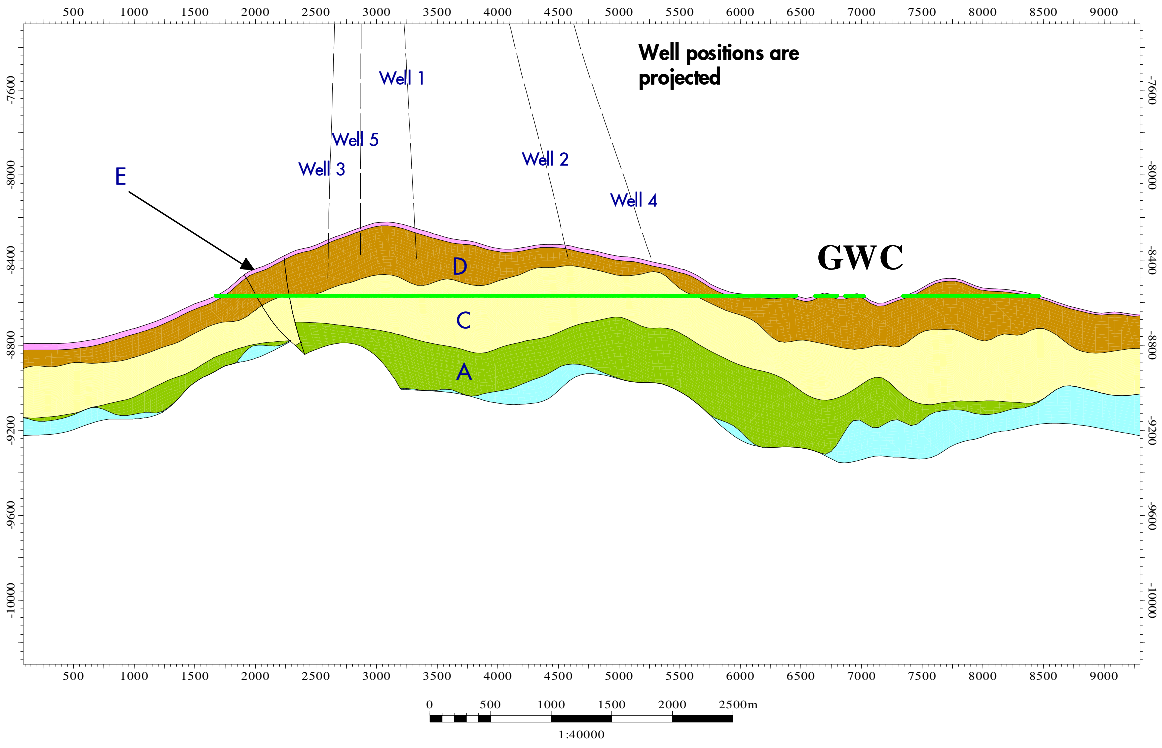

Figure 7.1. Lithostratigraphic x-section of the reservoir

Since primary depletion is the main drive mechanism, a pore volume multiplier is applied to the synthetic case (PV mult). A vertical transmissibility multiplier is also applied to the main D unit to accelerate the flow vertically and exacerbate any effect of coning (CTRZ Dsand). An integer variable is applied to the connectivity between the C & D units with the default being no connectivity (CTR CD). Since gas expansion is the primary drive mechanism, the connected volume would play an important role.

History Match Modifier	Min	Max	Truth
PV mult	0.8	1.2	0.9
CTRZ Dsand	20	50	45
CTR CD	0	1	0
AQFW Length	20000	50000	45000
AQFE Length	15000	35000	20000
AQFW Perm	50	300	250
AQFE Perm	400	800	650
Rock Compr.	2e-6	5e-6	3e-6
Res. Gas	0.1	0.25	0.14

Table 7.1. History Match Modifiers and their range

There are linear finite analytical aquifers attached to the grid on the western and eastern flanks of the field and their respective lengths and permeabilities are a source of uncertainty (AQFW Length, AQFE Length, AQFW Perm, AQFE Perm). Rock compressibility is thrown into the history match as a red herring to test whether the Flexi-PSO would concentrate its efforts on this variable. Finally the residual gas saturation is added to add to the effect of the primary drive mechanism as it affects the movable gas volumes. The simulator automatically scales the relative permeability according to whatever residual gas saturation is specified at initialisation.

A One-Parameter-at-a-Time (OPAT) sensitivity test is run on all the variables to get an initial gauge of the effect of each variable on the gas production. Figure 7.2 displays the tornado chart for this sensitivity analysis where the base case is taken as the mid-point of the modifier range. The production is especially sensitive to the pore volume multiplier and intuitively this makes sense as the gas volume is the main driving force in the system. The connectivity of the C & D units also appears to play a role, as this naturally would add more connected volume to the system.

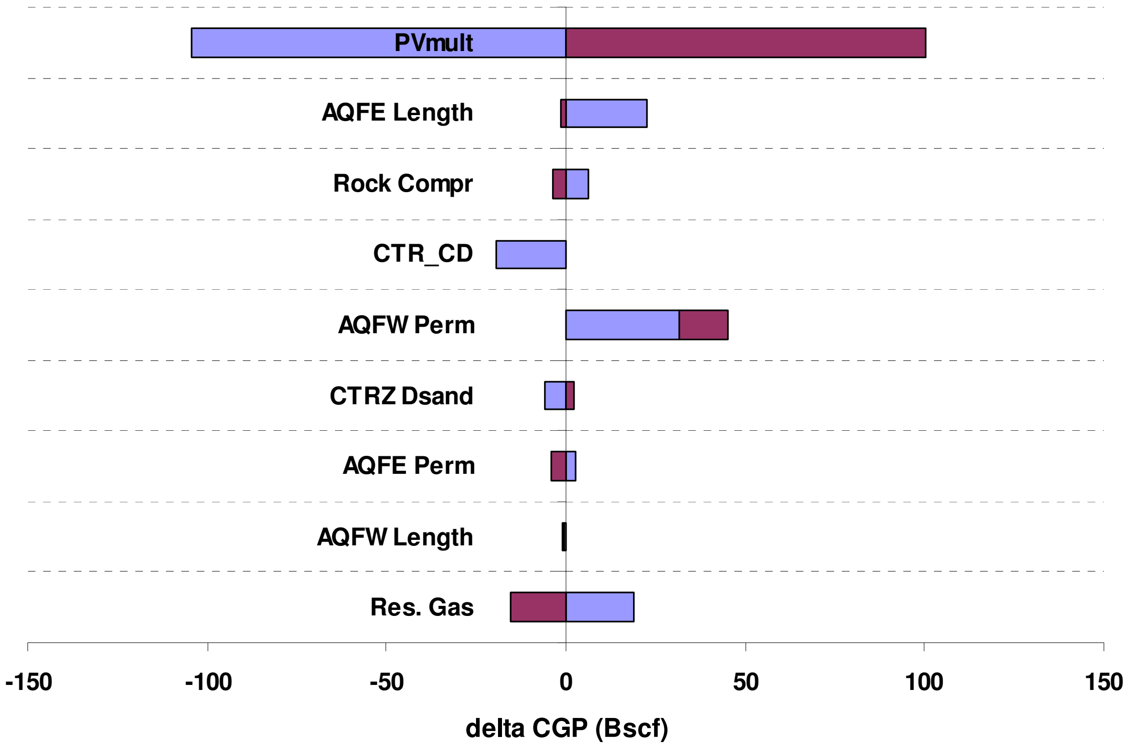

Figure 7.2. Tornado plot of OPAT sensitivity

The Faure Sequence presented in Chapter 6.1 is also useful as a designed experiment (since they are evenly space filling) to quickly screen variables and have a relative idea of their effect. Trends in the effect of variables can also be ascertained and variables with little/no effect can be discarded at this stage. To this end, one hundred runs were set up within the ranges specified in Table 7.1. Figure 7.3 shows the results of these runs.

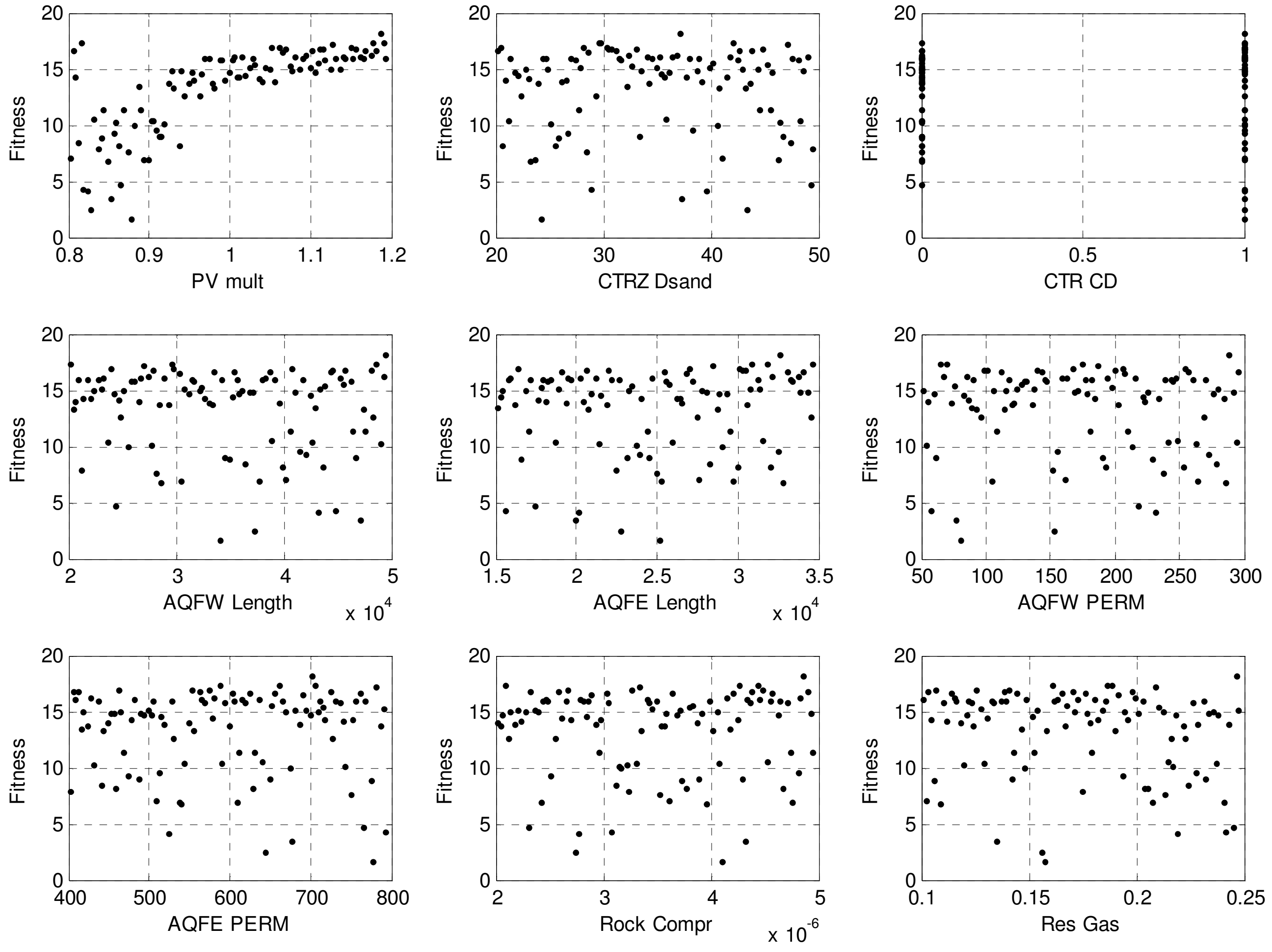

Figure 7.3. Faure Sequence “designed experiment”

Figure 7.4 plots the relative effect of each variable on the fitness using the well known correlation function (7.1.1) (μ - mean, σ- standard deviation).

$$\rho = \frac{\frac{1}{n}\sum_{i=1}^{n}(x_i - \mu_x)(y_i - \mu_y)}{\sigma_x . \sigma_y} \tag{7.1.1}$$

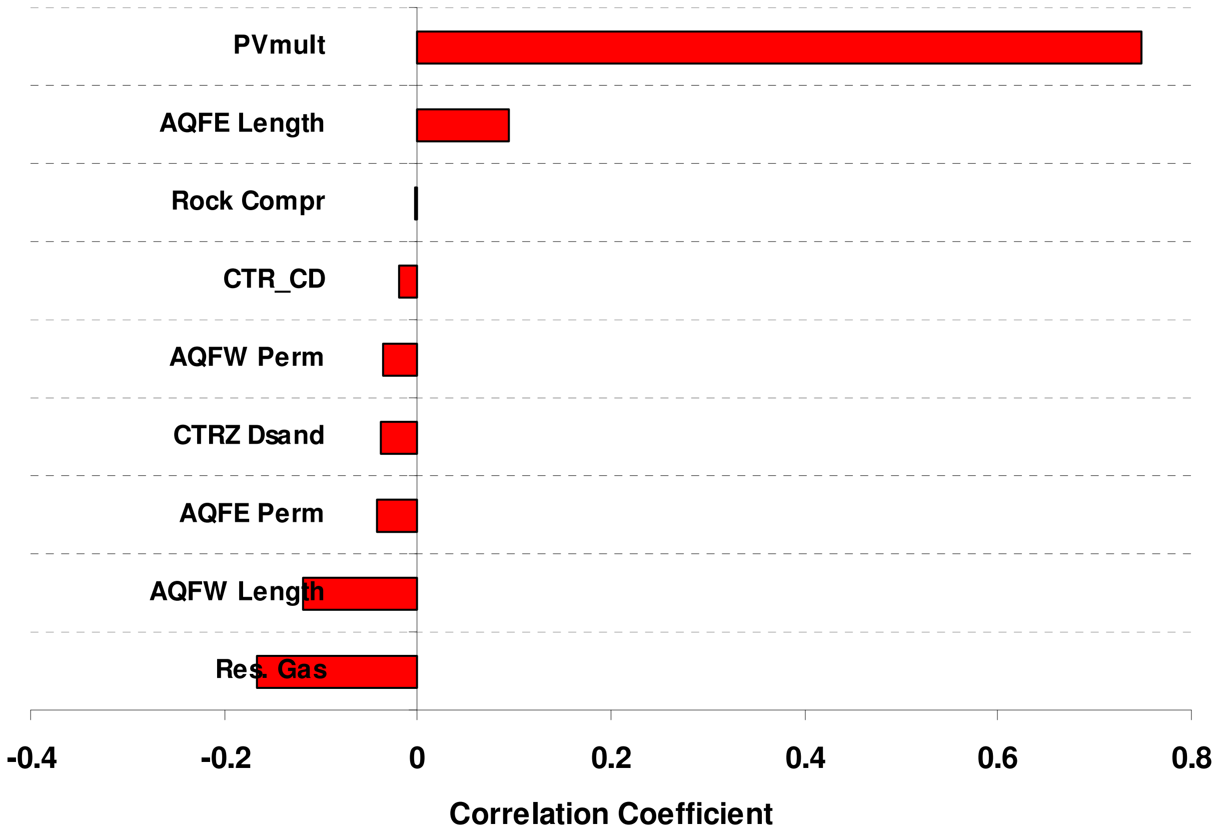

Figure 7.4. Correlation of each variable to fitness from Faure Sequence designed experiment

As expected the pore volume multiplier and residual gas saturation show a larger effect than the other variables. The aquifer properties also play a role while the rock compressibility plays little effect since the gas compressibility dominates.

There are ~ 170 000 gridblocks in the model with ~ 53 000 active. Figure 7.5 is a water saturation gridview of the model at an arbitrary point in time.

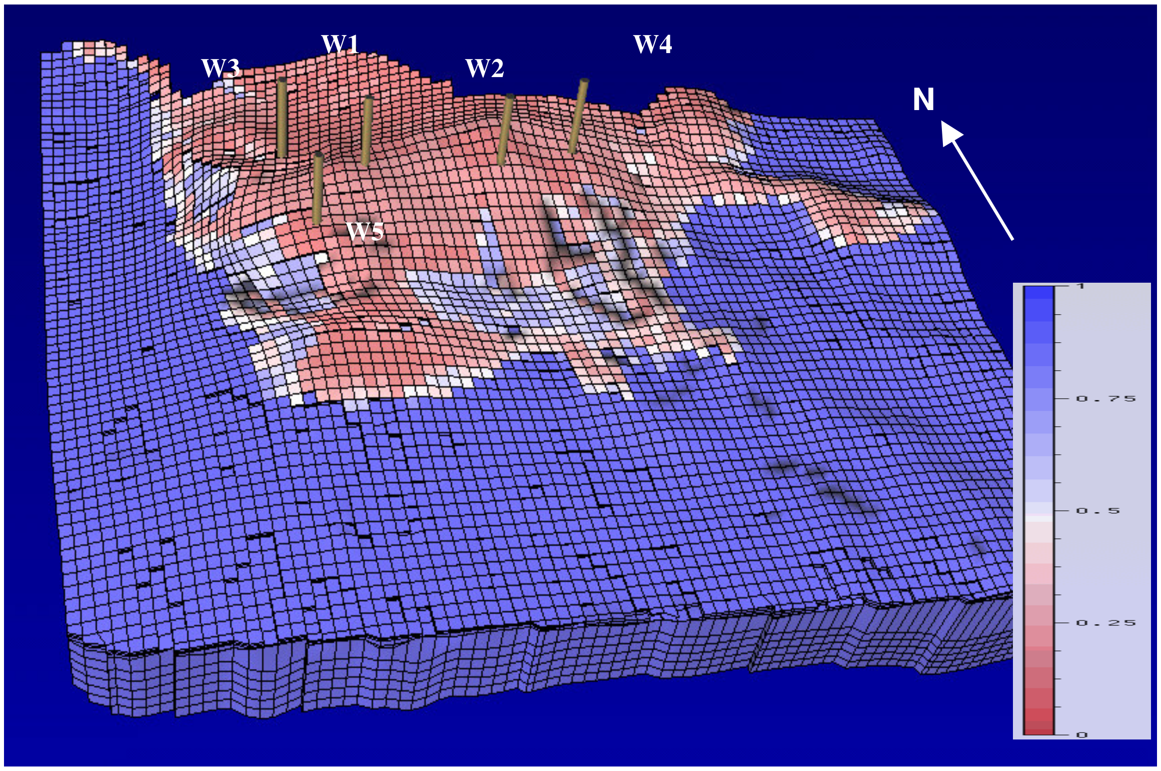

Figure 7.5. Overall S_w gridview of the model

7.2. Results and Discussion

The simulator used is MoReS (Shell proprietary). The Flexi-PSO was set up in the same way as in the ICF Model case study with a population of 20 particles and 50 iterations. Each run took about three hours and distributed over a cluster of CPU's the entire Flexi-PSO run took six days to complete.

All matches with RMSE less than 1 were considered acceptable from a visual judgement of the history match versus production plots. There were 50 acceptable matches, which were then clustered into 10 groups using average linkage hierarchical clustering. The match with the lowest fitness in each group was then taken forward into forecasting. Table 7.2 presents these final matches.

It is encouraging to note that the Flexi-PSO has performed well on this mixed-integer problem with all the acceptable matches having no transmissibility between the C & D units as in the truth case.

	PVmult	CTRZ Dsand	CTR_CD	AQFW Length	AQFE Length	AQFW Perm	AQFE Perm	Rock Compr	Res. Gas	Fitness
Truth	0.9	45	0	45000	20000	250	650	3e-6	0.14	0
Match 1	0.952	29.46	0	41249	34384	116.14	465.71	4.26E-06	0.158	0.813
Match 2	0.943	23.92	0	43293	25611	104.46	518.18	4.48E-06	0.151	0.239
Match 3	0.940	27.09	0	47665	29593	112.41	514.12	3.51E-06	0.135	0.317
Match 4	0.940	28.71	0	39158	24162	155.06	588.34	3.67E-06	0.164	0.768
Match 5	0.951	34.01	0	28844	23173	98.62	634.53	4.14E-06	0.176	0.526
Match 6	0.935	35.76	0	26781	23856	163.16	566.98	3.94E-06	0.166	0.439
Match 7	0.962	22.15	0	30491	33770	119.33	546.00	3.87E-06	0.150	0.932
Match 8	0.964	39.58	0	21796	28192	105.20	561.41	4.13E-06	0.200	0.871
Match 9	0.948	21.59	0	27098	22328	131.82	756.51	3.77E-06	0.158	0.887
Match 10	0.930	25.44	0	25547	22377	235.35	732.47	2.72E-06	0.168	0.771

Table 7.2. Final set of history matched models

Figure 7.6 displays the fitness history of the Flexi-PSO. The restarts are highlighted where the sequential niching process takes effect. The range of each niche is set to 10% of the dynamic range for each modifier. In this run there have been three restarts of the algorithm. On each restart the algorithm does reduce the fitness rapidly but still explores the search space.

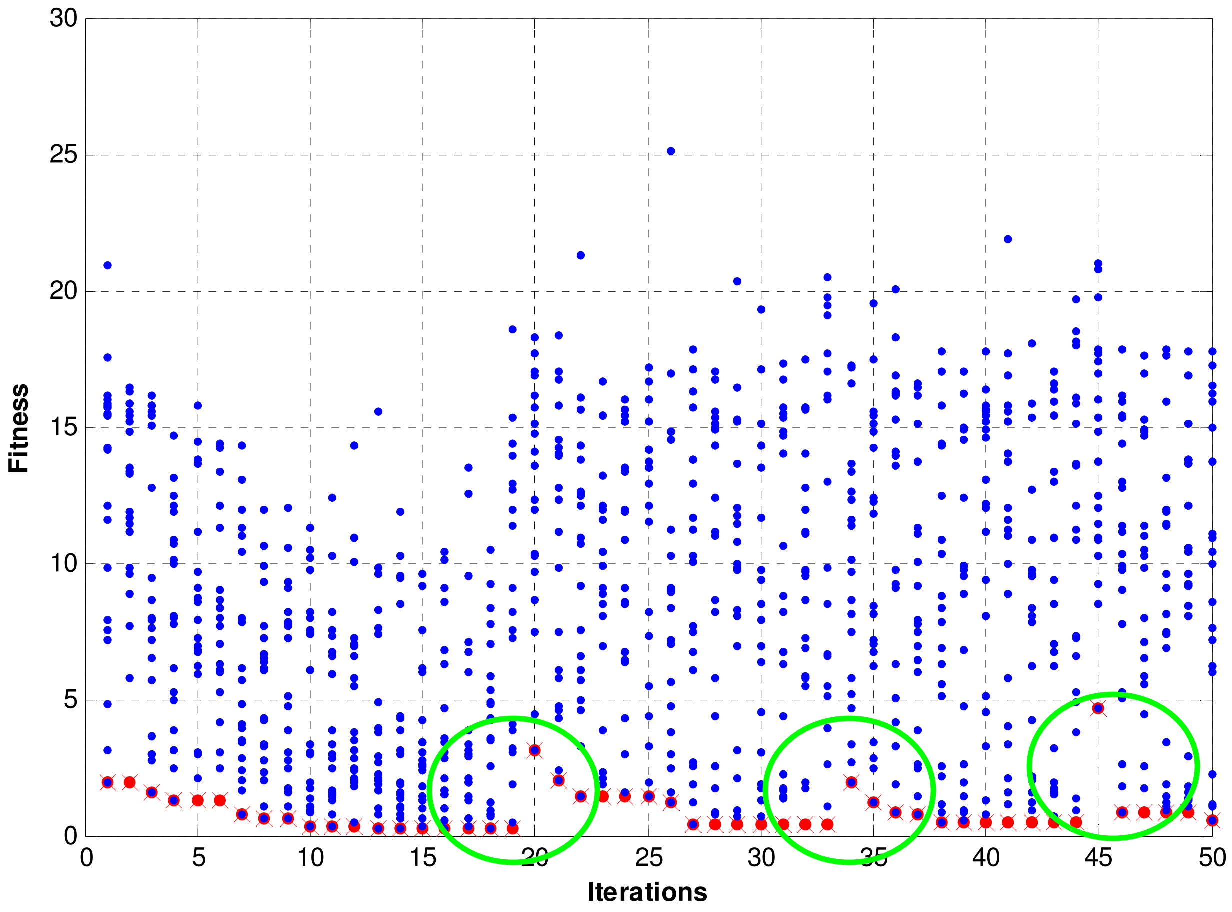

Figure 7.6. Fitness history of the Flexi-PSO (x – globalbest tracker in each niche sequence)

Figures 7.7 - 7.12 display the history match per well and field for each realisation. The history period starts at 01/11/2004 and ends at 01/03/2008 (demarcated on each plot). The forecast ends at 01/01/2011. To make the forecasting more challenging in terms of uncertainty modelling, it is assumed that the production facilities can no longer handle any more water throughput. In this way, the forecasts can now be analysed with respect to the truth case to see whether they do encapsulate it and if so, how wide is the forecasted uncertainty band. The forecast has a surface pipeline network with a compressor attached to it. The compression logic built into the deck states that whenever the tubing head pressure drops below a certain threshold, the compressor speed is then ramped up to compensate for this pressure drop which in turn leads to an increase in production.

Figure 7.7 shows the matches to Well 1 to be acceptable. Each match is able to produce the rates and track the flowing bottomhole pressure. The truth case forecast for this well is interesting as it is around 20 Bscf away from the ensemble as the truth case produces for a much longer duration that the rest of the cases. In Figure 7.8, the matches to Well 2 are also acceptable, with the flowing bottomhole pressure being tracked quite nicely. This well shuts in at the end of 2008 and hence its no surprise then that the ensemble does capture the truth case for the cumulative production for this well. In Figure 7.9, the matches to Well 3 are all acceptable with a slight deviation of the ensemble to the flowing bottomhole pressure near the end of history. The truth case for this well shuts in before the rest of the ensemble and hence has a cumulative production below the range of the ensemble.

In Figure 7.10, Well 4 has acceptable matches to the gas production and bottomhole pressure. This is the only well in the history that does produce water and its water production rate is in Figure 7.10. The ensemble does encapsulate the water production, but there is quite a wide uncertainty band (~ 3400 bbl/d to ~ 4200 bbl/d). In Figure 7.11, Well 5 has acceptable matches with the flowing bottomhole pressure deviating slightly towards the end of the history. The truth case shuts in before the rest of the ensemble and hence this well has a cumulative production that is lower than the ensemble. All the wells show an upturn in the bottomhole pressure towards the end of the forecast. This is due to the continuous charging of the reservoir from the aquifers.

In Figure 7.12, the ensemble does encapsulate the cumulative field production but not the field rate. This is because Well 1 continues to produce much later in the truth case than the history match cases. The results of this gasfield study are in stark similarity to that obtained with the ICF Model. Once again, we are faced with the likelihood that the ensemble will not be able to encapsulate the range on the production rate, but for the field as a whole it is more likely that the ensemble will encapsulate the truth case for the cumulative production. The reason for this is simple.

Lets assume we have a set of realisations, the only difference between them being pore volume multipliers while all other parameters are held constant. In this case, when the realisations are simulated the “likely outcome” will be a forecast range that is proportional to the pore volume multipliers. If we have a set of realisations that have similar volumes but differing properties, the “likely outcome” is that they will all produce similar forecasts in terms of the overall volume drained from the reservoir. As in this North Sea Gasfield study, the truth case sees Well 2 and Well 3 water out earlier than the history matches, but Well 1 sees more production than the history match cases as it now has a greater volume available to drain. Hence the reason for the fairly tight forecast envelope on the cumulative gas production.

It is important to note here that even with a perfect structural model, correct set of uncertainty parameters, ranges that cover the truth case and perfect measurements, as well as a set of excellent history matches, that the truth case production still cannot be encapsulated for the wells when forecasting! This makes the case for using uncertainty modelling to identify infill drilling targets somewhat tenuous. (Millar, 2005) quotes an example of an oil major identifying an infill location as being better than two other targets with similar average cumulative production because its forecast envelope was narrower. If as shown in this North Sea Gasfield case study, producing wells with a good set of matches and modifiers that are appropriately conditioned to historical production cannot encapsulate the truth case production for a gasfield, it hardly seems plausible that an infill location for an oil well (where relative permeability effects are more pronounced) can be identified to be better than any other location with similar production but a narrower forecast envelope.

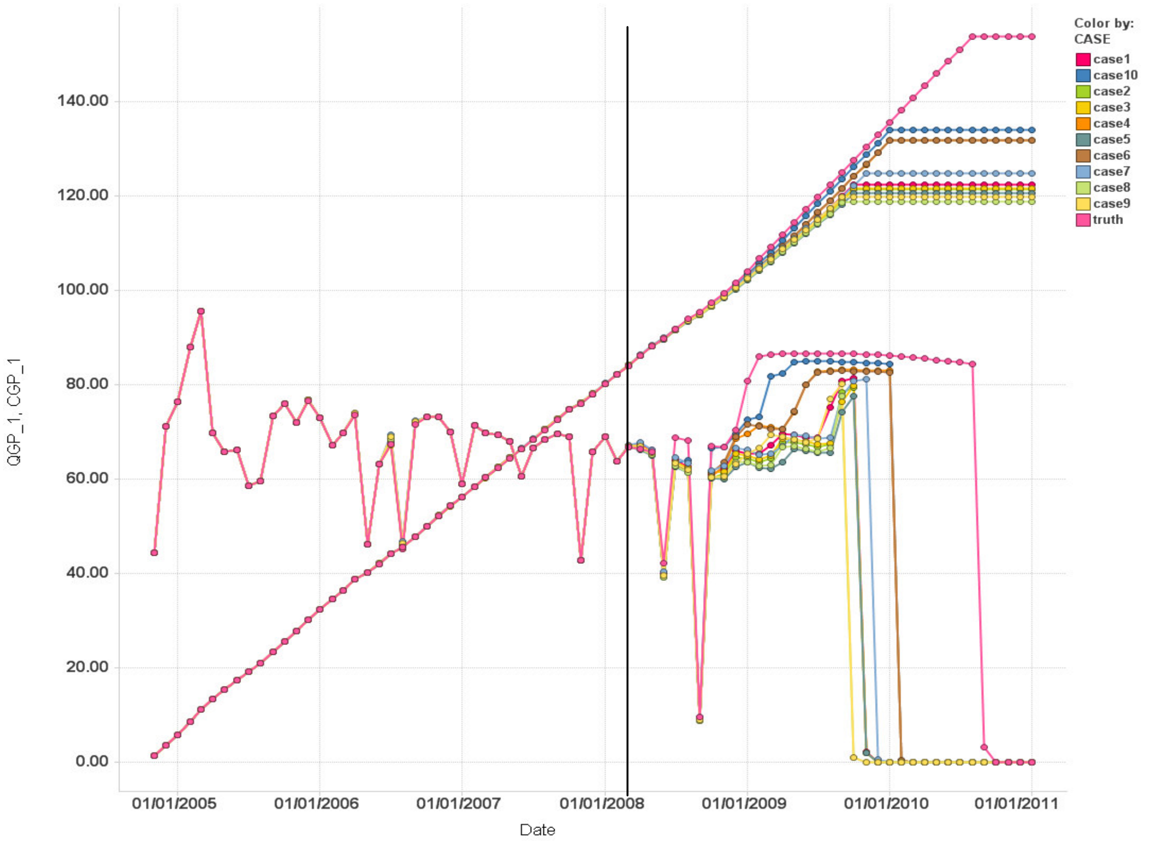

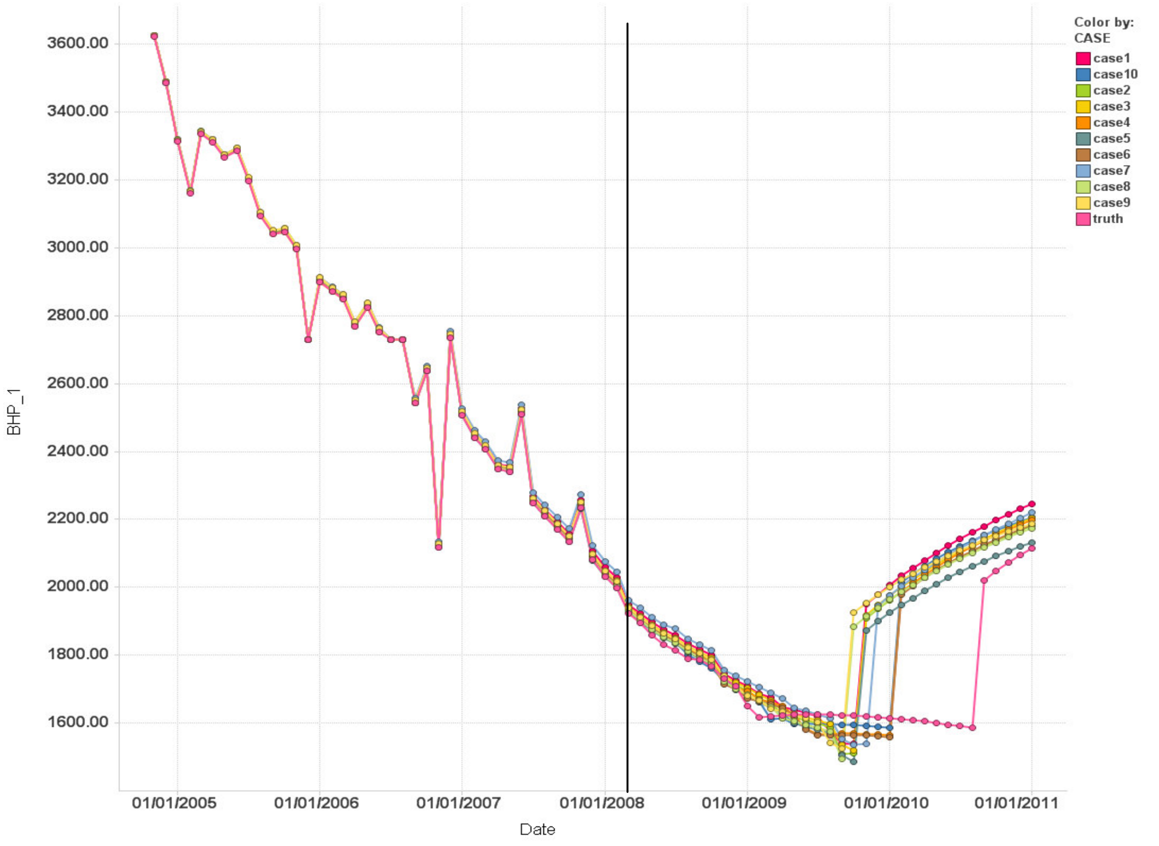

Figure 7.7. Well 1 matches (QGP – mmscfd, CGP - bscf, BHP - psia)

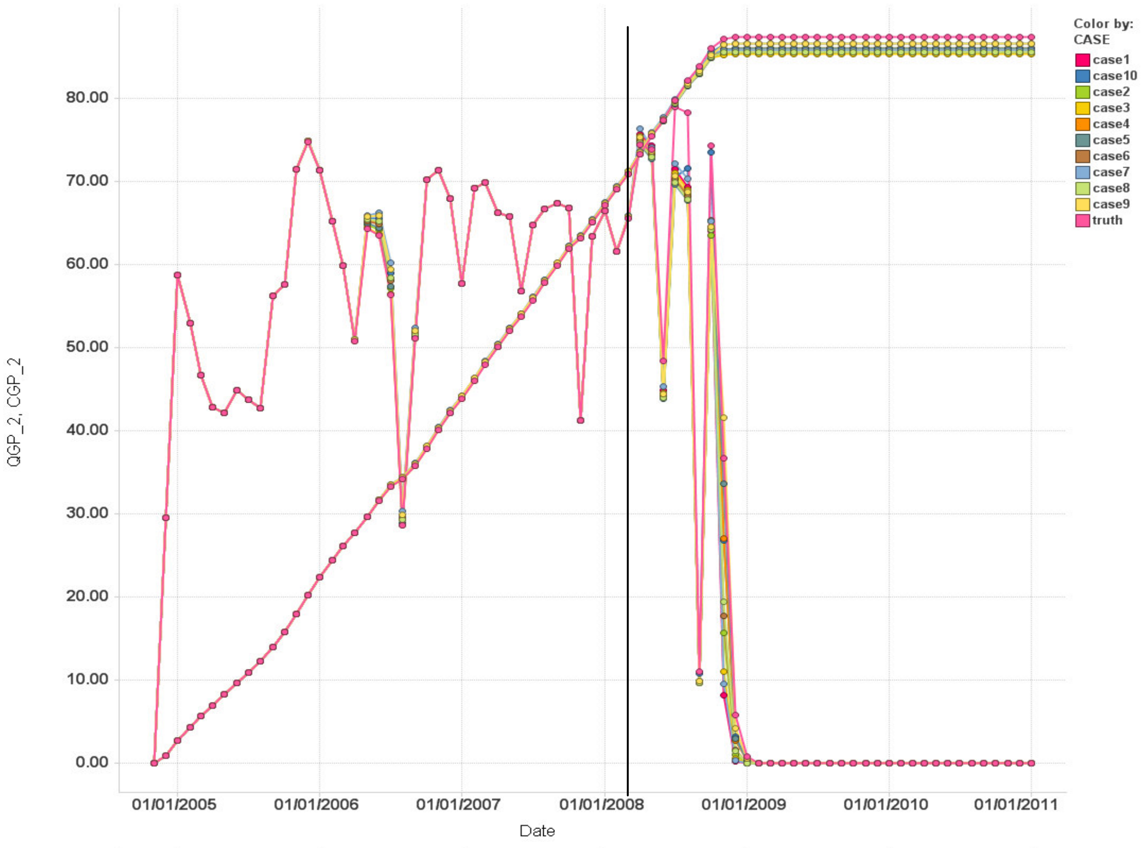

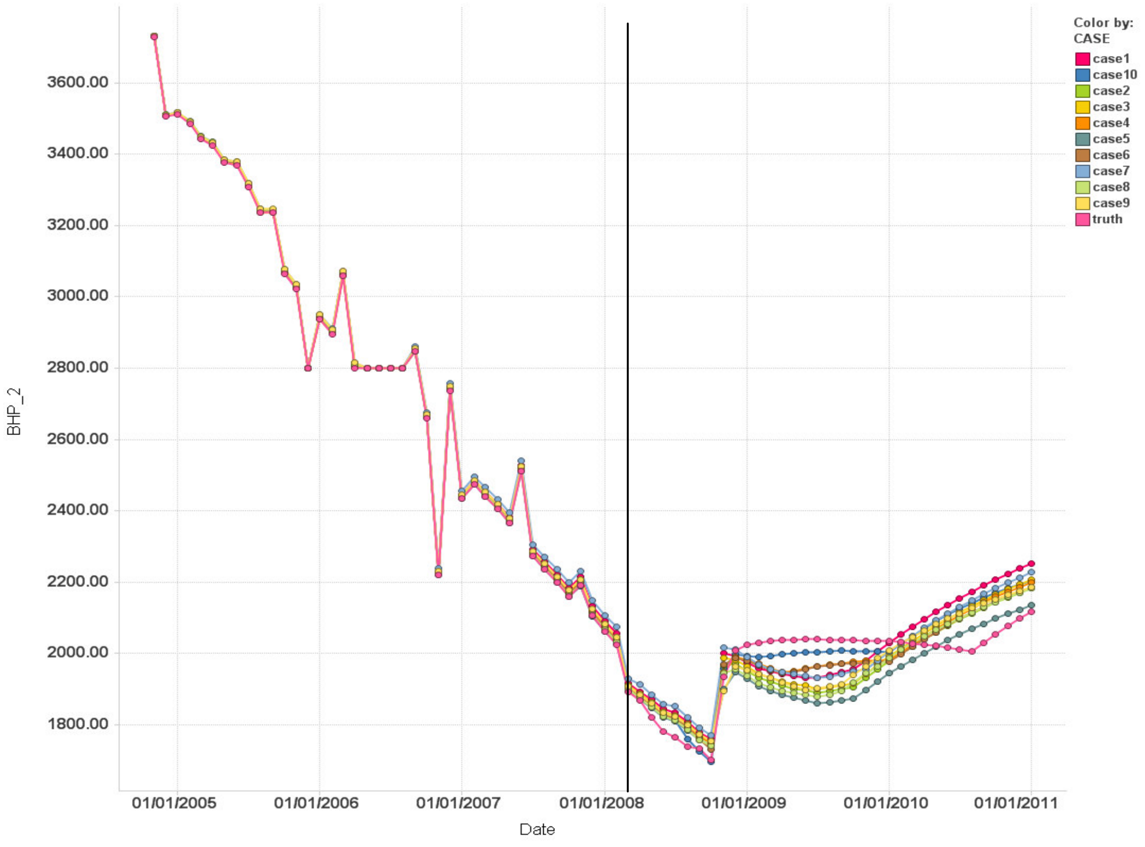

Figure 7.8. Well 2 matches (QGP – mmscfd, CGP - bscf, BHP- psia)

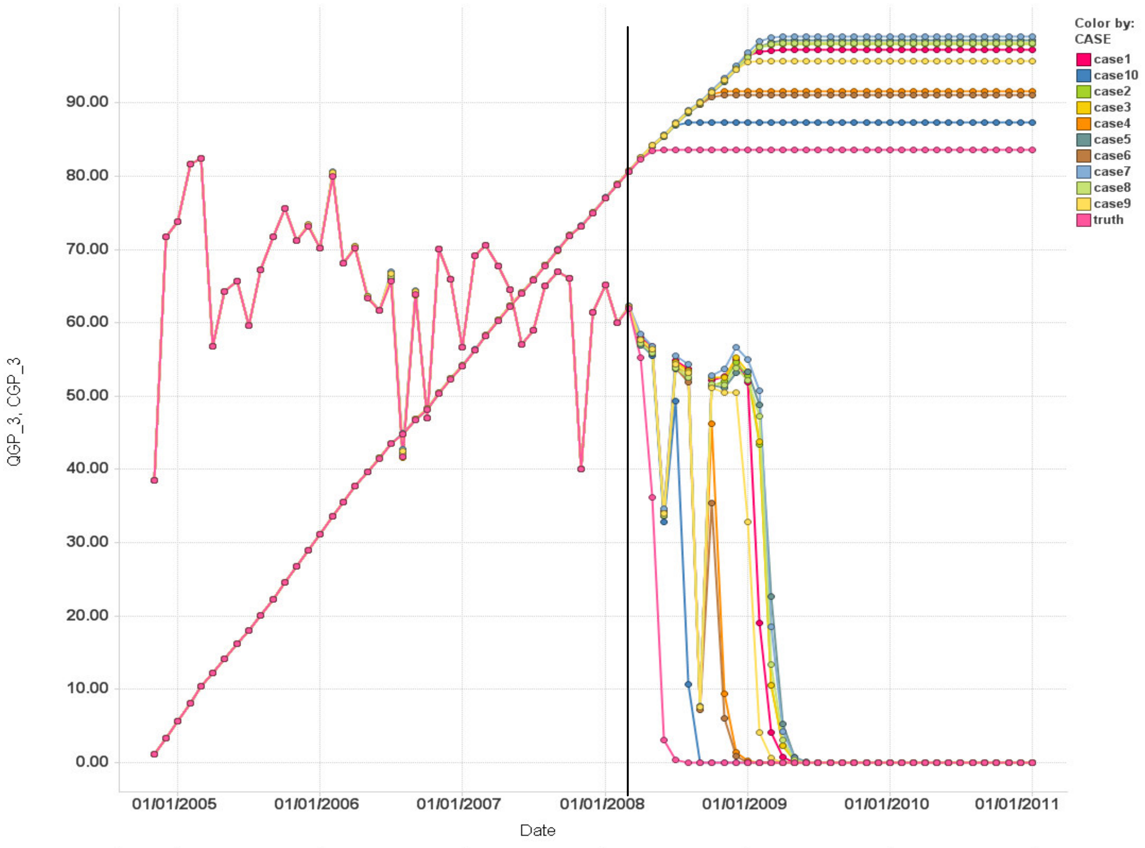

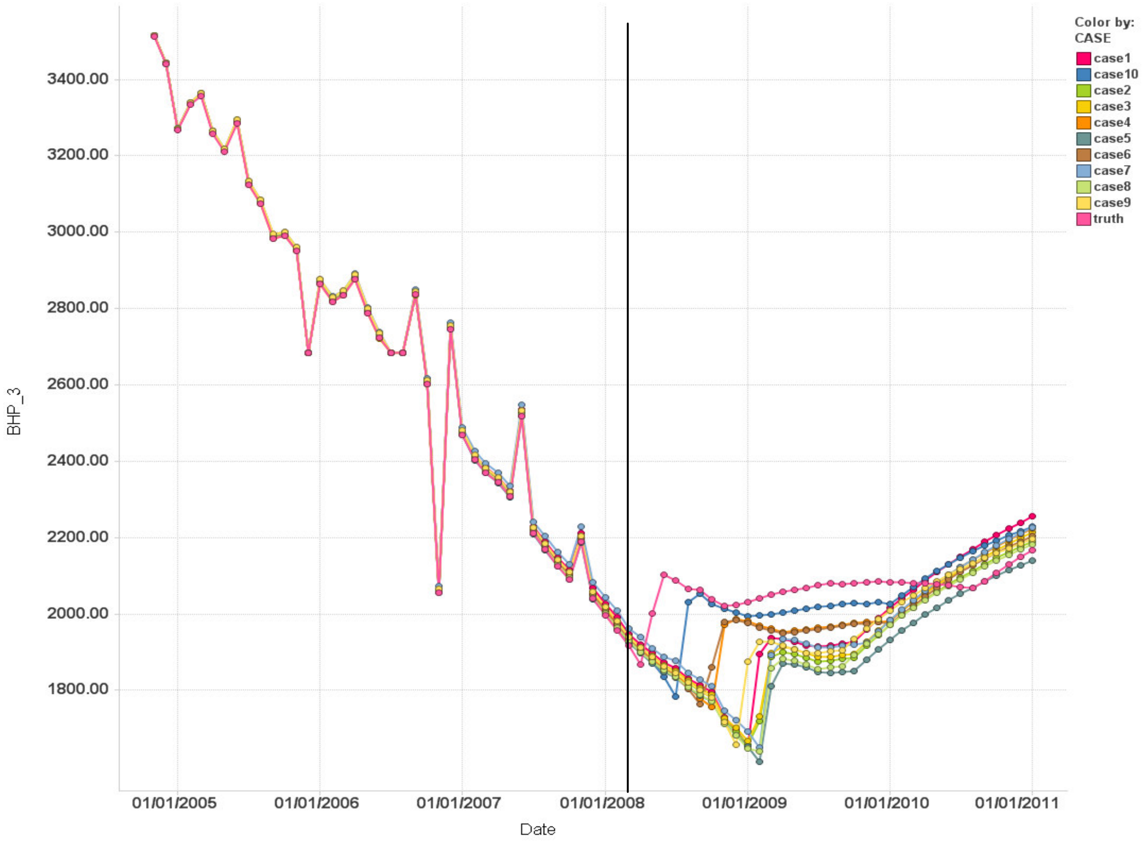

Figure 7.9. Well 3 matches (QGP – mmscfd, CGP - bscf, BHP - psia)

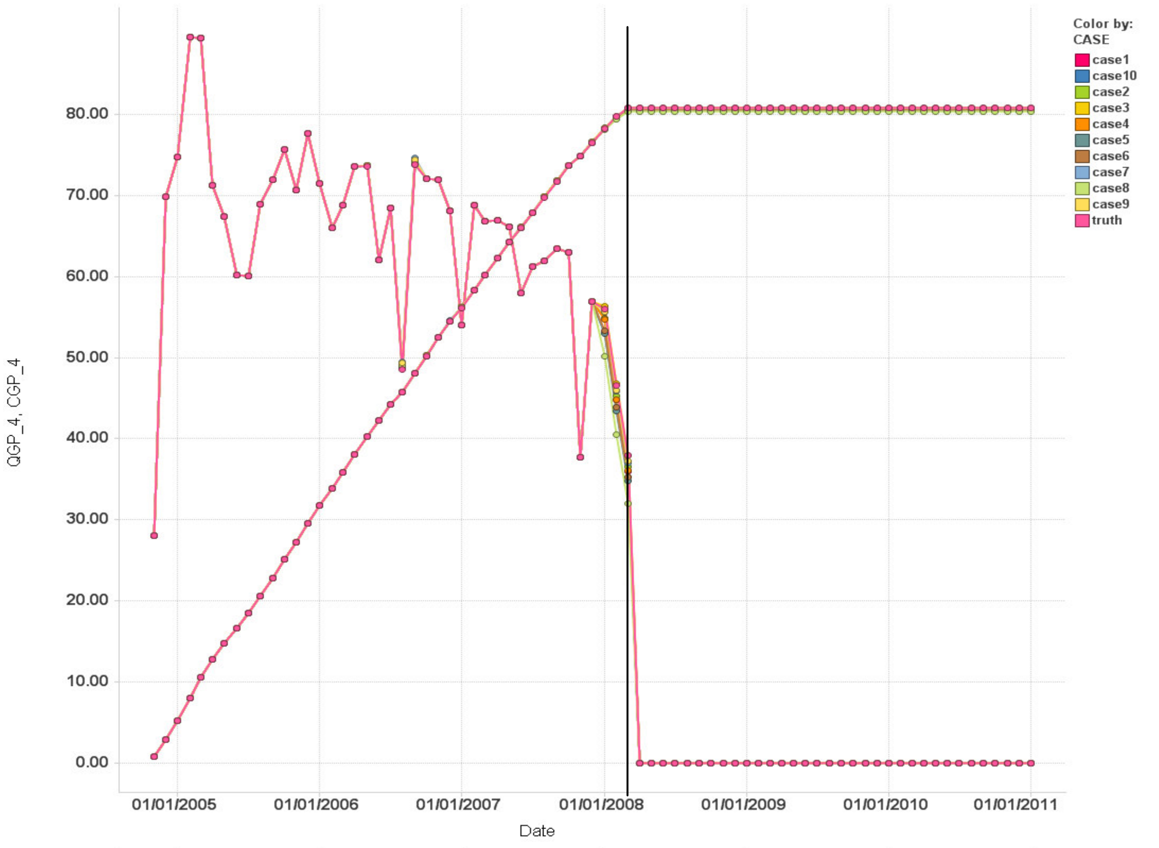

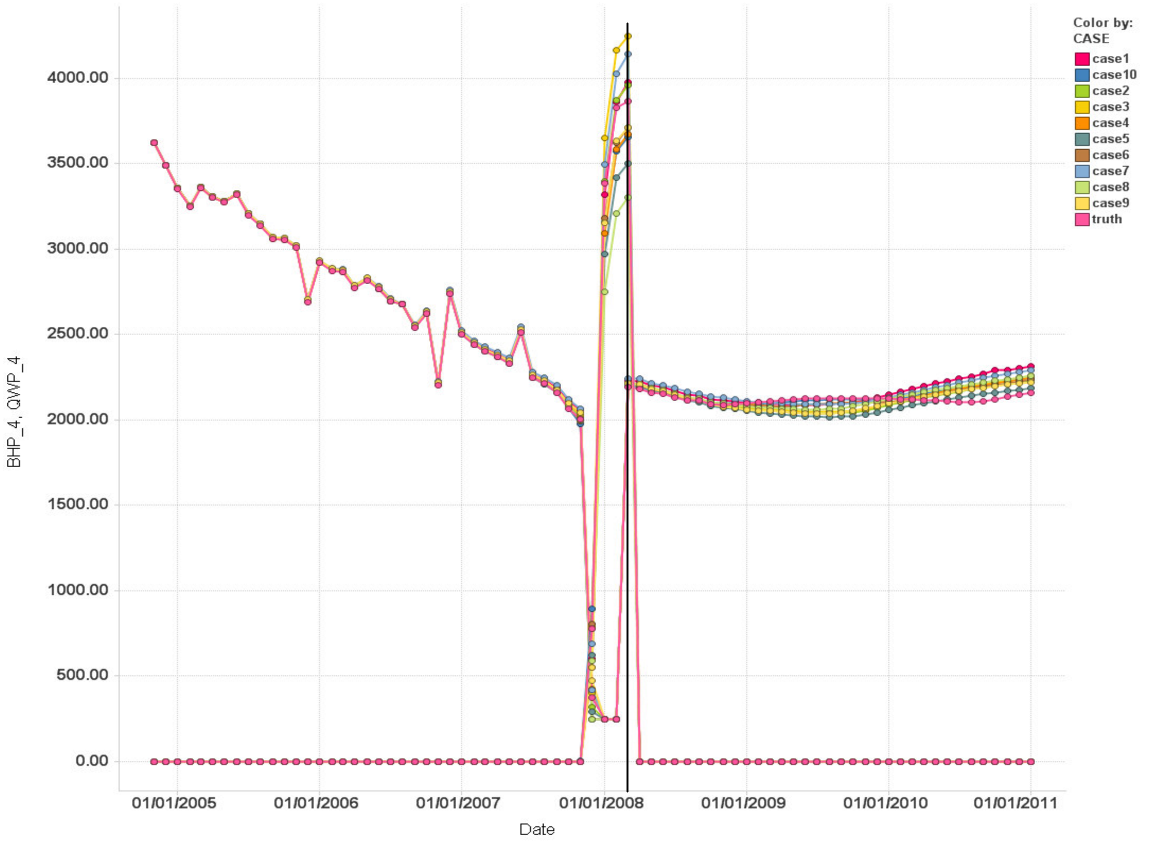

Figure 7.10. Well 4 matches (QGP – mmscfd, CGP - bscf, BHP - psia, QWP – bbl/d)

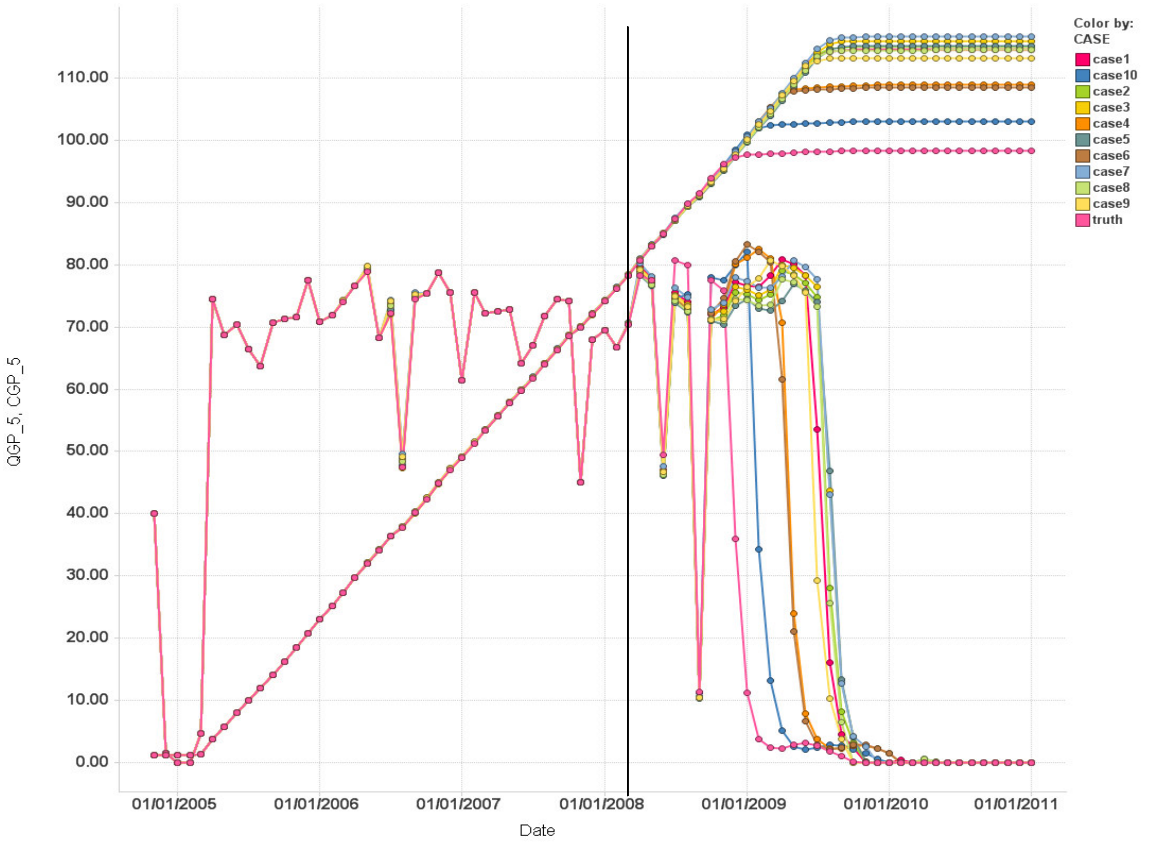

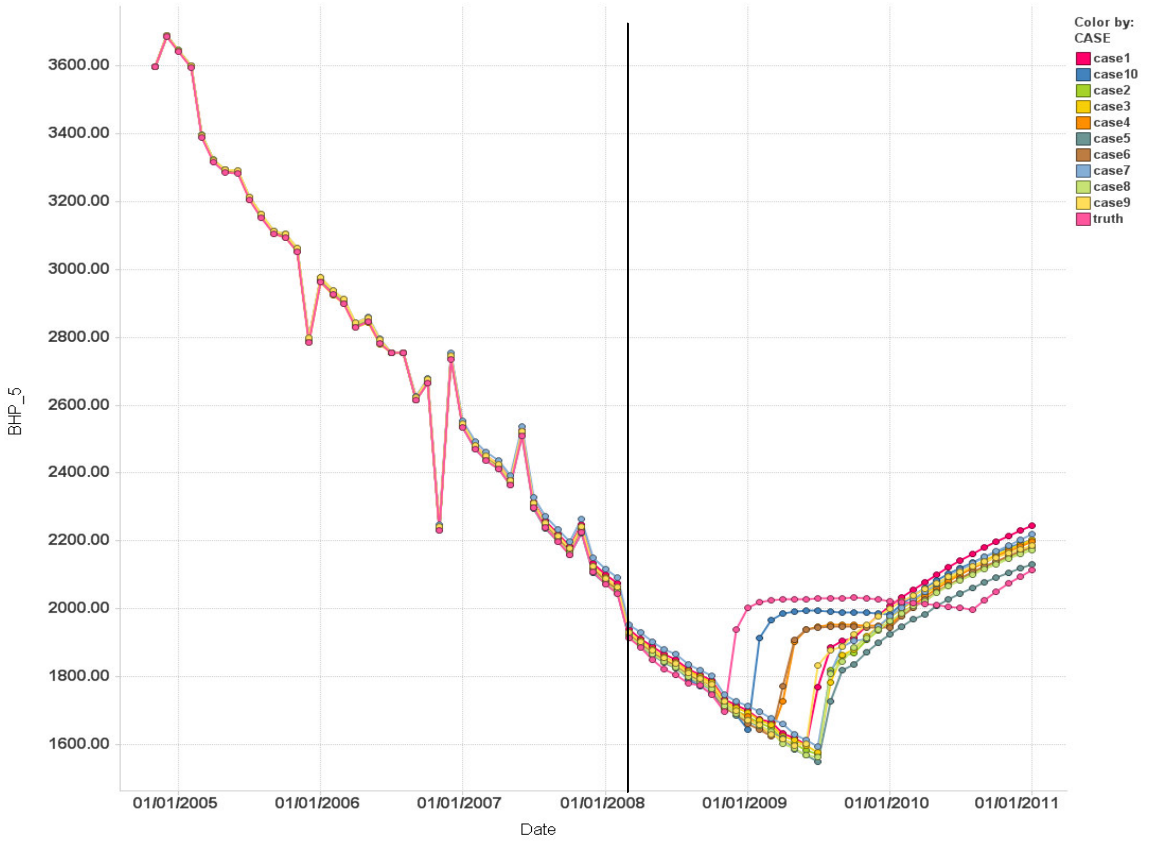

Figure 7.11. Well 5 matches (QGP – mmscfd, CGP - bscf, BHP - psia)

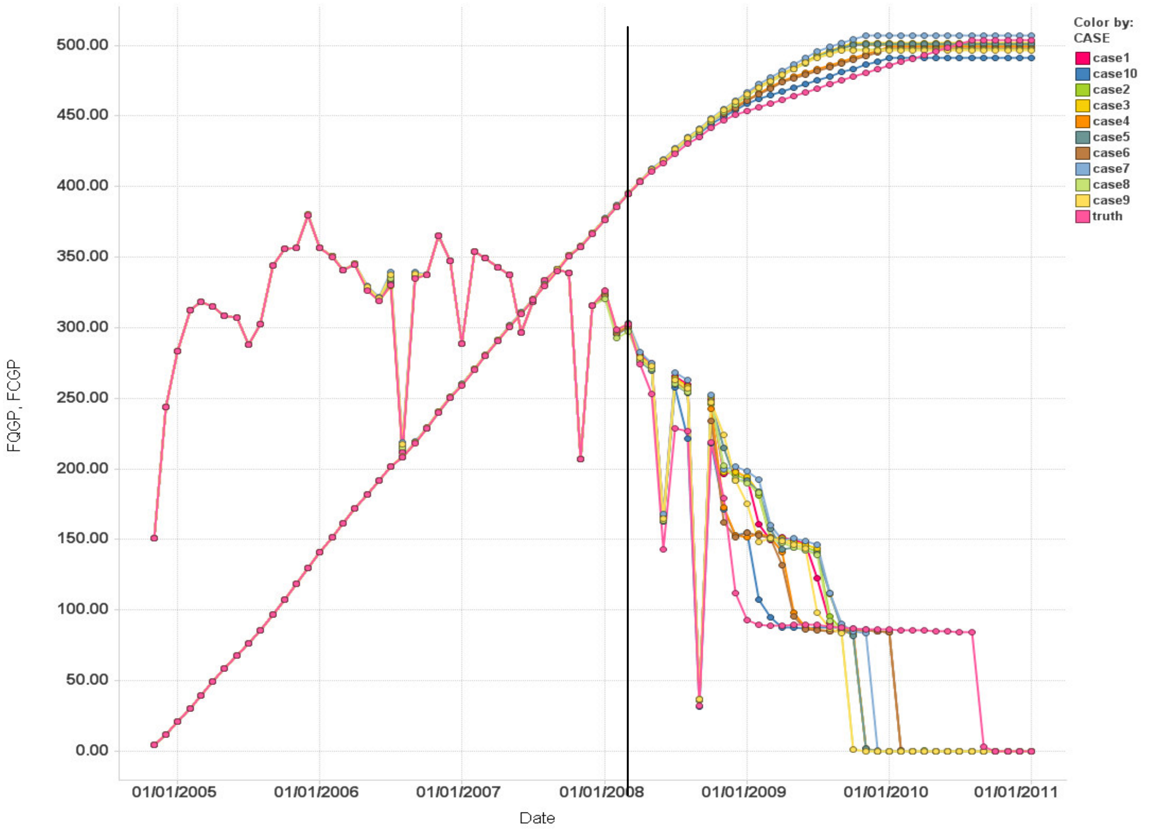

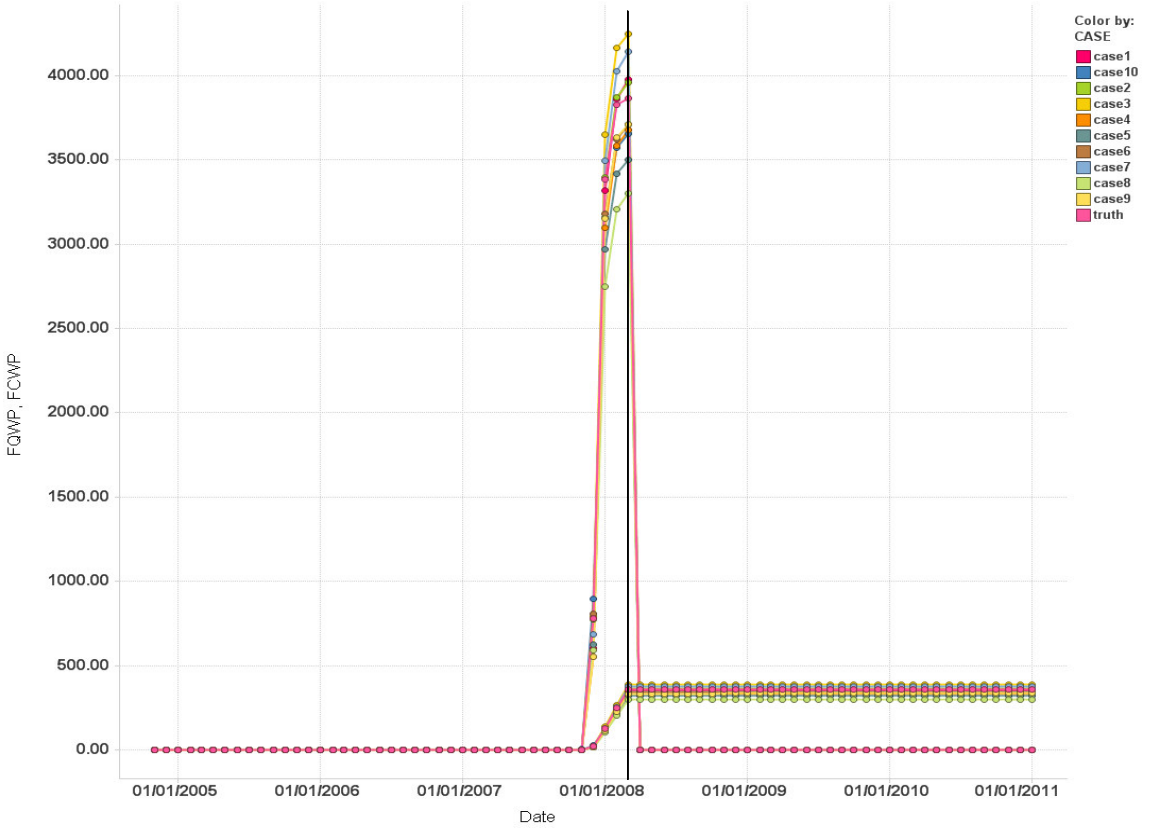

Figure 7.12. Field matches (QGP – mmscfd, CGP - bscf, QWP – bbl/d, CWP - mbbl/d)

CONCLUSIONS

Chapter 8

Conclusions

The theme of this thesis has been to examine key issues that we are faced with in history matching and try to develop an effective workflow in the history matching process that will generate meaningful results to practising reservoir engineers. In this regard, the focus is on further advancements in the area of assisted history matching. The key areas that this thesis contributes to can be summarised as follows :-

- Introduction of Particle Swarm Optimisation to the oil industry
- Understanding the effects of the parameters in the Particle Swarm Optimiser
- Development of a state of the art variant of the Particle Swarm Optimisation algorithm for history matching purposes (Flexi-PSO)
- Techniques of post-processing an assisted history match run
- Insight into the possible implications of the results of an uncertainty modelling exercise

Particle Swarms are a novel optimisation technique and are used in this thesis to history match finite difference reservoir simulation models. Particle

Swarms form part of the so-called evolutionary class of optimization algorithms that are population based and use various communication mechanisms to move towards optimal solutions. This is the first known implementation of particle swarms in the oil and gas industry and has been successfully applied to the Imperial College Fault Model to locate distinctly different history matches.

Particle swarms if designed properly can be very effective in moving through the search space and are effective in balancing global exploration and local exploitation. In this regard, a particle swarm variant dubbed “Flexi-PSO” has been specifically created that can quickly locate multiple niches and also handle multiple static realisations or discrete parameters. The motto behind the Flexi-PSO is “Big moves coupled with small moves”. This theme enables the swarm to scan niches more thoroughly and the reason behind its success in dealing with benchmark mathematical functions and the history matching case studies presented. The reason for this is that in the canonical and inertia weight versions of the PSO, particles concentrate on doing a global search and have high velocities from the outset which can lead to a particle that may be in a niche that contains the global optimum to fly out of that region. The Flexi-PSO reduces that possibility by enabling particles to also make local searches during the course of the run.

Before any optimisation algorithm can be deployed, it is best to test it against a wide range of problems to assess its robustness, and in doing so any shortcomings of the algorithm can be addressed. This thesis interrogated the Flexi-PSO with convex and highly non-convex mathematical functions, a neural network and integer problems. The Flexi-PSO is shown to have comparative efficacy as current state of the art algorithms. The algorithm is further modified to increase its effectiveness in dealing with multimodal problems via a sequential niching routine, which has shown to be effective in locating multiple optima.

The Flexi-PSO is then used to history match the Imperial College Fault Model and returns a match that is very close to the truth case, however this is not the case on every single run as was shown when function stretching was applied to niches. The results of the history matching procedure do require some post processing. A simple graphical approach combined with hierarchical clustering can be used to narrow down a final set of realizations to carry forward into prediction.

Even with the best algorithms and methods of processing results, it is still imperative to understand that the model is not a perfect reflection of the reservoir properties. This thesis shows that even with a highly effective algorithm like the "Flexi-PSO", the ensemble of matches that we are left with (even with one match that is very close to the truth case), there is no guarantee that their predictions will cover the true reservoir behaviour.

It is useful that unlike unstable systems in chaos theory which have a multiplicative effect if the starting point is incorrect and leads to less accurate behaviour over time, petroleum reservoirs are dissipative in energy and cumulative production predictions tend to flatten out the longer the prediction is in time. In this regard an ensemble is likely to create a prediction envelope that will cover the truth case with regards to field cumulative production (provided that the initial volumes in place are representative), however it is less likely that it will do so for well production rates.

The Flexi-PSO is then used to history match a synthetic version of a North Sea Gasfield. The results of this case study are indeed very interesting. Although the Flexi-PSO has successfully managed to find multiple matched cases, the matched cases in fact point to an interesting insight into evaluating uncertainty. All the history match cases have similar volumes in place and their narrow forecast range does encapsulate the cumulative production of the truth case. However, as was observed in the ICF Model case study, the same cannot be said of the production rate. It becomes even more interesting on a well level, where we see that it is much more difficult for the ensemble to track the truth case production. In this case where wells are being shut in due to the limit on the water handling capacity, the remaining gas volume is then left available for other wells to drain.

Essentially, it appears that the wider the hydrocarbon in place volume range there is from a set of history match realisations, the wider it can be expected the reserves forecast will be. For a narrow in place volume range, the wells will compete for production and wells that are shut-in will just leave more volume for the remaining wells to access.

As shown in the North Sea Gasfield case study, producing wells with a good set of matches and modifiers that are appropriately conditioned to historical production cannot encapsulate the truth case for a gasfield, it hardly seems plausible that an infill location for an oil well can be identified to be better than any other location with similar production but a narrower forecast envelope. This criteria needs to reviewed very carefully, and other environmental factors should be called into account e.g. drilling cost when making a final decision.

In short any history matching exercise requires a good optimisation algorithm together with post processing of results to take meaningful realisations forward into prediction. The end result is as is commonly quipped only as good as the model itself, hence some degree of common sense needs to be exercised in the allocation of time and resources with respect to any history matching exercise.

APPENDIX

Appendix A

Problem Definitions for the CEC 2005 Special Session on Real-Parameter Optimisation

Summary of the 25 Test Functions

- **Unimodal Functions (5):**
  - F_1: Shifted Sphere Function
  - F_2: Shifted Schwefel's Problem 1.2
  - F_3: Shifted Rotated High Conditioned Elliptic Function
  - F_4: Shifted Schwefel's Problem 1.2 with Noise in Fitness
  - F_5: Schwefel's Problem 2.6 with Global Optimum on Bounds

- **Multimodal Functions (20):**
  - **Basic Functions** (7):
    - F_6: Shifted Rosenbrock's Function
    - F_7: Shifted Rotated Griewank's Function without Bounds
    - F_8: Shifted Rotated Ackley's Function with Global Optimum on Bounds
    - F_9: Shifted Rastrigin's Function
    - F_{10}: Shifted Rotated Rastrigin's Function
    - F_{11}: Shifted Rotated Weierstrass Function
    - F_{12}: Schwefel's Problem 2.13

- **Expanded Functions** (2):
  - F_{13}: Expanded Extended Griewank's plus Rosenbrock's Function (F8F2)
  - F_{14}: Shifted Rotated Expanded Scaffer's F6
- **Hybrid Composition Functions** (11):
  - F_{15}: Hybrid Composition Function
  - F_{16}: Rotated Hybrid Composition Function
  - F_{17}: Rotated Hybrid Composition Function with Noise in Fitness
  - F_{18}: Rotated Hybrid Composition Function
  - F_{19}: Rotated Hybrid Composition Function with a Narrow Basin for the Global Optimum
  - F_{20}: Rotated Hybrid Composition Function with the Global Optimum on the Bounds
  - F_{21}: Rotated Hybrid Composition Function
  - F_{22}: Rotated Hybrid Composition Function with High Condition Number Matrix
  - F_{23}: Non-Continuous Rotated Hybrid Composition Function
  - F_{24}: Rotated Hybrid Composition Function
  - F_{25}: Rotated Hybrid Composition Function without Bounds

Unimodal Functions

F_1: Shifted Sphere Function

$$F_1(\mathbf{x}) = \sum_{i=1}^{D} z_i^{\,2} + f\_bias_1 \,, \mathbf{z} = \mathbf{x} - \mathbf{o} \,, \mathbf{x} = [x_1, x_2, ..., x_D]$$

D: dimensions. $\mathbf{o} = [o_1, o_2, ..., o_D]$: the shifted global optimum.

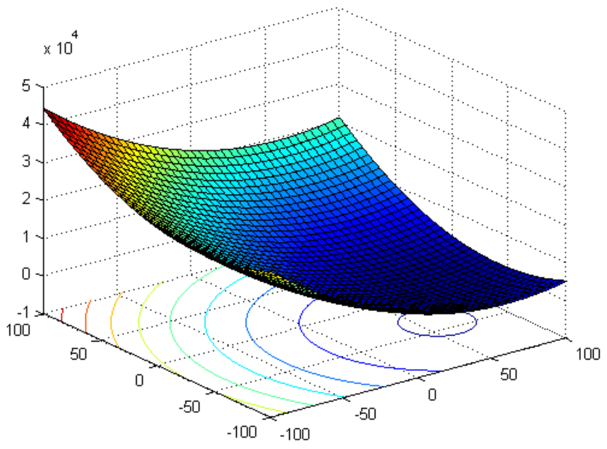

Figure A-1. 3-*D* map for 2-*D* function

Properties:

- Unimodal
- Shifted
- Separable
- Scalable
- $\mathbf{x} \in [-100,100]^D$, Global optimum: $\mathbf{x}^* = \mathbf{o}$, $F_1(\mathbf{x}^*) = f\_bias_1 = -450$

F$_2$: Shifted Schwefel's Problem 1.2

$$F_2(\mathbf{x}) = \sum_{i=1}^{D}(\sum_{j=1}^{i} z_j)^2 + f\_bias_2,\ \mathbf{z} = \mathbf{x} - \mathbf{o}, \mathbf{x} = [x_1, x_2, ..., x_D]$$

D: dimensions, $\mathbf{o} = [o_1, o_2, ..., o_D]$: the shifted global optimum

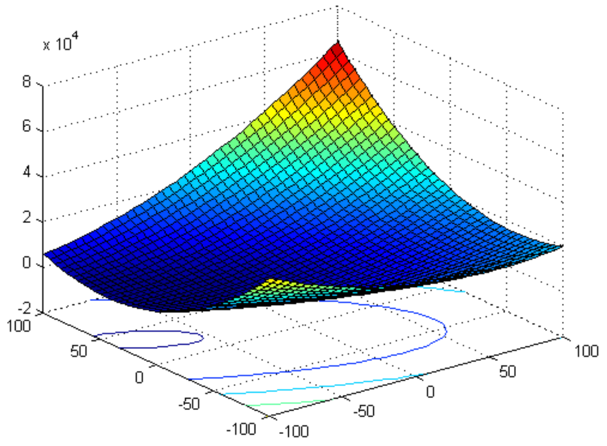

Figure A-2. 3-*D* map for 2-*D* function

Properties:

- Unimodal
- Shifted
- Non-separable
- Scalable
- $\mathbf{x} \in [-100, 100]^D$, Global optimum $\mathbf{x}^* = \mathbf{o}$, $F_2(\mathbf{x}^*) = f\_bias_2 = -450$

F$_3$: Shifted Rotated High Conditioned Elliptic Function

$$F_3(\mathbf{x}) = \sum_{i=1}^{D} (10^6)^{\frac{i-1}{D-1}} z_i^2 + f\_bias_3, \ \mathbf{z} = (\mathbf{x} - \mathbf{o}) * \mathbf{M}, \mathbf{x} = [x_1, x_2, ..., x_D]$$

D: dimensions, $\mathbf{o} = [o_1, o_2, ..., o_D]$: the shifted global optimum
M: orthogonal matrix

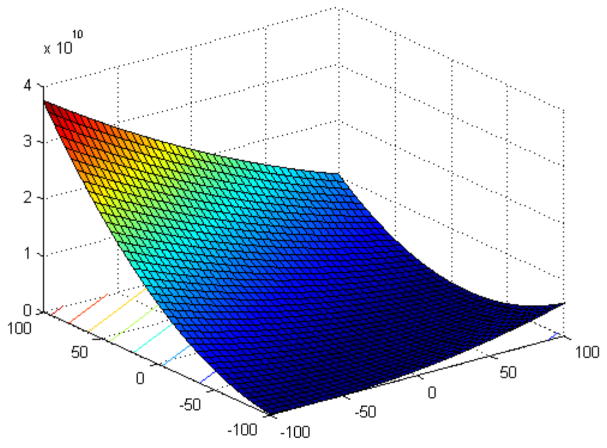

Figure A-3. 3-*D* map for 2-*D* function

Properties:

- Unimodal
- Shifted
- Rotated
- Non-separable
- Scalable
- $\mathbf{x} \in [-100,100]^D$, Global optimum $\mathbf{x}^* = \mathbf{o}$, $F_3(\mathbf{x}^*) = f\_bias_3$ =- 450

F$_4$: Shifted Schwefel's Problem 1.2 with Noise in Fitness

$$F_4(\mathbf{x}) = (\sum_{i=1}^{D}(\sum_{j=1}^{i} z_j)^2) * (1+0.4|N(0,1)|) + f\_bias_4 \text{ , } \mathbf{z} = \mathbf{x}-\mathbf{o} \text{ , } \mathbf{x} = [x_1, x_2, ..., x_D]$$

D: dimensions, $\mathbf{o} = [o_1, o_2, ..., o_D]$: the shifted global optimum

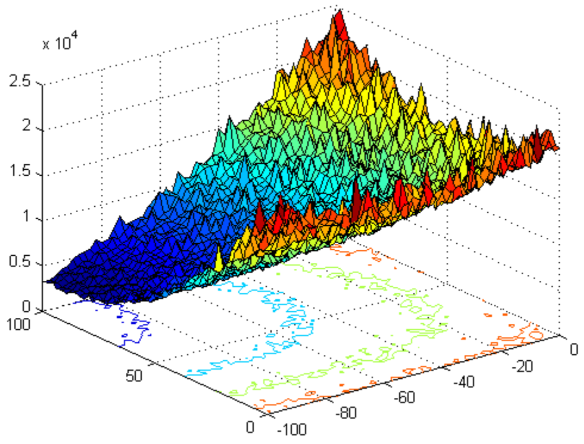

Figure A-4. 3-*D* map for 2-*D* function

Properties:

- Unimodal
- Shifted
- Non-separable
- Scalable
- Noise in fitness
- $\mathbf{x} \in [-100,100]^D$, Global optimum $\mathbf{x}^* = \mathbf{o}$, $F_4(\mathbf{x}^*) = f\_bias_4 = -450$

F_5: Schwefel's Problem 2.6 with Global Optimum on Bounds

$f(\mathbf{x}) = \max\{|x_1 + 2x_2 - 7|, |2x_1 + x_2 - 5|\}, i = 1,...,n$, $\mathbf{x}^* = [1,3]$, $f(\mathbf{x}^*) = 0$

Extend to D dimensions:

$F_5(\mathbf{x}) = \max\{|\mathbf{A}_i\mathbf{x} - \mathbf{B}_i|\} + f\_bias_5, i = 1,...,D$, $\mathbf{x} = [x_1, x_2, ..., x_D]$

D: dimensions

A is a *D*D* matrix, a_{ij} are integer random numbers in the range [*-500, 500*],

$\det(\mathbf{A}) \neq 0$, $\mathbf{A}_i$ is the i^{th} row of **A**.

$\mathbf{B}_i = \mathbf{A}_i * \mathbf{o}$, **o** is a *D**1 vector, o_i are random number in the range [-100,100]

set $o_i = -100$, for $i = 1,2,...,\lceil D/4 \rceil$, $o_i = 100$, for $i = \lfloor 3D/4 \rfloor,...,D$

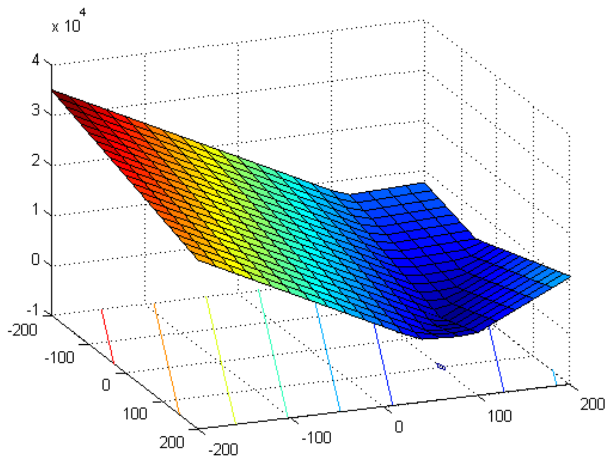

Figure A-5. 3-*D* map for 2-*D* function

Properties:

- Unimodal
- Non-separable
- Scalable
- If the initialization procedure initializes the population at the bounds, this problem will be solved easily.
- $\mathbf{x} \in [-100,100]^D$, Global optimum $\mathbf{x}^* = \mathbf{o}$, $F_5(\mathbf{x}^*) = f\_bias_5 = -310$

Basic Multimodal Functions

F_6: Shifted Rosenbrock's Function

$$F_6(\mathbf{x}) = \sum_{i=1}^{D-1} (100(z_i^2 - z_{i+1})^2 + (z_i - 1)^2) + f\_bias_6 \text{, } \mathbf{z} = \mathbf{x} - \mathbf{o} + 1, \mathbf{x} = [x_1, x_2, ..., x_D]$$

D: dimensions, $\mathbf{o} = [o_1, o_2, ..., o_D]$: the shifted global optimum

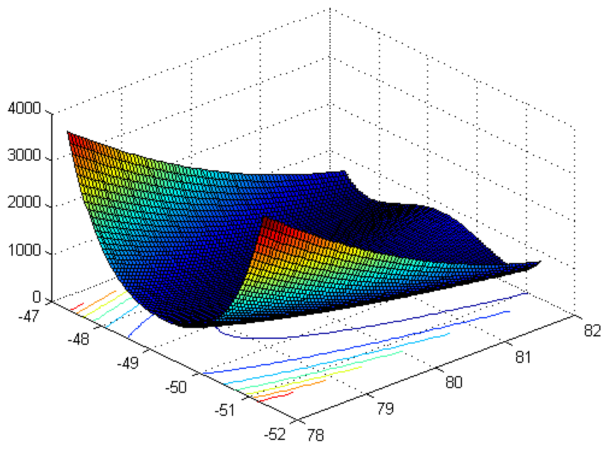

Figure A-6. 3-*D* map for 2-*D* function

Properties:

- Multi-modal
- Shifted
- Non-separable
- Scalable
- Having a very narrow valley from local optimum to global optimum
- $\mathbf{x} \in [-100, 100]^D$, Global optimum $\mathbf{x}^* = \mathbf{o}$, $F_6(\mathbf{x}^*) = f\_bias_6 = 390$

F7: Shifted Rotated Griewank's Function without Bounds

$$F_7(\mathbf{x}) = \sum_{i=1}^{D} \frac{z_i^{\,2}}{4000} - \prod_{i=1}^{D} \cos(\frac{z_i}{\sqrt{i}}) + 1 + f\_bias_7 \ , \ \mathbf{z} = (\mathbf{x} - \mathbf{o}) * \mathbf{M}, \ \mathbf{x} = [x_1, x_2, ..., x_D]$$

D: dimensions

$\mathbf{o} = [o_1, o_2, ..., o_D]$: the shifted global optimum

M': linear transformation matrix, condition number=3

M =**M'**(1+0.3|N(0,1)|)

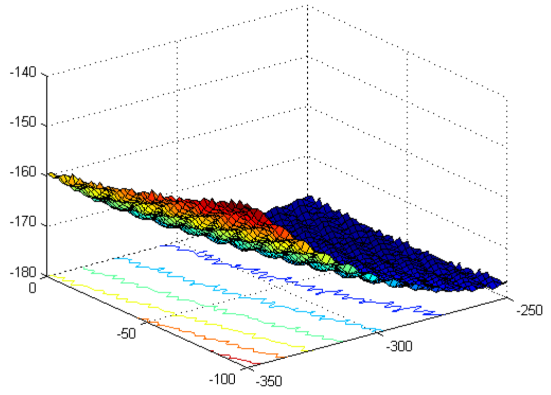

Figure A-7. 3-*D* map for 2-*D* function

Properties:

- Multi-modal
- Rotated
- Shifted
- Non-separable
- Scalable
- No bounds for variables *x*
- Initialize population in $[0, 600]^D$, Global optimum $\mathbf{x}^* = \mathbf{o}$ is outside of the initialization range, $F_7(\mathbf{x}^*) = f\_bias_7 = -180$

F_8: Shifted Rotated Ackley's Function with Global Optimum on Bounds

$$F_8(\mathbf{x}) = -20\exp(-0.2\sqrt{\frac{1}{D}\sum_{i=1}^{D} z_i^2}) - \exp(\frac{1}{D}\sum_{i=1}^{D}\cos(2\pi z_i)) + 20 + e + f\_bias_8,$$

$\mathbf{z} = (\mathbf{x} - \mathbf{o}) * \mathbf{M}$, $\mathbf{x} = [x_1, x_2, ..., x_D]$, D: dimensions

$\mathbf{o} = [o_1, o_2, ..., o_D]$: the shifted global optimum;

After load the data file, set $o_{2j-1} = -32$ o_{2j} are randomly distributed in the search range, for $j = 1, 2, ..., \lfloor D/2 \rfloor$

M: linear transformation matrix, condition number=100

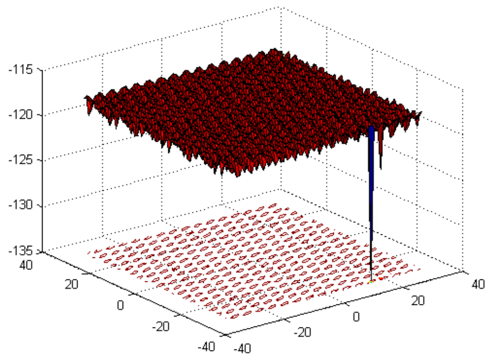

Figure A-8. 3-*D* map for 2-*D* function

Properties:

- Multi-modal
- Rotated
- Shifted
- Non-separable
- Scalable
- **A**'s condition number Cond(**A**) increases with the number of variables as $O(D^2)$
- Global optimum on the bound
- If the initialization procedure initializes the population at the bounds, this problem will be solved easily.
- $\mathbf{x} \in [-32, 32]^D$, Global optimum $\mathbf{x}^* = \mathbf{o}$, $F_8(\mathbf{x}^*) = f\_bias_8 = -140$

F*9*: Shifted Rastrigin's Function

$$F_9(\mathbf{x}) = \sum_{i=1}^{D} (z_i^2 - 10\cos(2\pi z_i) + 10) + f\_bias_9, \ \mathbf{z} = \mathbf{x} - \mathbf{o}, \ \mathbf{x} = [x_1, x_2, ..., x_D]$$

D: dimensions, $\boldsymbol{o} = [o_1, o_2, ..., o_D]$: the shifted global optimum

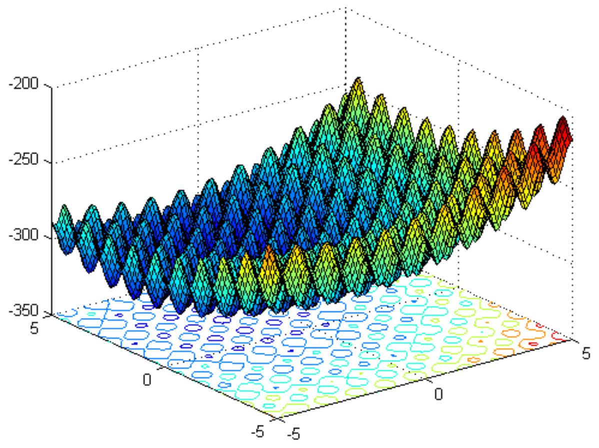

Figure A-9. 3-*D* map for 2-*D* function

Properties:

- Multi-modal
- Shifted
- Separable
- Scalable
- Local optima's number is huge
- $\mathbf{x} \in [-5, 5]^D$, Global optimum $\mathbf{x}^* = \mathbf{o}$, $F_9(\boldsymbol{x}^*) = f\_bias_9 = -330$

F₁₀: Shifted Rotated Rastrigin's Function

$$F_{10}(\mathbf{x}) = \sum_{i=1}^{D} (z_i^{\,2} - 10\cos(2\pi z_i) + 10) + f\_bias_{10}\,,\ \mathbf{z} = (\mathbf{x} - \mathbf{o}) * \mathbf{M}\,, \mathbf{x} = [x_1, x_2, ..., x_D]$$

D: dimensions, $\mathbf{o} = [o_1, o_2, ..., o_D]$: the shifted global optimum

M: linear transformation matrix, condition number=2

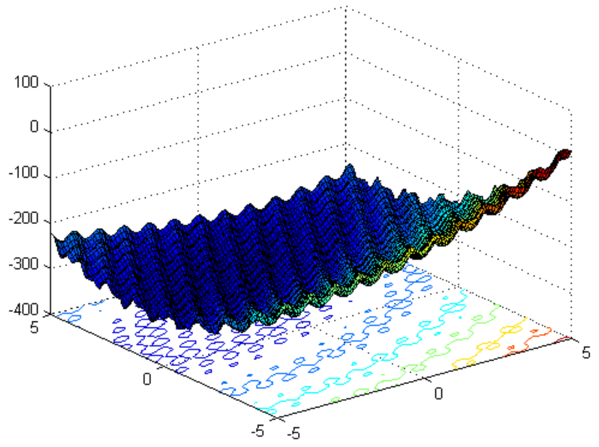

Figure A-10. 3-*D* map for 2-*D* function

Properties:

- Multi-modal
- Shifted
- Rotated
- Non-separable
- Scalable
- Local optima's number is huge
- $\mathbf{x} \in [-5,5]^D$, Global optimum $\mathbf{x}^* = \mathbf{o}$, $F_{10}(\mathbf{x}^*) = f\_bias_{10} = -330$

F_{11}: Shifted Rotated Weierstrass Function

$$F_{11}(\mathbf{x}) = \sum_{i=1}^{D} \left(\sum_{k=0}^{k\max} [a^k \cos(2\pi b^k (z_i + 0.5))] \right) - D \sum_{k=0}^{k\max} [a^k \cos(2\pi b^k \cdot 0.5)] + f\_bias_{11},$$

a=0.5, b=3, $k_{\max}$=20, $\mathbf{z} = (\mathbf{x} - \mathbf{o}) * \mathbf{M}$, $\mathbf{x} = [x_1, x_2, ..., x_D]$

D: dimensions, $\mathbf{o} = [o_1, o_2, ..., o_D]$: the shifted global optimum

M: linear transformation matrix, condition number=5

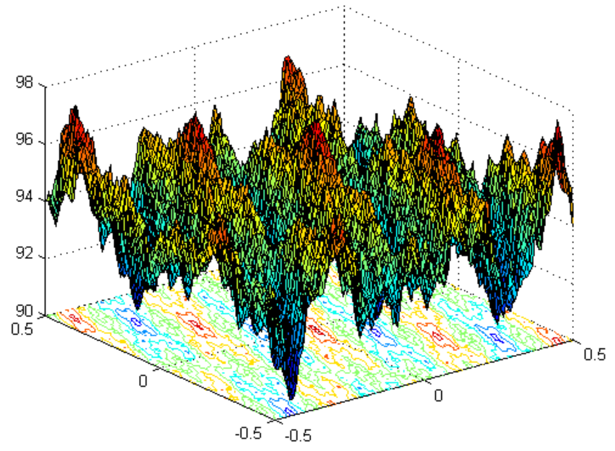

Figure A-11. 3-*D* map for 2-*D* function

Properties:

- Multi-modal
- Shifted
- Rotated
- Non-separable
- Scalable
- Continuous but differentiable only on a set of points
- $\mathbf{x} \in [-0.5, 0.5]^D$, Global optimum $\mathbf{x}^* = \mathbf{o}$, $F_{11}(\mathbf{x}^*) = f\_bias_{11} = 90$

F*12*: Schwefel's Problem 2.13

$$F_{12}(\mathbf{x}) = \sum_{i=1}^{D} (\mathbf{A}_i - \mathbf{B}_i(\boldsymbol{x}))^2 + f\_bias_{12}, \mathbf{x} = [x_1, x_2, ..., x_D]$$

$$\mathbf{A}_i = \sum_{j=1}^{D} (a_{ij} \sin \alpha_j + b_{ij} \cos \alpha_j), \mathbf{B}_i(x) = \sum_{j=1}^{D} (a_{ij} \sin x_j + b_{ij} \cos x_j), \text{ for } i = 1, ..., D$$

D: dimensions

A, **B** are two *D*D* matrix, a_{ij}, b_{ij} are integer random numbers in the range [-100,100],

$\boldsymbol{\alpha} = [\alpha_1, \alpha_2, ..., \alpha_D], \alpha_j$ are random numbers in the range $[-\pi, \pi]$.

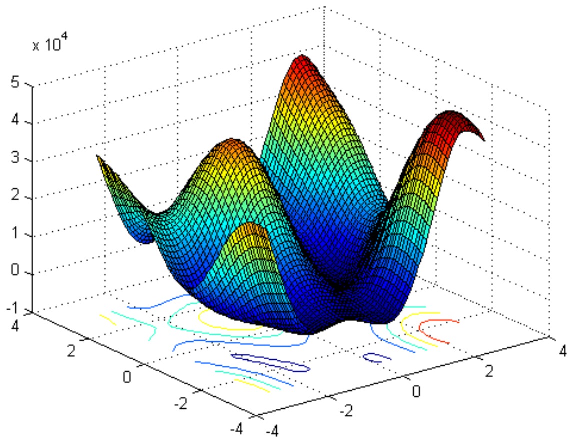

Figure A-12. 3-*D* map for 2-*D* function

Properties:

- Multi-modal
- Shifted
- Non-separable
- Scalable
- $\mathbf{x} \in [-\pi, \pi]^D$, Global optimum $\mathbf{x}^* = \boldsymbol{\alpha}$, $F_{12}(\mathbf{x}^*) = f\_bias_{12} = -460$

Expanded Functions

Using a 2-*D* function $F(x, y)$ as a starting function, corresponding expanded function is:
$EF(x_1, x_2, ..., x_D) = F(x_1, x_2) + F(x_2, x_3) + ... + F(x_{D-1}, x_D) + F(x_D, x_1)$

F*13*: Shifted Expanded Griewank's plus Rosenbrock's Function (F8F2)

F8: Griewank's Function: $F8(\boldsymbol{x}) = \sum_{i=1}^{D} \frac{x_i^2}{4000} - \prod_{i=1}^{D} \cos(\frac{x_i}{\sqrt{i}}) + 1$

F2: Rosenbrock's Function: $F2(\boldsymbol{x}) = \sum_{i=1}^{D-1} (100(x_i^2 - x_{i+1})^2 + (x_i - 1)^2)$

$F8F2(x_1, x_2, ..., x_D) = F8(F2(x_1, x_2)) + F8(F2(x_2, x_3)) + ... + F8(F2(x_{D-1}, x_D)) + F8(F2(x_D, x_1))$

Shift to
$F_{13}(\mathbf{x}) = F8(F2(z_1, z_2)) + F8(F2(z_2, z_3)) + ... + F8(F2(z_{D-1}, z_D)) + F8(F2(z_D, z_1)) + f\_bias_{13}$
$\mathbf{z} = \mathbf{x} - \mathbf{o} + 1$, $\mathbf{x} = [x_1, x_2, ..., x_D]$
D: dimensions $\mathbf{o} = [o_1, o_2, ..., o_D]$: the shifted global optimum

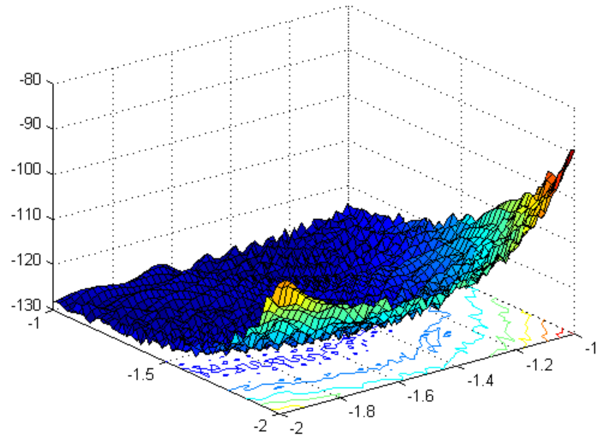

Figure A-13. 3-*D* map for 2-*D* function

Properties:

- Multi-modal
- Shifted
- Non-separable
- Scalable
- $\mathbf{x} \in [-3,1]^D$, Global optimum $\mathbf{x}^* = \mathbf{o}$, $F_{13}(\mathbf{x}^*) = f\_bias_{13}(13)$=-130

F*14*: Shifted Rotated Expanded Scaffer's F6 Function

$$F(x,y) = 0.5 + \frac{(\sin^2(\sqrt{x^2+y^2}) - 0.5)}{(1+0.001(x^2+y^2))^2}$$

Expanded to

$F_{14}(\mathbf{x}) = EF(z_1, z_2, ..., z_D) = F(z_1, z_2) + F(z_2, z_3) + ... + F(z_{D-1}, z_D) + F(z_D, z_1) + f\_bias_{14}$,

$\mathbf{z} = (\mathbf{x} - \mathbf{o}) * \mathbf{M}$, $\mathbf{x} = [x_1, x_2, ..., x_D]$

D: dimensions, $\mathbf{o} = [o_1, o_2, ..., o_D]$: the shifted global optimum

M: linear transformation matrix, condition number=3

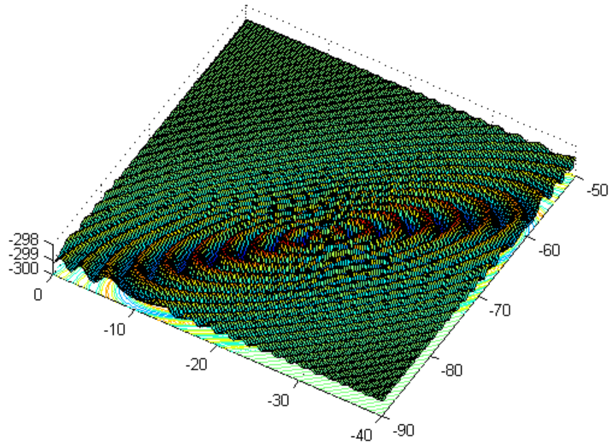

Figure A-14. 3-*D* map for 2-*D* function

Properties:

- Multi-modal
- Shifted
- Non-separable
- Scalable
- $\mathbf{x} \in [-100,100]^D$, Global optimum $\mathbf{x}^* = \mathbf{o}$, $F_{14}(\mathbf{x}^*) = f\_bias_{14}$ (14)= -300

Composition functions

$F(\mathbf{x})$: new composition function
$f_i(\mathbf{x})$: ith basic function used to construct the composition function

n: number of basic functions
D: dimensions
$\mathbf{M}_i$: linear transformation matrix for each $f_i(\boldsymbol{x})$
$\mathbf{o}_i$: new shifted optimum position for each $f_i(\boldsymbol{x})$

$$F(\mathbf{x}) = \sum_{i=1}^{n} \{w_i * [f_i'((\mathbf{x}-\mathbf{o}_i)/\lambda_i * \mathbf{M}_i) + bias_i]\} + f\_bias$$

w_i: weight value for each $f_i(\mathbf{x})$, calculated as below:

$$w_i = \exp\left(-\frac{\sum_{k=1}^{D}(x_k - o_{ik})^2}{2D\sigma_i^2}\right),$$

$$w_i = \begin{cases} w_i & w_i == \max(w_i) \\ w_i*(1\text{-}\max(w_i).\text{^}10) & w_i \neq \max(w_i) \end{cases}$$

then normalize the weight $w_i = w_i / \sum_{i=1}^{n} w_i$

σ_i: used to control each $f_i(\mathbf{x})$'s coverage range, a small σ_i give a narrow range for that $f_i(\mathbf{x})$

λ_i : used to stretch compress the function, λ_i>1 means stretch, λ_i<1 means compress

$\mathbf{o}_i$ define the global and local optima's position, $bias_i$ define which optimum is global optimum. Using $\mathbf{o}_i$, $bias_i$, a global optimum can be placed anywhere.

If $f_i(\mathbf{x})$ are different functions, different functions have different properties and height, in order to get a better mixture, estimate a biggest function value $f_{\max i}$ for 10 functions $f_i(\mathbf{x})$, then normalize each basic functions to similar heights as below:

$f_i'(\mathbf{x}) = C * f_i(\mathbf{x}) / \left|f_{\max i}\right|$, C is a predefined constant.

$\left|f_{\max i}\right|$ is estimated using $\left|f_{\max i}\right| = f_i((\mathbf{x}'/\lambda_i) * \mathbf{M}_i)$, $\mathbf{x}'$=[5,5…,5].

In the following composition functions,
Number of basic functions n=10.
D: dimensions
o: n*D matrix, defines $f_i(\mathbf{x})$'s global optimal positions

bias=[0, 100, 200, 300, 400, 500, 600, 700, 800, 900]. Hence, the first function $f_1(\mathbf{x})$ always the function with the global optimum.
C=2000

Pseudo Code:

```
Define f1-f10, $\sigma$, $\lambda$, bias, C, load data file o and rotated linear transformation matrix **M1-M10**
$\mathbf{y}$=[5,5…,5].
For i=1:10
        $w_i = \exp(-\frac{\sum_{k=1}^{D}(x_k - o_{ik})^2}{2D\sigma_i^2})$ ,
        $fit_i = f_i(((\mathbf{x}-\mathbf{o}_i)/\lambda_i)*\mathbf{M}_i)$
        $f\max_i = f_i((\mathbf{y}/\lambda_i)*\mathbf{M}_i)$,
        $fit_i = C * fit_i / f\max_i$

EndFor

$SW = \sum_{i=1}^{n} w_i$
$MaxW = \max(w_i)$

For i=1:10
$w_i = \begin{cases} w_i & if \quad w_i == MaxW \\ w_i*(1\text{-}MaxW.\hat{}10) & if \quad w_i \neq MaxW \end{cases}$
$w_i = w_i / SW$
EndFor

$F(\mathbf{x}) = \sum_{i=1}^{n}\{w_i*[fit_i + bias_i]\}$
$F(\mathbf{x}) = F(\boldsymbol{x}) + f\_bias$
```

F₁₅: Hybrid Composition Function

$f_{1-2}(\mathbf{x})$: Rastrigin's Function

$$f_i(\mathbf{x}) = \sum_{i=1}^{D} (x_i^2 - 10\cos(2\pi x_i) + 10)$$

$f_{3-4}(\mathbf{x})$: Weierstrass Function

$$f_i(\mathbf{x}) = \sum_{i=1}^{D} \left(\sum_{k=0}^{k\max} [a^k \cos(2\pi b^k (x_i + 0.5))] \right) - D \sum_{k=0}^{k\max} [a^k \cos(2\pi b^k \cdot 0.5)],$$

a=0.5, b=3, $k_{\max}$=20

$f_{5-6}(\mathbf{x})$: Griewank's Function

$$f_i(\mathbf{x}) = \sum_{i=1}^{D} \frac{x_i^2}{4000} - \prod_{i=1}^{D} \cos\left(\frac{x_i}{\sqrt{i}}\right) + 1$$

$f_{7-8}(\mathbf{x})$: Ackley's Function

$$f_i(\mathbf{x}) = -20\exp\left(-0.2\sqrt{\frac{1}{D}\sum_{i=1}^{D} x_i^2}\right) - \exp\left(\frac{1}{D}\sum_{i=1}^{D}\cos(2\pi x_i)\right) + 20 + e$$

$f_{9-10}(\mathbf{x})$: Sphere Function

$$f_i(\mathbf{x}) = \sum_{i=1}^{D} x_i^2$$

$\sigma_i = 1$ for $i = 1, 2, ..., D$

$\boldsymbol{\lambda}$ = [1, 1, 10, 10, 5/60, 5/60, 5/32, 5/32, 5/100, 5/100]

$\mathbf{M}_i$ are all identity matrices

Please notice that these formulas are just for the basic functions, no shift or rotation is included in these expressions. x here is just a variable in a function.

Take f_1 as an example, when we calculate $f_1(((\mathbf{x} - \mathbf{o}_1) / \lambda_1) * \mathbf{M}_1)$, we need calculate $f_1(\mathbf{z}) = \sum_{i=1}^{D} (z_i^2 - 10\cos(2\pi z_i) + 10)$, $\mathbf{z} = ((\mathbf{x} - \mathbf{o}_1) / \lambda_1) * \mathbf{M}_1$.

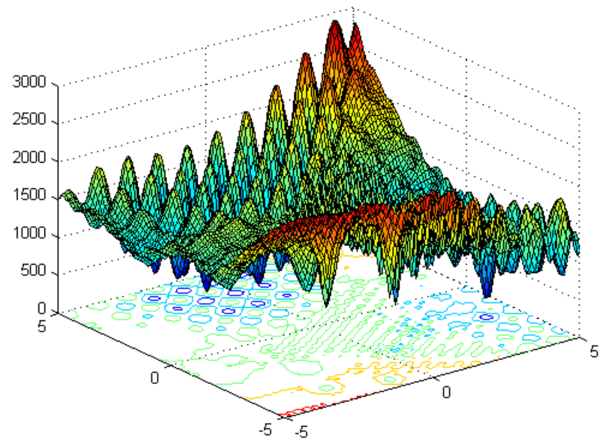

Figure A-15. 3-*D* map for 2-*D* function

Properties:

- Multi-modal
- Separable near the global optimum (Rastrigin)
- Scalable
- A huge number of local optima
- Different function's properties are mixed together
- Sphere Functions give two flat areas for the function
- $\mathbf{x} \in [-5,5]^D$, Global optimum $\mathbf{x}^* = \mathbf{o}_1$, $F_{15}(\mathbf{x}^*) = f\_bias_{15} = 120$

F_{16}: Rotated Version of Hybrid Composition Function F_{15}

Except $\mathbf{M}_i$ are different linear transformation matrixes with condition number of 2, all other settings are the same as F_{15}.

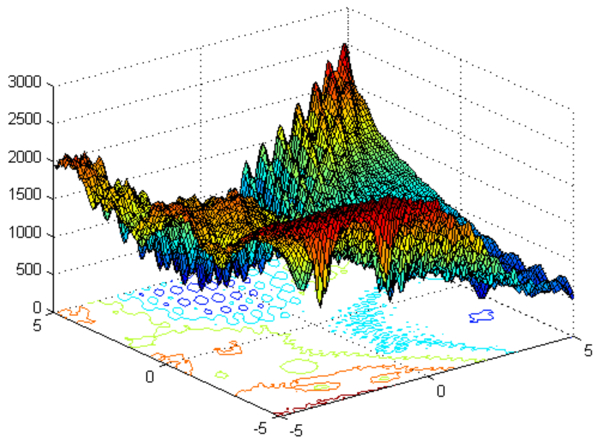

Figure A-16. 3-*D* map for 2-*D* function

Properties:

- Multi-modal
- Rotated
- Non-Separable
- Scalable
- A huge number of local optima
- Different function's properties are mixed together
- Sphere Functions give two flat areas for the function.
- $\mathbf{x} \in [-5,5]^D$, Global optimum $\mathbf{x}^* = \mathbf{o}_1$, $F_{16}(\boldsymbol{x}^*) = f\_bias_{16}$ =120

F_{17}: F_{16} with Noise in Fitness

Let (F_{16} - f_bias_{16}) be $G(\boldsymbol{x})$, then

$$F_{17}(\mathbf{x}) = G(\mathbf{x})*(1+0.2|N(0,1)|) + f\_bias_{17}$$

All settings are the same as F_{16}.

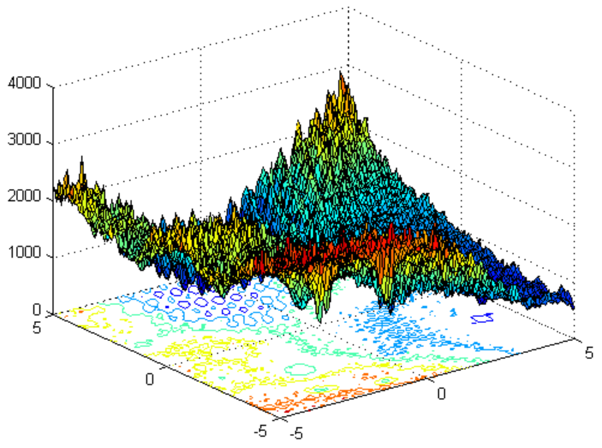

Figure A-17. 3-*D* map for 2-*D* function

Properties:

- Multi-modal
- Rotated
- Non-Separable
- Scalable
- A huge number of local optima
- Different function's properties are mixed together
- Sphere Functions give two flat areas for the function.
- With Gaussian noise in fitness
- $\mathbf{x} \in [-5,5]^D$, Global optimum $\mathbf{x}^* = \mathbf{o}_1$, $F_{17}(\mathbf{x}^*) = f\_bias_{17}$ =120

F_{18}: Rotated Hybrid Composition Function

$f_{1-2}(\mathbf{x})$: Ackley's Function

$$f_i(\mathbf{x}) = -20\exp(-0.2\sqrt{\frac{1}{D}\sum_{i=1}^{D} x_i^2}) - \exp(\frac{1}{D}\sum_{i=1}^{D}\cos(2\pi x_i)) + 20 + e$$

$f_{3-4}(\mathbf{x})$: Rastrigin's Function

$$f_i(\mathbf{x}) = \sum_{i=1}^{D}(x_i^2 - 10\cos(2\pi x_i) + 10)$$

$f_{5-6}(\mathbf{x})$: Sphere Function

$$f_i(\mathbf{x}) = \sum_{i=1}^{D} x_i^2$$

$f_{7-8}(\mathbf{x})$: Weierstrass Function

$$f_i(\mathbf{x}) = \sum_{i=1}^{D}(\sum_{k=0}^{k\max}[a^k\cos(2\pi b^k(x_i + 0.5))]) - D\sum_{k=0}^{k\max}[a^k\cos(2\pi b^k \cdot 0.5)],$$

a=0.5, b=3, k_{max}=20

$f_{9-10}(\mathbf{x})$: Griewank's Function

$$f_i(\mathbf{x}) = \sum_{i=1}^{D}\frac{x_i^2}{4000} - \prod_{i=1}^{D}\cos(\frac{x_i}{\sqrt{i}}) + 1$$

$\boldsymbol{\sigma}$=[1, 2, 1.5, 1.5, 1, 1, 1.5, 1.5, 2, 2];

$\boldsymbol{\lambda}$= [2*5/32; 5/32; 2*1; 1; 2*5/100; 5/100; 2*10; 10; 2*5/60; 5/60]

$\mathbf{M}_i$ are all rotation matrices. Condition numbers are [2 3 2 3 2 3 20 30 200 300]

$\mathbf{o}_{10} = [0, 0, ..., 0]$

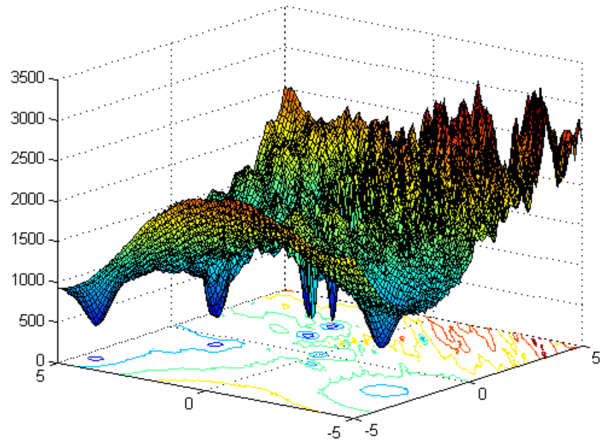

Figure A-18. 3-*D* map for 2-*D* function

Properties:

- Multi-modal
- Rotated
- Non-Separable
- Scalable
- A huge number of local optima
- Different function's properties are mixed together
- Sphere Functions give two flat areas for the function.
- A local optimum is set on the origin
- $\mathbf{x} \in [-5,5]^D$, Global optimum $\mathbf{x}^* = \mathbf{o}_1$, $F_{18}(\boldsymbol{x}^*) = f\_bias_{18} = 10$

F_{19}: Rotated Hybrid Composition Function with narrow basin global optimum

All settings are the same as F_{18} except
$\boldsymbol{\sigma}$=[0.1, 2, 1.5, 1.5, 1, 1, 1.5, 1.5, 2, 2];,
$\boldsymbol{\lambda}$ = [0.1*5/32; 5/32; 2*1; 1; 2*5/100; 5/100; 2*10; 10; 2*5/60; 5/60]

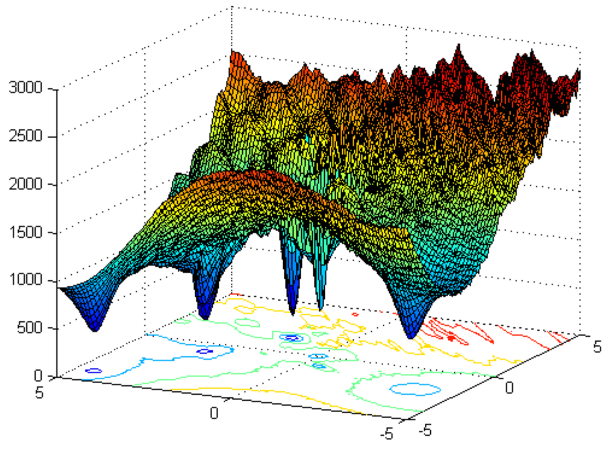

Figure A-19. 3-*D* map for 2-*D* function

Properties:

- Multi-modal
- Non-separable
- Scalable
- A huge number of local optima
- Different function's properties are mixed together
- Sphere Functions give two flat areas for the function.
- A local optimum is set on the origin
- A narrow basin for the global optimum
- $\mathbf{x} \in [-5,5]^D$, Global optimum $\mathbf{x}^* = \mathbf{o}_1$, $F_{19}(\mathbf{x}^*) = f\_bias_{19}$ (19)=10

F$_{20}$: Rotated Hybrid Composition Function with Global Optimum on the Bounds

All settings are the same as F_{18} except after load the data file, set $o_{1(2j)} = 5$, for $j = 1, 2, ..., \lfloor D/2 \rfloor$

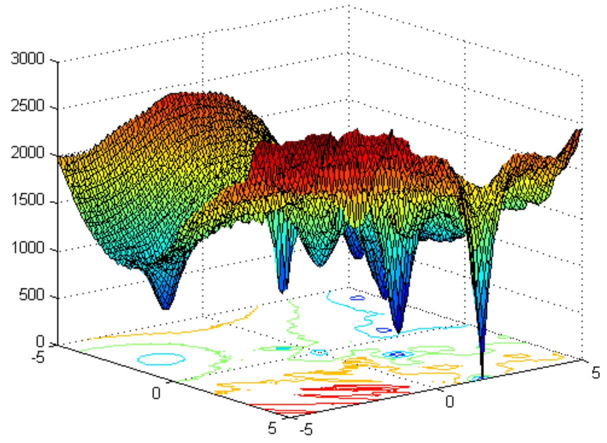

Figure A-20. 3-*D* map for 2-*D* function

Properties:

- Multi-modal
- Non-separable
- Scalable
- A huge number of local optima
- Different function's properties are mixed together
- Sphere Functions give two flat areas for the function.
- A local optimum is set on the origin
- Global optimum is on the bound
- If the initialization procedure initializes the population at the bounds, this problem will be solved easily.
- $\mathbf{x} \in [-5,5]^D$, Global optimum $\mathbf{x}^* = \mathbf{o}_1$, $F_{20}(\mathbf{x}^*) = f\_bias_{20} = 10$

F$_{21}$: Rotated Hybrid Composition Function

$f_{1-2}(\mathbf{x})$: Rotated Expanded Scaffer's F6 Function

$$F(x,y)=0.5+\frac{(\sin^2(\sqrt{x^2+y^2})-0.5)}{(1+0.001(x^2+y^2))^2}$$

$$f_i(\mathbf{x})=F(x_1,x_2)+F(x_2,x_3)+\ldots+F(x_{D-1},x_D)+F(x_D,x_1)$$

$f_{3-4}(\mathbf{x})$: Rastrigin's Function

$$f_i(\mathbf{x})=\sum_{i=1}^{D}(x_i^2-10\cos(2\pi x_i)+10)$$

$f_{5-6}(\mathbf{x})$: F8F2 Function

$$F8(\mathbf{x})=\sum_{i=1}^{D}\frac{x_i^2}{4000}-\prod_{i=1}^{D}\cos(\frac{x_i}{\sqrt{i}})+1$$

$$F2(\mathbf{x})=\sum_{i=1}^{D-1}(100(x_i^2-x_{i+1})^2+(x_i-1)^2)$$

$$f_i(\mathbf{x})=F8(F2(x_1,x_2))+F8(F2(x_2,x_3))+\ldots+F8(F2(x_{D-1},x_D))+F8(F2(x_D,x_1))$$

$f_{7-8}(\mathbf{x})$: Weierstrass Function

$$f_i(\mathbf{x})=\sum_{i=1}^{D}(\sum_{k=0}^{k\max}[a^k\cos(2\pi b^k(x_i+0.5))])-D\sum_{k=0}^{k\max}[a^k\cos(2\pi b^k\cdot 0.5)],$$

a=0.5, b=3, k$_{max}$=20

$f_{9-10}(\mathbf{x})$: Griewank's Function

$$f_i(\mathbf{x})=\sum_{i=1}^{D}\frac{x_i^2}{4000}-\prod_{i=1}^{D}\cos(\frac{x_i}{\sqrt{i}})+1$$

$\boldsymbol{\sigma}=[1,1,1,1,1,2,2,2,2,2]$,

$\boldsymbol{\lambda}=$ [5*5/100; 5/100; 5*1; 1; 5*1; 1; 5*10; 10; 5*5/200; 5/200];

$\mathbf{M}_i$ are all orthogonal matrix

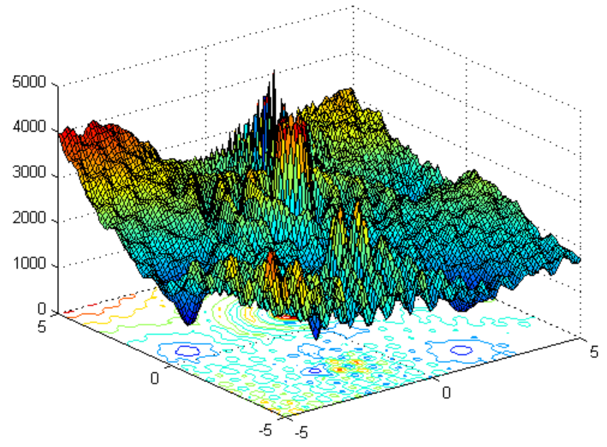

Figure A-21. 3-*D* map for 2-*D* function

Properties:

- Multi-modal
- Rotated
- Non-Separable
- Scalable
- A huge number of local optima
- Different function's properties are mixed together
- $\mathbf{x} \in [-5,5]^D$, Global optimum $\mathbf{x}^* = \mathbf{o}_1$, $F_{21}(\mathbf{x}^*) = f\_bias_{21}$ =360

F_{22}: Rotated Hybrid Composition Function with High Condition Number Matrix

All settings are the same as F_{21} except $\mathbf{M}_i$'s condition numbers are [10 20 50 100 200 1000 2000 3000 4000 5000]

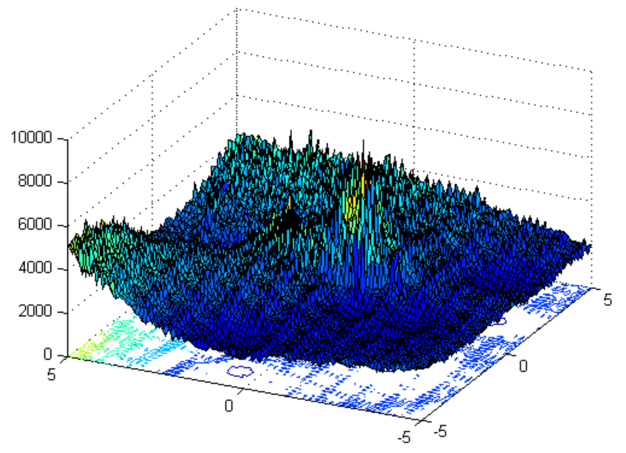

Figure A-22. 3-*D* map for 2-*D* function

Properties:

- Multi-modal
- Non-separable
- Scalable
- A huge number of local optima
- Different function's properties are mixed together
- Global optimum is on the bound
- $\mathbf{x} \in [-5,5]^D$, Global optimum $\mathbf{x}^* = \mathbf{o}_1$, $F_{22}(\mathbf{x}^*) = f\_bias_{22}$ =360

F$_{23}$: Non-Continuous Rotated Hybrid Composition Function

All settings are the same as F_{21}.

Except $x_j = \begin{cases} x_j & |x_j - o_{1j}| < 1/2 \\ round(2x_j)/2 & |x_j - o_{1j}| >= 1/2 \end{cases}$ for $j = 1, 2, .., D$

$$round(x) = \begin{cases} a-1 & if \quad x <= 0 \,\&\, b >= 0.5 \\ a & if \quad b < 0.5 \\ a+1 & if \quad x > 0 \,\&\, b >= 0.5 \end{cases},$$

where a is x's integral part and b is x's decimal part

All "round" operators in this document use the same schedule.

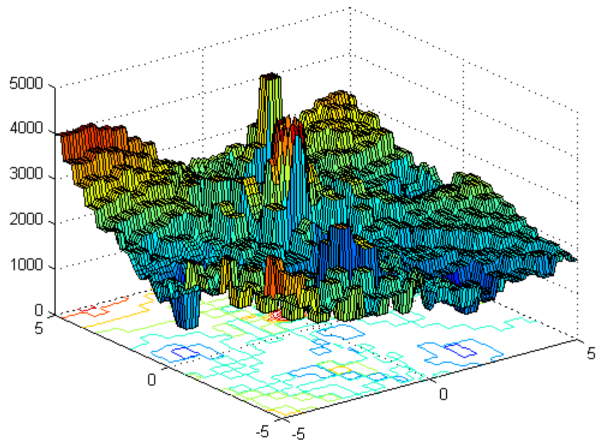

Figure A-23. 3-*D* map for 2-*D* function

Properties:

- Multi-modal
- Non-separable
- Scalable
- A huge number of local optima
- Different function's properties are mixed together
- Non-continuous
- Global optimum is on the bound
- $\mathbf{x} \in [-5, 5]^D$, Global optimum $\mathbf{x}^* = \mathbf{o}_1$, $f(\boldsymbol{x}^*) \approx$ ***f_bias*** (23)=360

F_{24}: Rotated Hybrid Composition Function

$f_1(\mathbf{x})$: Weierstrass Function

$$f_i(\mathbf{x}) = \sum_{i=1}^{D}\left(\sum_{k=0}^{k\max}[a^k\cos(2\pi b^k(x_i+0.5))]\right) - D\sum_{k=0}^{k\max}[a^k\cos(2\pi b^k 0.5)],$$

a=0.5, b=3, k_{max}=20

$f_2(\mathbf{x})$: Rotated Expanded Scaffer's F6 Function

$$F(x,y) = 0.5 + \frac{(\sin^2(\sqrt{x^2+y^2})-0.5)}{(1+0.001(x^2+y^2))^2}$$

$$f_i(\mathbf{x}) = F(x_1,x_2)+F(x_2,x_3)+\ldots+F(x_{D-1},x_D)+F(x_D,x_1)$$

$f_3(\mathbf{x})$: F8F2 Function

$$F8(\mathbf{x}) = \sum_{i=1}^{D}\frac{{x_i}^2}{4000} - \prod_{i=1}^{D}\cos\left(\frac{x_i}{\sqrt{i}}\right)+1$$

$$F2(\mathbf{x}) = \sum_{i=1}^{D-1}(100(x_i^2-x_{i+1})^2+(x_i-1)^2)$$

$$f_i(\mathbf{x}) = F8(F2(x_1,x_2))+F8(F2(x_2,x_3))+\ldots+F8(F2(x_{D-1},x_D))+F8(F2(x_D,x_1))$$

$f_4(\mathbf{x})$: Ackley's Function

$$f_i(\mathbf{x}) = -20\exp\left(-0.2\sqrt{\frac{1}{D}\sum_{i=1}^{D}x_i^2}\right)-\exp\left(\frac{1}{D}\sum_{i=1}^{D}\cos(2\pi x_i)\right)+20+e$$

$f_5(\mathbf{x})$: Rastrigin's Function

$$f_i(\mathbf{x}) = \sum_{i=1}^{D}({x_i}^2-10\cos(2\pi x_i)+10)$$

$f_6(\mathbf{x})$: Griewank's Function

$$f_i(\mathbf{x}) = \sum_{i=1}^{D}\frac{{x_i}^2}{4000} - \prod_{i=1}^{D}\cos\left(\frac{x_i}{\sqrt{i}}\right)+1$$

$f_7(\mathbf{x})$: Non-Continuous Expanded Scaffer's F6 Function

$$F(x,y) = 0.5 + \frac{(\sin^2(\sqrt{x^2+y^2})-0.5)}{(1+0.001(x^2+y^2))^2}$$

$$f(\boldsymbol{x}) = F(y_1,y_2)+F(y_2,y_3)+\ldots+F(y_{D-1},y_D)+F(y_D,y_1)$$

$$y_j = \begin{cases} x_j & |x_j| < 1/2 \\ round(2x_j)/2 & |x_j| >= 1/2 \end{cases} \quad \text{for } j = 1,2,..,D$$

$f_8(\mathbf{x})$: Non-Continuous Rastrigin's Function

$$f(\mathbf{x}) = \sum_{i=1}^{D}({y_i}^2-10\cos(2\pi y_i)+10)$$

$$y_j = \begin{cases} x_j & |x_j| < 1/2 \\ round(2x_j)/2 & |x_j| >= 1/2 \end{cases} \quad \text{for } j = 1, 2, .., D$$

$f_9(\mathbf{x})$: High Conditioned Elliptic Function

$$f(\mathbf{x}) = \sum_{i=1}^{D} (10^6)^{\frac{i-1}{D-1}} x_i^2$$

$f_{10}(\mathbf{x})$: Sphere Function with Noise in Fitness

$$f_i(\mathbf{x}) = (\sum_{i=1}^{D} x_i^2)(1 + 0.1|N(0,1)|)$$

$\sigma_i = 2$,for $i = 1, 2..., D$

$\boldsymbol{\lambda}$ =[10; 5/20; 1; 5/32; 1; 5/100; 5/50; 1; 5/100; 5/100]

$\mathbf{M}_i$ are all rotation matrices, condition numbers are [100 50 30 10 5 5 4 3 2 2];

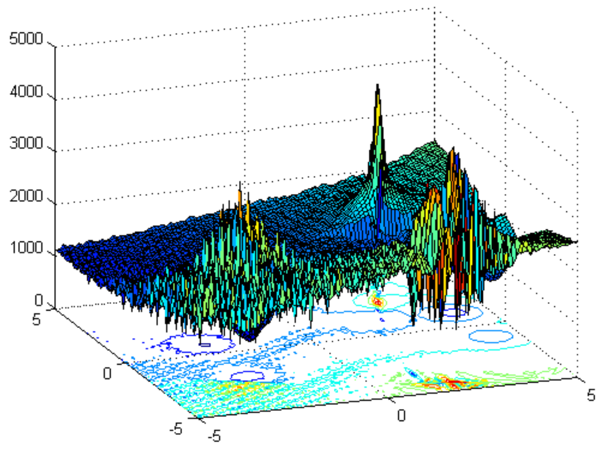

Figure A-24. 3-*D* map for 2-*D* function

Properties:

- Multi-modal
- Rotated
- Non-Separable
- Scalable
- A huge number of local optima
- Different function’s properties are mixed together
- Unimodal Functions give flat areas for the function.
- $\mathbf{x} \in [-5,5]^D$, Global optimum $\mathbf{x}^* = \mathbf{o}_1$, $F_{24}(\mathbf{x}^*) = f\_bias_{24} = 260$

F_{25}: Rotated Hybrid Composition Function without bounds

All settings are the same as F_{24} except no exact search range set for this test function.

Properties:

- Multi-modal
- Non-separable
- Scalable
- A huge number of local optima
- Different function's properties are mixed together
- Unimodal Functions give flat areas for the function.
- Global optimum is on the bound
- No bounds
- Initialize population in $[2,5]^D$, Global optimum $\boldsymbol{x}^* = \boldsymbol{o}_1$ is outside of the initialization range, $F_{25}(\mathbf{x}^*) = f\_bias_{25}$ =260

Appendix B

Iris Dataset

Sample #	Sepal Length	Sepal Width	Petal Length	Petal Width	Type
1	5.1	3.5	1.4	0.2	Setosa
2	4.9	3	1.4	0.2	Setosa
3	4.7	3.2	1.3	0.2	Setosa
4	4.6	3.1	1.5	0.2	Setosa
5	5	3.6	1.4	0.2	Setosa
6	5.4	3.9	1.7	0.4	Setosa
7	4.6	3.4	1.4	0.3	Setosa
8	5	3.4	1.5	0.2	Setosa
9	4.4	2.9	1.4	0.2	Setosa
10	4.9	3.1	1.5	0.1	Setosa
11	5.4	3.7	1.5	0.2	Setosa
12	4.8	3.4	1.6	0.2	Setosa
13	4.8	3	1.4	0.1	Setosa
14	4.3	3	1.1	0.1	Setosa
15	5.8	4	1.2	0.2	Setosa
16	5.7	4.4	1.5	0.4	Setosa
17	5.4	3.9	1.3	0.4	Setosa
18	5.1	3.5	1.4	0.3	Setosa
19	5.7	3.8	1.7	0.3	Setosa
20	5.1	3.8	1.5	0.3	Setosa
21	5.4	3.4	1.7	0.2	Setosa
22	5.1	3.7	1.5	0.4	Setosa
23	4.6	3.6	1	0.2	Setosa
24	5.1	3.3	1.7	0.5	Setosa
25	4.8	3.4	1.9	0.2	Setosa
26	5	3	1.6	0.2	Setosa
27	5	3.4	1.6	0.4	Setosa
28	5.2	3.5	1.5	0.2	Setosa
29	5.2	3.4	1.4	0.2	Setosa
30	4.7	3.2	1.6	0.2	Setosa
31	4.8	3.1	1.6	0.2	Setosa
32	5.4	3.4	1.5	0.4	Setosa
33	5.2	4.1	1.5	0.1	Setosa
34	5.5	4.2	1.4	0.2	Setosa
35	4.9	3.1	1.5	0.1	Setosa

Sample #	Sepal Length	Sepal Width	Petal Length	Petal Width	Type
36	5	3.2	1.2	0.2	Setosa
37	5.5	3.5	1.3	0.2	Setosa
38	4.9	3.1	1.5	0.1	Setosa
39	4.4	3	1.3	0.2	Setosa
40	5.1	3.4	1.5	0.2	Setosa
41	5	3.5	1.3	0.3	Setosa
42	4.5	2.3	1.3	0.3	Setosa
43	4.4	3.2	1.3	0.2	Setosa
44	5	3.5	1.6	0.6	Setosa
45	5.1	3.8	1.9	0.4	Setosa
46	4.8	3	1.4	0.3	Setosa
47	5.1	3.8	1.6	0.2	Setosa
48	4.6	3.2	1.4	0.2	Setosa
49	5.3	3.7	1.5	0.2	Setosa
50	5	3.3	1.4	0.2	Setosa
51	7	3.2	4.7	1.4	Versicolor
52	6.4	3.2	4.5	1.5	Versicolor
53	6.9	3.1	4.9	1.5	Versicolor
54	5.5	2.3	4	1.3	Versicolor
55	6.5	2.8	4.6	1.5	Versicolor
56	5.7	2.8	4.5	1.3	Versicolor
57	6.3	3.3	4.7	1.6	Versicolor
58	4.9	2.4	3.3	1	Versicolor
59	6.6	2.9	4.6	1.3	Versicolor
60	5.2	2.7	3.9	1.4	Versicolor
61	5	2	3.5	1	Versicolor
62	5.9	3	4.2	1.5	Versicolor
63	6	2.2	4	1	Versicolor
64	6.1	2.9	4.7	1.4	Versicolor
65	5.6	2.9	3.6	1.3	Versicolor
66	6.7	3.1	4.4	1.4	Versicolor
67	5.6	3	4.5	1.5	Versicolor
68	5.8	2.7	4.1	1	Versicolor
69	6.2	2.2	4.5	1.5	Versicolor
70	5.6	2.5	3.9	1.1	Versicolor
71	5.9	3.2	4.8	1.8	Versicolor
72	6.1	2.8	4	1.3	Versicolor
73	6.3	2.5	4.9	1.5	Versicolor
74	6.1	2.8	4.7	1.2	Versicolor
75	6.4	2.9	4.3	1.3	Versicolor
76	6.6	3	4.4	1.4	Versicolor
77	6.8	2.8	4.8	1.4	Versicolor

Sample #	Sepal Length	Sepal Width	Petal Length	Petal Width	Type
78	6.7	3	5	1.7	Versicolor
79	6	2.9	4.5	1.5	Versicolor
80	5.7	2.6	3.5	1	Versicolor
81	5.5	2.4	3.8	1.1	Versicolor
82	5.5	2.4	3.7	1	Versicolor
83	5.8	2.7	3.9	1.2	Versicolor
84	6	2.7	5.1	1.6	Versicolor
85	5.4	3	4.5	1.5	Versicolor
86	6	3.4	4.5	1.6	Versicolor
87	6.7	3.1	4.7	1.5	Versicolor
88	6.3	2.3	4.4	1.3	Versicolor
89	5.6	3	4.1	1.3	Versicolor
90	5.5	2.5	4	1.3	Versicolor
91	5.5	2.6	4.4	1.2	Versicolor
92	6.1	3	4.6	1.4	Versicolor
93	5.8	2.6	4	1.2	Versicolor
94	5	2.3	3.3	1	Versicolor
95	5.6	2.7	4.2	1.3	Versicolor
96	5.7	3	4.2	1.2	Versicolor
97	5.7	2.9	4.2	1.3	Versicolor
98	6.2	2.9	4.3	1.3	Versicolor
99	5.1	2.5	3	1.1	Versicolor
100	5.7	2.8	4.1	1.3	Versicolor
101	6.3	3.3	6	2.5	Virginica
102	5.8	2.7	5.1	1.9	Virginica
103	7.1	3	5.9	2.1	Virginica
104	6.3	2.9	5.6	1.8	Virginica
105	6.5	3	5.8	2.2	Virginica
106	7.6	3	6.6	2.1	Virginica
107	4.9	2.5	4.5	1.7	Virginica
108	7.3	2.9	6.3	1.8	Virginica
109	6.7	2.5	5.8	1.8	Virginica
110	7.2	3.6	6.1	2.5	Virginica
111	6.5	3.2	5.1	2	Virginica
112	6.4	2.7	5.3	1.9	Virginica
113	6.8	3	5.5	2.1	Virginica
114	5.7	2.5	5	2	Virginica
115	5.8	2.8	5.1	2.4	Virginica
116	6.4	3.2	5.3	2.3	Virginica
117	6.5	3	5.5	1.8	Virginica
118	7.7	3.8	6.7	2.2	Virginica
119	7.7	2.6	6.9	2.3	Virginica

Sample #	Sepal Length	Sepal Width	Petal Length	Petal Width	Type
120	6	2.2	5	1.5	Virginica
121	6.9	3.2	5.7	2.3	Virginica
122	5.6	2.8	4.9	2	Virginica
123	7.7	2.8	6.7	2	Virginica
124	6.3	2.7	4.9	1.8	Virginica
125	6.7	3.3	5.7	2.1	Virginica
126	7.2	3.2	6	1.8	Virginica
127	6.2	2.8	4.8	1.8	Virginica
128	6.1	3	4.9	1.8	Virginica
129	6.4	2.8	5.6	2.1	Virginica
130	7.2	3	5.8	1.6	Virginica
131	7.4	2.8	6.1	1.9	Virginica
132	7.9	3.8	6.4	2	Virginica
133	6.4	2.8	5.6	2.2	Virginica
134	6.3	2.8	5.1	1.5	Virginica
135	6.1	2.6	5.6	1.4	Virginica
136	7.7	3	6.1	2.3	Virginica
137	6.3	3.4	5.6	2.4	Virginica
138	6.4	3.1	5.5	1.8	Virginica
139	6	3	4.8	1.8	Virginica
140	6.9	3.1	5.4	2.1	Virginica
141	6.7	3.1	5.6	2.4	Virginica
142	6.9	3.1	5.1	2.3	Virginica
143	5.8	2.7	5.1	1.9	Virginica
144	6.8	3.2	5.9	2.3	Virginica
145	6.7	3.3	5.7	2.5	Virginica
146	6.7	3	5.2	2.3	Virginica
147	6.3	2.5	5	1.9	Virginica
148	6.5	3	5.2	2	Virginica
149	6.2	3.4	5.4	2.3	Virginica
150	5.9	3	5.1	1.8	Virginica

BIBLIOGRAPHY

Alessio, L., Coca, S., Bourbon, L., "*Experimental Design as a framework for Multiple Realisation History Matching : F6 Further Development Studies*," paper SPE 93164 presented at the 2005 Asia Pacific Oil & Gas Conference and Exhibition held in Jakarta, Indonesia, 5-7 Apr 2005.

Al-kazemi, B. & Mohan, C.K., "*Training Feedforward Neural Networks using Multi-phase Particle Swarm Optimisation*," in Proceedings of the 9th International Conference on Neural Information Processing, **5**, 2002.

Alonso, S., Jimenez, J., Carmona, H., Galvan, B. & Winter, G., "*Performance of a Flexible Evolutionary Algorithm*," Proc. of IEEE Congress on Evolutionary Computation (CEC 2005), **1**, 02-05, Sept. 2005.

Angeline, P., "*Evolutionary Optimization versus Particle Swarm Optimization: Philosophy and Performance Difference*," The 7th Annual Conference on Evolutionary Programming, San Diego, USA. 1998, pp 600-610.

Ballester, P.J., Stephenson, J., Carter, J.N. & Gallagher, K., "*Real-Parameter Optimization Performance Study on the CEC-2005 benchmark with SPC-PNX*," Proc. of IEEE Congress on Evolutionary Computation (CEC 2005), **1**, 02-05, Sept. 2005.

Bayes, T. "*An Essay towards solving a problem in the Doctrine of Chances*," Philosophical Transactions of the Royal Society," Vol. 53, 1763.

Beasley, D., Bull, D. R., Martin, R. R., "*A Sequential Niche Technique for Multimodal Function Optimisation*," Evolutionary Computation, 1, No. 2, 1993.

Bissell, R.C. Yogeshwar, S., and Killough, J.E., "*History Matching using the method of Gradients: Two Case Studies*, " paper SPE 28590 presented at the SPE 69th Annual Technical Conference and Exhibition, New Orleans, Louisiana, Sep 25-28, 1994.

Blackwell, T. and Branke, J.,: "*Multi-swarm Optimisation in Dynamic Environments*," Applications of Evolutionary Computing (2004) pp. 489-500.

Blake, C. Keogh, E. & Merz, C.J., "*UCI Repository of Machine Learning Databases*," University of California, Irvine, Dept. of Information and Computer Sciences, 1998.

Brits, R., Engelbrecht, A.P., F. van den Bergh, "*A Niching Particle Swarm Optimiser*," Fourth Asia-Pacific Conference on Simulated Evolution and Learning, (2002) pp 692-696.

Brun, B., Gosseling, O., and Barker, J. W., "*Use of Prior Information in Gradient Based History Matching*," SPEJ (March 2004) **9**, No. 1, 67.

Carter, JN, Ballester, PJ, Tavassoli, Z, "*Our calibrated model has poor predictive value: An example from the petroleum industry*," RELIAB ENG SYST SAFE, 2006, **91**, Pages: 1373 – 1381.

Chavent, G., Dupuy, M., and Lemonnier, P., "*History Matching by use of Optimal Control Theory*, " SPEJ (Feb. 1975) 74-86, Trans., AIME, **259**.

Chen, W. H. et al., "*A New Algorithm for Automatic History Matching*," SPEJ (Dec. 1974) 593-608; Trans., AIME, **257**.

Chrichton, M., "*PREY*," Harper Collins, 2002.

Christie, M.A., Glimm, J., Grove, J.W., Higdon, D.M., Sharp, D.H. & Wood-Schultz, M.M. "*Error Analysis and Simulations of Complex Phenomena*," Los Alamos Science, No. 29, 2005.

Clerc, M., "*The Swarm and the Queen : Towards a deterministic and adaptive particle swarm optimisation*," Proceedings of the 1999 IEEE Congress on Evolutionary Computation, Washington D.C., p1951-1957, 1999.

Cohen, S.C.M & de Castro, L.N., "*Data Clustering with Particle Swarms*," IEEE Congress on Evolutionary Computation, 2006, p1792-1798.

Costa, A.P.A, Schiozer, D.J., Poletto, C.A., "*Use of Uncertainty Analysis to Improve Production History Matching Decision-Making Process*," paper SPE 99324 presented at the SPE Europe/EAGE Annual Conference and Exhibition held in Vienna, Austria, 12-15 Jun 2006.

Cui, H., and Kelkar, M., "*Automatic History Matching of Naturally Fractured Reservoirs and a Case Study*," paper SPE 94037-MS presented at SPE Western Regional Meeting, Irvine, California, Mar 30 - Apr 01, 2005.

Cullick, A.S., Johnson, D., Shi, G., "*Improved and More-Rapid History Matching with a Non-linear Proxy and Global Optimisation*," paper SPE 101933 presented at the 2006 SPE Annual Technical Conference and Exhibition held in San Antonio, Texas, 24-27 Sep 2006.

Darcy, H. "*Les Fontaines Publiques de la Ville de Dijon*," Dalmont, Paris, 1856.

D'Errico, J. "fminsearchbnd, Bound constrained optimisation using fminsearch, " Mathworks File Exchange, 2006, http://www.mathworks.com/matlabcentral/fileexchange/8277.

Eberhart, R.C. and Hu, X., "*Human Tremor Analysis using Particle Swarm Optimisation*," Proceedings of the Congress on Evolutionary Computation, (Washington D.C. USA), IEEE Service Centre, Piscataway, NJ, 1995, pp. 1927-1930.

Eberhart, R. & Shi, Y., "*Evolving Artificial Neural Networks*," Proc. of the Intl. Conf. on Neural Networks and Brain. Beijing, P. R. of China, 1998.

Eberhart,R., and Shi, Y. "*Comparing inertia weights and constriction factors in particle swarm optimization*," in Proceedings of the Congress on Evolutionary Computing, pages 84-89, 2000.

Engelbrecht, A.P., Masiye, B.S., Pampara,G., "*Niching ability of basic particle swarm optimization algorithms*," in Proceedings of the IEEE Swarm Intelligence Symposium, 2005.

Erbas, D., Christie, M.A, "*Effect of Sampling Strategies on Prediction Uncertainty Estimation*," paper SPE 106299 presented at the 2007 SPE Reservoir Simulation Symposium held in Houston, Texas, 26-28 Feb 2007.

Ertekin, T., Abou-Kassem, J.H., King, G.R. "*Basic Applied Reservoir Simulation*," Society of Petroleum Engineers, 2001.

Faure, H., "*Good Permutations for Extreme Discrepancy*," Journal of Number Theory, **42**, 1992.

Fletcher, R., "*A New Approach to Variable Metric Algorithms*," Computer Journal, **13**, pp. 317-322, 1970.

Fox, B.L., "*Implementation and Relative Efficiency of Quasirandom Sequence Generators*," ACM Transactions on Mathematical Software, **12**, No. 4, 1986.

Gaing, Z, "*Constrained optimal power flow by mixed integer particle swarm optimisation*," in Power Engineering Society General Meeting IEEE, **1**, 2005.

Goldberg, D. E. & Richardson, J., "*Genetic algorithms with sharing for multimodal function optimisation*," in Proceedings of the 2nd International

Conference on Genetic Algorithms, J.J. Grefensette, Ed. Hillsdale, NJ: Lawrence Erlbaum, 1989.

Gomez, S., Gosselin, O. and Barker, J.W., "*Gradient-Based History Matching With a Global Optimization Method*," SPEJ (June 2001), **6**, No. 2, 200.

Joy, C., Boyle, P.P., Tan, K.S., "*Quasi-Monte Carlo Methods in Numerical Finance*," Management Science, **42**, No. 6, 1996.

Jun-jie, X., Zhan-hong, X., "*An Extended Particle Swarm Optimizer*," 19th IEEE International Parallel and Distributed Processing Symposium (IPDPS'05) - Workshop 6, 2005, p.193a.

Kaipio, J., Somersalo, E. "*Statistical and Computational Inverse Problems*," Applied Mathematical Sciences, Vol. 160, Springer, 2005.

Kathrada, M. "*The Flexi-PSO: Towards a more flexible Particle Swarm Optimiser*," OPSEARCH, Vol. 2, Springer, 2009.

Kennedy, J. and Eberhart, R. C., "*Particle Swarm Optimization*," Proceedings of IEEE International Conference on Neural Networks, **4**, (Perth, Australia), IEEE Service Centre, Piscataway, NJ, 1995, pp 1942-1948.

Kennedy, J., "*The Particle Swarm: Social Adaptation of Knowledge*", Proceedings of the International Conference on Evolutionary Computation, pp. 303-308, 1997.

Kennedy, J., "*Stereotyping: improving particle swarm performance with cluster analysis*," in Congress on Evolutionary Computation (CEC 2000), **2**, 2000.

Kennedy, J., Eberhart, R. C. and Shi, Y., "*Swarm Intelligence*", Morgan Kauffman, 2001.

Koederitz, L.F., "*Lecture Notes on Applied Reservoir Simulation*," World Scientific Publishing Co., 2005.

Lagarias, J.C., J. A. Reeds, M. H. Wright, and P. E. Wright, "*Convergence Properties of the Nelder-Mead Simplex Method in Low Dimensions*," SIAM Journal of Optimization, Vol. 9 No. 1, pp. 112-147, 1998.

Laskari, E.C., Parsopoulos, K.E. & Vrahatis, M.N., "*Particle swarm optimization for integer programming*," Proceedings of the 2002 Congress on Evolutionary Computation, Vol. 2, 2002.

Li, B., Friedmann, F., "*Semiautomatic Multiple Resolution Design for History Matching*," paper SPE 102277 presented at the 2006 SPE Annual Technical Conference and Exhibition held in San Antonio, Texas, 24-27 Sep 2006.

Liang, J.J. & Suganthan, P.N., "*Dynamic Multi-Swarm Particle Swarm Optimizer with Local Search*," Proc. of IEEE Congress on Evolutionary Computation (CEC 2005)*,* **1**, 02-05, Sept. 2005

Løvbjerg, M., Rasmussen, T. K., and Krink, T., "*Hybrid particle swarm optimiser with breeding and subpopulations*," Proceedings of the Genetic and Evolutionary Computation Conference (GECCO 2001).

Kirkpatrick, S., C. D. Gelatt Jr., M. P. Vecchi, "*Optimization by Simulated Annealing*", Science, **220**, 4598, 671-680, 1983.

Kitayama, S. & Yasuda, K., "*A method for mixed-integer programming problems by particle swarm optimisation*," Electrical Engineering in Japan, **157**, No. 2, 2006.

Maeterlinck, M., "*The Life of the Bee*," Dodd, Mead and Company, 1901.

Mantica, S. and Cominelli, A., "*Combining Global and Local Optimization Techniques for Automatic History Matching Production and Seismic Data*," paper 66355 presented at the SPE Reservoir Simulation Symposium held in Houston, Texas, 11–14 Feb 2001.

Masters, T., "*Practical Neural Network Recipes in C++*," Morgan Kaufmann, 1993.

Mathworks, "*Neural Network Toolbox,*" Matlab Online Help, Mathworks 2005.

Millar, D., "Assisted history matching gives better production forecasts," *Oil Review Middle East*, **5**, 2005.

Molina, D., Herrera, F. & Lozano, M., "*Adaptive Local Search Parameters for Real-Coded Memetic Algorithms*," Proc. of IEEE Congress on Evolutionary Computation (CEC 2005)*,* **1**, 02-05, Sept. 2005.

Oliver, D.S., Reynolds, A.C. & Liu, N. "*Inverse Theory for Petroleum Reservoir Characterisation and History Matching*," Cambridge University Press, 2008.

Ouenes, A., Brefort, B., Meunier, G., and Dupéré, S., "*A New Algorithm for Automatic History Matching: Application of Simulated Annealing Method to Reservoir Inverse Modeling*," paper SPE 26297 (1983).

Ouenes, A., and Bhagavan, S., "*Application of Simulated Annealing and Other Global Optimization Methods to Reservoir Description: Myths and Realities*," paper SPE 28415 presented at the 1994 SPE Annual Technical Conference and Exhibition, New Orleans, Sept. 25-28.

Parish et al., "*Effective History Matching : The Application of Advanced Software Techniques to the History Matching process*," paper 25250 presented at the 12th SPE Symposium on Reservoir Simulation, New Orleans, Louisiana, Feb 28 – Mar 03, 1993.

Parsopoulos, K.E., Vrahatis, M.N., "*On the Computation of all Global Minimzers through Particle Swarm Optimisation*," IEEE Transactions on Evolutionary Computation, 8(3), 2004.

Ramgulam, A., Ertekin, T., Flemings, P. B., "*Utilization of Artificial Neural Networks in the Optimisation of History Matching*," paper SPE 107468 presented at the 2007 SPE Latin American and Caribbean Petroleum Engineering Conference held in Beunos Aires, Argentina, 15-16 Apr 2007.

Ratnaweera, A., Halgamuge, S. K.,Watson, H.C., "*Self-Organizing Hierarchical Particle Swarm Optimizer With Time-Varying Acceleration Coefficients*," IEEE Transactions on Evolutionary Computation, 8, No. 3, : (2004), pp 240-255

Reuben, A., "*What is it like being an oil trader?*," BBC News, http://news.bbc.co.uk/2/hi/business/7250554.stm, 2008.

Ribeiro, P.F. & Schlansker, W.K.,: "*A Hybrid Particle Swarm and Neural Network Approach for Reactive Power Control*," online article - http://webapps.calvin.edu/~pribeiro/courses/engr302/Samples/ReactivePower-PSO-wks.pdf, 2004.

Rodrigues, J.R.P., Wachter, A. & Conn, A. "*Combining Adjoint Calculations and Quasi-Newton Methods for Automatic History Matching*," paper presented at SPE Europec/EAGE Annual Conference, SPE 99996, 2006.

Romero, C.E., Carter, C.E., Gringarten, A.C., Zimmerman, R.W., "*A Modified Genetic Algorithm for Reservoir Characterisation*," paper SPE presented at the SPE International Oil and Gas Conference and Exhibition in China held in Beijing, China, 7–10 November 2000.

Rongshan, B. & Yang, X., "*Using Particle Swarm Optimisation for Mixed-Integer Nonlinear Programming in Process Synthesis*," eprints for the optimization community, http://www.optimization-online.org/DB_HTML/2004/01/807.html.

Schulze-Riegert, R.W., Axmann, J.K., Haase, O., Rian, D.T., You, Y. L., "*Optimization Methods for History Matching of Complex Reservoirs*," paper SPE 66393 presented at the SPE Reservoir Simulation Symposium held in Houston, Texas, 11–14 Feb 2001.

Schutte, J.F., Reinbolt, J.A., Fregly, B.J. Haftka, R.T., George, A.D., "*Parallel Global Optimisation with the Particle Swarm Algorithm*," International Journal of Numerical Methods in Engineering, **61**, 2004.

Sen, M.K., Datta-Gupta, A., Stoffa, P.L., Lake, L.W. and Pope, G.A., "*Stochastic Reservoir Modelling Using Simulated Annealing and Genetic Algorithms*," SPE Formation Evaluation (March 1995) 49.

Shi, Y. and Eberhart, R.C., "*Empirical Study of Particle Swarm Optimisation*," Proceedings of the Congress on Evolutionary Computation, (Washington D.C. USA), IEEE Service Centre, Piscataway, NJ, 1995, pp. 1945-1949.

Shi, Y.H. and Eberhart, R.C., "*Parameter selection in particle swarm optimisation*," Annual Conference on Evolutionary Programming, San Diego, 1998.

Silva, A., Neves, A., Costa, E., "*Chasing the Swarm: A Predator Prey Approach to Function Optimisation*", Proceedings of the MENDEL2002 8th International Conference on Soft Computing, Brno, Czech Republic. 2002.

Silva, A., Neves, A., and Costa, E., "*SAPPO: a simple, adaptable, predator prey optimiser,*" Lecture Notes in Computer Science(LNCS) No. 2902: Progress in Artificial Intelligence, Proceedings of 11th Protuguese Conference on Artificial Intelligence (EPIA 2003), Beja, Portugal. pp. 59-73, 2003

Socha, K., Dorigo, M., "*Ant colony optimisation for continuous domains*," European Journal of Operations Research, **185**, 2008.

Solorzanom L. N., Arredando, S.E., "*Method for Automatic History Matching of Reservoir Simulation Models*," paper SPE 4594 presented at 48th Annual Fall Meeting, Las Vegas, Nevada 1973.

de Sousa, S.H.G., "*Scatter Search Heuristic Applied to the History Matching Problem*," paper SPE 113610-STU presented at the 2007 SPE International Student Paper contest, 2007.

Suganthan, P.N., "*Particle Swarm Optimiser with Neighbourhood Operator*," Proceedings of the 1999 Congress of Evolutionary Computation, vol. 3, 1999, pp 1958-1962. IEEE Press.

Suganthan, P.N.,: "*Problem Definitions and Evaluation Criteria for the 2005 Special Session on Real Parameter Optimisation*," http://www.ntu.edu.sg/home/EPNSugan/, 2005.

Tarantola, A. "*Popper, Bayes and the inverse problem*," Nature Physics, Vol. 2, 2006.

Tasgetiren, M.F., Liang, Y., Gencyilmaz, G. & Eker, I., "*A Differential Evolution algorithm for Continuous Function Optimisation*," Proc. of IEEE Congress on Evolutionary Computation (CEC 2005)*,* 1, 02-05, Sept. 2005 van den Bergh, F. and Engelbrecht, A. P., "*Cooperative learning in neural networks using particle swarm optimizers*," South African Computer Journal, **26** pp. 84-90, 2000.

van der Corput, J., "Verteilungsfunktionen I & II," Nederlandse Akademie van Wetenschappen, **38**, 1935.

Vaz, I.F., Fernandes, M.G.P., "*Particle swarm algorithms for multi-local optimisation*," in Congreso Galego de Estatística e Investigación de Operacións Guimarães 26, 27 e 28 de Outubro de 2005.

Vesterstroem, J.S., Riget, J., Krink, T., "*Division of labor in particle swarm optimisation,*" *Proceedings of the IEEE Congress on Evolutionary Computation*, Honolulu, Hawaii (2002).

Wasserman, M. L., Emanuel, A.S., and Seinfeld, J.H., "*Practical Applications of Optimal Control Theory to History Matching Multiphase Simulator Models*," SPEJ (Aug.1975) 347-55; Trans., AIME, **259**.

Watson, A.T., "*History Matching in Two Phase Petroleum Reservoirs*," *SPEJ* (Dec 1980) 521-32.

Yang, P.H. & Watson, A.T., "Automatic History Matching with Variable Metric Methods," paper 16977 presented at the SPE Annual Technical Conference and Exhibition, Dallas, Sep. 1987.

Yamada, T., "*Non-Uniqueness of History Matching*," paper SPE 59434 presented at the SPE Asia Pacific Conference on Integrated Modelling for Asset Management held in Yokohama, Japan, 25–26 Apr 2000.

Zhang, J., Zhang, J.R., Li, K., "*A Sequential Niching Technique for Particle Swarm Optimisation*," in Advances in Intelligent Computing. Springer Berlin / Heidelberg, 2005.

Zhang, L., Yu, H., Hu, S., "*Optimal choice of parameters for particle swarm optimisation*," Journal of Zhejiang University SCIENCE, 6A(6), p528-534, 2005.

Zhang, W., Liu, Y. and Clerc, M., "*An Adaptive PSO Algorithm for Reactive Power Optimization,*" Advances in Power System Control Operation and Management (APSCOM) 2003, Hong Kong.